TIME-VARYING DOPPLER COMPENSATION FOR UNDERWATER ACOUSTIC COMMUNICATION

by

Habib Mirhedayati

Submitted in partial fulfillment of the requirements
for the degree of Master of Applied Science

at

Dalhousie University
Halifax, Nova Scotia
March 2017

Table of Contents

List of Figures

List of Tables

Abstract

This thesis focuses on time-varying Doppler compensation for underwater acoustic communications using an orthogonal frequency division multiplexing (OFDM) system. An underwater acoustic channel simulator is developed based on the geometry of the system deployment and by considering the statistics of the random variation of the channel. This channel simulator is capable of modeling any relative motion between the transmitter and receiver. The effect of the underwater acoustic (UWA) channel on OFDM system is studied by incorporating a model in system level simulation of the communication link. The time-varying Doppler compensation method is then introduced as an innovative method which is able to compensate for Doppler shift due to time-varying relative velocity between the transmitter and receiver. Finally, the proposed Doppler compensation method is integrated to an ultrasonic OFDM system and the communication reliability is evaluated through simulations and measurements in realistic deployment conditions. Specifically, for a distance of 150 m a net throughput after synchronization, channel estimation and decoding 760 bit/s was demonstrated with a bit error rate of 0.035 for a low SNR of 5.5 dB. More importantly, it will be shown that the assessment of the communication performance realized using simulations is very close to that of the measured performance.

Acknowledgements

First and foremost, I would like to express my sincere gratitude to my supervisor, Dr. Jean-François Bousquet, for his guidance, support and insight throughout my Master's degree program. I would like to thank him for providing me with the friendly and productive environment of UW-Stream research lab.

I would also like to thank my committee members, Dr. Mae Seto and Dr. Jacek Ilow for sparing their precious time and dedicating their consideration to enrich my work.

I've had the unique opportunity of sharing my Master's degree journey with my lab-mate and best friend, Graham McIntyre, who always is a source of support and inspiration. I thank him for sharing his knowledge as well as the many valuable and insightful discussions we had during my research. My sincere gratitude also goes to Dr. Mark McIntyre for his unsparing support during my graduate school career. I have no doubt to count myself fortunate to have his mentorship.

I'm indebted to my colleague at Vemco, Dr. Sara Stout-Grandy, for her priceless feedback and advice during the preparation process of this thesis. I would also like to thank Amirix System Inc for the use of their equipment and their technical support. A special thanks to my colleagues Terry Fraser and Gary Marsh, for the valuable discussions throughout the experimental process.

Finally, this work would not have been possible without the love, encouragement and support of my parents. I would like to extend my sincere appreciation and heartfelt gratitude to them for all the love and inspiration.

Chapter 1

Introduction

1.1 Background

The water covers about 71 percent of the Earth's surface. This water is found mainly in oceans which have significant impact on human life. For example, the ocean moderates the Earth's climate and influences the weather. Also it provides food, mineral and energy resources. These natural benefits, in addition to being an important source of inspiration, recreation and discovery for human beings, motivate scientists, oceanographers, and politicians to explore the oceans more closely.

There are some obstacles which make the widespread exploration of the oceans extremely difficult. One obstacle is the pressure under water. As an object goes deeper underwater, the pressure of the water on that object is increased. The second obstacle is the darkness. At great depths, even powerful lights fail to illuminate an area sufficiently. Because of these difficulties, the ocean discoverers started developing tools and technologies to enable scientific exploration of the deep sea. These efforts can be traced as far as 1521 when Ferdinand Magellan tried to measure the depth of the Pacific ocean with a 2400 ft weighted line [2].

In addition to the eagerness of ocean explorers to solve the mystery of the undersea world, there has always been a need for coastal people to survey the littoral coast for sea activities, and particularly to maintain the security of their lands. This need, motivated the scientists to develop some tools for underwater sensing. The first attempt in underwater sensing was conducted in 1490 by Leonardo Da Vinci who tried to listen for a ship from a long distance using a tube submerged in the sea. This experiment encouraged other scientists to pursue studying underwater acoustics further in the 18th century. The first successful measurements of the speed of sound

underwater were done by Colladon and Sturm in early 1800's. At about the same time, scientists began to think about the practical applications of underwater sound, such as using sound to measure the depth of the ocean [2].

In the early 1900's, because of increasing ship traffic and ineffectiveness of lighthouses and lightships, the necessity of a reliable warning system was raised. Among the first works, a group of scientists proposed a navigational safety system which consisted of some underwater bells located under lightships and a series of waterproof microphones installed on ships. Later in 1912, a Canadian engineer, Reginald Fessenden, proposed to replace the bells with electric-powered sound generators and more selective underwater microphones, which they referred to as hydrophones [2].

After World War I, scientists developed a massive number of experiments in the field of underwater acoustics propagation which led to a good understanding of the physical effects of the underwater medium on sound propagation. The results of this research were used in the development of sonars and weapons during World War II and the Cold War.

Since then, an extensive effort has been dedicated to research and development of underwater communication systems, in addition to underwater navigation systems. Underwater sensor networks, still rely on fiber optic or copper cabling, particularly to serve sufficiently large and stationary devices. However, a wireless link is desirable in many situations. Some of the applications of underwater wireless communications systems are monitoring the health of the ocean, discovery of new natural resources in oil and gas industry, fish tracking, and communication between autonomous underwater vehicles (AUVs).

During the last 30 years, a few underwater RF systems have been developed. The use of electromagnetic (EM) waves in RF systems has several advantages over acoustic waves, such as higher data rate and robustness to Doppler effect in mobile applications in which the platforms are moving. The freshwater is a low-loss medium for EM waves which attracts a lot of interest in using RF systems. However, the need for a big antenna size for EM underwater transmitter, i.e. a couple of meters for a 50 MHz antenna, make these systems unpractical in low power applications [3]. In addition,

seawater is a high-loss medium for EM waves because of the high degree of salinity [3]. Therefore, these disadvantages makes the underwater RF communications systems unpractical in low power and wide-range applications.

Acoustic wave is used as primary carrier for underwater wireless communications, due to its low-loss property at low frequencies (on the order of 100 Hz to 100 kHz). However, due to low speed of sound underwater, these systems suffer from large latency. Also, underwater acoustic communication systems are adversely affected by multipath propagation due to reflection and refraction.

Recent advances in optical communications have resulted in the development of underwater optical communications systems such as the one which was developed by Sonardyne for high data-rate communications (up to 500 Mbps) for a short range (less than 100 m) [4] in clear water. Although optical communication systems may perform well in short range underwater applications, there are a couple of disadvantages for these systems. First, absorption of optical signals under water is way faster than acoustic waves. Second, turbidity underwater causes significant optical scattering. Third, strong ambient level of light, emitted from surface, has an adverse effect on shallow water applications [3].

Besides all the efforts that have been made to enable RF and optical communications for the underwater environments, acoustic communication is still the most prevalent method. Although these systems also suffer from low data rates, time-variance, and multipath issues, researchers are finding new ways to deal with the issues of underwater acoustic systems by applying advanced signal processing techniques.

1.2 Motivations

The underwater environment is a highly distortive medium for acoustic propagation. The distortions are directly related to the physical characteristics of the underwater environment.

Firstly, this environment is bounded by the surface, bottom and other obstacles. When an acoustic wave hits a boundary, a part of its energy passes through the

boundary or gets absorbed by the medium. The rest of the energy is reflected. When reflections happen, the receiver may observe different copies of the transmitted signal with different delays, amplitudes, and phases. This phenomenon is called *multipath arrival* which effectively degrades the performance of the communication system, because it distorts the received signal. This phenomenon is shown in Figure 1.1.

Secondly, the power intensity of the acoustic signal gets attenuated while traveling underwater. The rate of attenuation depends on different physical parameters such as the range, frequency, and type of chemicals underwater. This attenuation can reduce the ratio of the signal to noise (background noise or electronics noise) power.

The last major physical shortcoming of acoustic propagation underwater is its low speed. The speed of sound underwater is approximately 1500 $\frac{\mathrm{m}}{\mathrm{s}}$, which in comparison with the speed of electromagnetic waves in the air $300,000,000$ $\frac{\mathrm{m}}{\mathrm{s}}$, is very slow. This means, a wireless communication algorithm which performs well in the air, may experience high latency and long delays when it propagates acoustically underwater. Moreover, the low speed of sound underwater makes the communication system very sensitive to the relative velocity between transmitter and receiver and any kind of random motion of the medium. The effect of this phenomenon is usually observed as a timing offset and frequency distortion.

There are other effects underwater that impact communications, such as wave bending (refraction) in deep water and scattering of the waves due to reflections from small objects, bubbles, rocks, or fishes. These physical impairments motivate scientists to study and analyze this communication medium and its challenges more closely.

One of the main purposes of this work is to analyze the physical phenomena which affects the performance of an underwater acoustic communication system. Also, because of the critical requirement for computer modeling in present day research, the need for a realistic software tool for underwater sound propagation modeling is essential. Because of this, in this work a software channel simulator will be developed by considering the essential physical impairments of the underwater environment. This

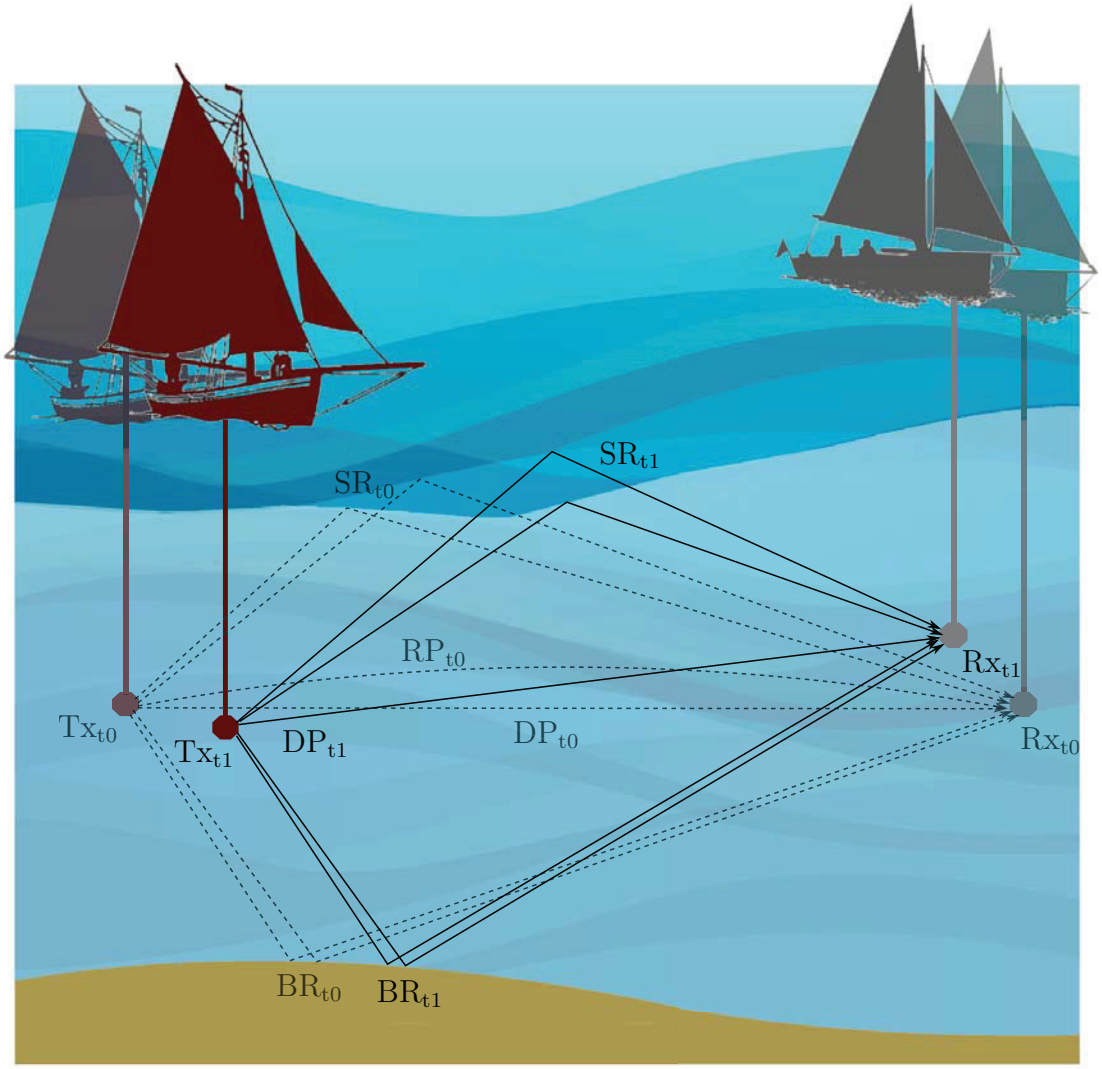

Figure 1.1: An underwater acoustic communication deployment with dynamic transmitter (Tx) and receiver (Rx) at two instances, $t0$ and $t1$. DP, RP, SR and BR demonstrate direct path, refracted path, surface reflection and bottom reflection, respectively.

thesis focuses on modeling propagation through a highly time-varying underwater environment either due to relative receiver/transmitter motion or due to random movement of the medium. As will be shown the proposed channel simulator is a flexible

and efficient tool for simulating the underwater communication system deployments in which the relative velocity between the receiver and transmitter is changing with time.

The considerable advances in wireless systems in the past thirty years in the RF world, above the water, has produced a number of techniques for communications that may be useful to mitigate some of the problems in underwater acoustic communications. The capabilities of the advanced RF land wireless communications systems have encouraged a lot of engineers to adjust the RF techniques in a way to be applied in underwater acoustic systems. Therefore, the second motivation for this thesis is to apply advanced RF land communication techniques to underwater acoustic communications in order to improve the reliability of a wireless underwater acoustic link. Particularly, developing the algorithms to compensate for the distortions which happen due to the time-varying effect of the underwater environment. The techniques presented in this work will help improve the data rate performance for longer ranges, and in a time-varying underwater medium.

1.3 Thesis Contributions

This thesis presents a wideband digital underwater communication system that can provide a reliable communication link in a time-varying channel scenario, in which the transmitter and receiver are moving relative to each other with a time-varying acceleration.

In this thesis, *Orthogonal Frequency Division Multiplexing (OFDM)* is used to modulate the data, because of its capability to estimate and compensate for the communication channel impairments such as multipath propagation and time-variance.

This thesis will focus on the synchronization and compensation for the time-variance of the channel, which in a communication system, is usually referred to as *Doppler compensation and synchronization* unit. In particular, an innovative Doppler compensation method will be presented in this thesis, which is its main contribution. This Doppler estimation technique is able to estimate the Doppler shift in ultra sound

communications (170 kHz), in a deployment which is subject to high degree of acceleration. Then the system compensates for Doppler using a novel resampling method which is called *time-varying fractional delay line (TVFDL)*. Moreover in this work, the synchronization and Doppler compensation blocks will be integrated into a full receiver design to evaluate the performance of this technique in both simulation and practice.

The other contribution of this thesis is the characterization and modeling of the underwater communication medium, which is called *underwater acoustic (UWA) communication channel*. After mathematical modeling of the channel, a software channel simulator is developed which considers both geometrical parameters of a specific deployment, as well as the statistical characteristics of the measured channels. The TVFDL is also used in this channel simulator to implement the Doppler effect due to time-varying acceleration between the transmitter and receiver. Using TVFDL makes the channel simulator very flexible in software implementation of any time-varying deployment.

Finally, to evaluate the performance of the communication system and channel simulator, a series of sea trials were preformed at Amirix Systems Inc.'s facilities in Shad Bay, Nova Scotia. It will be demonstrated that the assessment of the communication performance realized using a software model of the entire system is very close to that of the measured performance.

1.4 Thesis Outline

The outline of the thesis is reviewed here. Chapter 2 analyzes the characteristics of the UWA channel and presents the software channel simulator. In Chapter 3 the characteristics of the OFDM system is introduced and the effect of the UWA channel on OFDM will be analyzed. Chapter 4 will review the advantages and disadvantages of the conventional Doppler compensation methods and will present a new Doppler compensation and synchronization technique relying on pilot sub-carriers of the OFDM symbol. Chapter 5 will show the development of the transmitter and receiver architecture and explore the scientific methods which are used to evaluate the performance

of the communication system, as well as discussing the essential considerations in the communications system design procedure. Finally, the conclusions and future works are presented in Chapter 6.

Chapter 2

The Underwater Acoustic Channel

In telecommunications, the medium between the transmitter and receiver, which affects the signal characteristics is called the *communication channel*. It has been recognized that the underwater communication system deployment is expensive and complicated. Also, underwater acoustic (UWA) communication channels show different characteristics in different deployment settings and environmental conditions. Therefore, developing a tool to predict the UWA channel characteristics to evaluate the performance of the system before deployment is essential. In this Chapter a computationally efficient software model is utilized to develop a geometry based stochastic model for highly mobile deployments, when all the components of the deployment are moving.

The existing underwater acoustic channel models will be reviewed in Section 2.1 and the mathematical model of the channel is presented in Section 2.2, while in Section 2.3 the time variability of the channel is analyzed accurately. Finally, a software channel model will be developed in Section 2.4.

2.1 Review of Underwater Acoustic Channel Challenges

In underwater acoustic channel design, a variety of conditions such as changes in system geometry and environmental conditions must be considered [5]. Ray tracing tools, such as Bellhop [6], have been used traditionally to predict acoustic wave propagation for a given geometry, but these deterministic models typically do not consider the random variation of the channel with time. The authors in [7] have developed a less complex ray tracing model that takes into account the channel variations caused

by the moving sea surface. This model is called *Virtual Timeseries Experiment (VirTEX)* and referring to [5], "it operates by tracing multiple interrelated beams to assess the cumulative effect on the signal of a given frequency."

In addition to the efforts that researchers have put into deterministic UWA software channel modelling, considerable studies have been conducted to model the channel stochastically [5, 8, 9, 10, 11, 12, 13]. These studies are based on analysis of the measurements and the variety of the models is a result of differences between the deployment sites and probing signals. Although these tools can represent a time-varying underwater environment for a given geometry, they do not account for the time-varying velocity between the transmitter and receiver, such as in the presence of a constant relative acceleration between the transmitter and receiver.

Similar to the other wireless channels, the underwater channel impairments can be classified into four groups which are explained here.

1) Transmission Loss: This phenomenon describes the reduction in the signal intensity as it propagates away from the source. In underwater acoustic propagation the transmission loss is a consequence of spreading, absorption and reflection [10, 12]. The spreading of the sound energy is a result of the expansion of the wavefront. In addition to spreading, as sound propagates underwater, its energy gets absorbed by the molecules in water and is converted to heat. This phenomenon reduces the amplitude of the wave-front and it is known as absorption loss. This loss is a function of range and frequency [14]. Reflection loss is the third type of transmission loss. As the acoustic rays are reflected from the surface, bottom, walls and, moving objects, the energy of the wave is decreased as a result of discontinuity or impedance mismatch between the water and other mediums.

An important consideration about transmission loss is that it depends on the distance between the transmitter and receiver. In a mobile scenario, this distance can vary significantly. The transmission loss affects the path amplitudes directly. So, the path amplitude varies with time due to time-varying distance. This effect will be explained in detail in Section 2.3.2.

2) Multipath Propagation: In the UWA channel, the multipath propagation is due to two phenomena: 1) reflection, and 2) refraction [12, 14]. The underwater environments such as ocean, rivers, and water tanks are bounded by their surface, walls and the floor, as well as other objects, on which the acoustic waves will reflect. Furthermore, the speed of sound underwater depends on the temperature, pressure and salinity, and it can vary significantly over large depth variations. The variable sound speed profile will cause refraction, which can be observed as a bending of the wave in any direction off the line of sight [12, 14]. As a result of reflection and refraction, the receiver observes multiple distorted copies of the transmitted signal with different delays, amplitudes and phases. This observation is called multipath arrival which results in a multipath channel.

In addition, some of the minor effects which can result in scattering of the energy around the *eigenpaths* are surface waves, internal waves and the bubbles [12, 14, 15]. Eigenpath is referred to a path which contains multiple copies of the transmitted signal which are scattered around a stronger arrival. In fact, each eigenpath is a cluster of arrivals which includes numerous small paths with an approximately equal delay but different Doppler shifts and phases. The small paths which form the eigenpath are called a *micropaths*. In this work in ray theory description the eigenpath is called eigenray.

3) Time-variance: The time-variance in the UWA channel is due to the motion of scatterers and transmitter/receiver displacements. Surface waves, internal currents, tides, bubbles and moving objects, like undersea creatures, are scattering objects that create time-varying delays and amplitudes in a multipath channel. Waves, currents and tides can force the underwater instruments to drift or move [12]. The fundamental principle that accounts for time-variance is the *Doppler effect* which accounts for the change in frequency of the received signal [12]. Generally, this frequency shift happens due to relative motion between the receiver and transmitter. The channel time-variance can be described by time-varying path delay and time-varying path amplitude. These parameters are discussed in detail in Section 2.3.1 and Section 2.3.2.

4) Noise: In most communication system designs, the main source of noise is the thermal noise, which is produced by transducer instruments. This kind of noise is usually modelled as an additive white Gaussian distributed term. The term *white noise* indicates that the power of the noise remains constant for all frequencies. According to [12], while the background noise in UWA channel can usually be approximated as Gaussian, it is not white. The background noise below the sea is referred to as *ambient noise*. This noise comes from different sources such as, surface waves, distant ships, tides, rain, biological sounds underwater mamals, turbulence and even ice-cracking in polar regions [12, 14]. More details on underwater acoustic noise can be found in [12, 14]. In this thesis, only the background additive white Gaussian noise is considered in simulations.

2.2 Mathematical Representation of the Channel

The UWA channel can be characterized mathematically by its *impulse response*. The UWA channel impulse response (CIR) is time-variant. This CIR of a time-varying multipath channel can be modelled as a sum of time delayed and amplitude scaled versions of the transmitted impulse function [16], explained as

$$h(t,\tau) = \sum_{p=1}^{N_p} h_p(t)\delta\left(\tau - \tau_p(t)\right), \tag{2.1}$$

where t, τ, h_p, τ_p, and N_p represent time, delay, time-varying amplitude of the pth path, time-varying delay of the pth path, and the number of eigenpaths, respectively. The other parameter that must be used in mathematical time-varyig channel representation is the *spreading function*. According to [16], the values of the spreading function, $S(\nu,\tau)$, characterizes the overall complex attenuation and reflections from the scatterers, associated with all paths of delay, τ, and Doppler frequency shift, ν. The spreading function can be obtained as the Fourier transform of the $h(t,\tau)$ with respect to t as

$$S(\nu,\tau) = \int_{-\infty}^{\infty} h(t,\tau)\mathrm{e}^{-j2\pi\nu t}dt. \tag{2.2}$$

The time-varying channel impulse response or the spreading function can describe a

deterministic UWA channel, completely. However, to account the random variation of UWA channel, stochastic characterization should be considered.

When the statistical channel model is developed, a stochastic process is used to vary the channel characteristics as a function of time and delay. Then, the auto-correlation function is used to characterize a stochastic channel with second order statistics. The auto-correlation function of a two-dimensional channel impulse response, $h(t, \tau)$, is a four-dimensional function. Therefore the second order statistics of the UWA channel will be described by a four dimensional correlation function [16], as

$$R_{hh}(t, t'; \tau, \tau') = \mathrm{E}\left[h(t, \tau)h^*(t', \tau')\right], \tag{2.3}$$

where E[·] is the expected value operator. To simplify the correlation function in terms of only two variables, *Wide-Sense Stationary Uncorrelated Scattering* (WSSUS) condition is assumed which is defined here.

Uncorrelated Scattering: *If different paths interpreted to belong to different scatterers, then under the uncorrelated scattering (US) assumption, the eigenpaths are uncorrelated as a function of delay*, i.e.,

$$\mathrm{E}\left[h(t, \tau)h^*(t', \tau')\right] = R_{hh}(t, t'; \tau)\delta(\tau' - \tau). \tag{2.4}$$

Wide-Sense Stationary: *The random amplitude of the channel is considered wide-sense stationary (WSS) if it is independent of single time instances, t_i. In other words, the autocorrelation function of the channel is independent of time, but it depends on the difference between time instants, $\Delta t = t' - t$. The autocorrelation function of a WSS channel is represented by*

$$\mathrm{E}\left[h(t, \tau)h^*(t', \tau')\right] = R_{hh}(\Delta t; \tau, \tau'). \tag{2.5}$$

By combining both concepts, the autocorrelation function $R_{hh}(\Delta t, \tau)$ becomes

$$R_{hh}(\Delta t, \tau) = \mathrm{E}\left[h(t, \tau)h^*(t + \Delta t, \tau)\right]. \tag{2.6}$$

Referring to [16], under WSSUS assumption the second-order statistics of a channel are fully described by the 2D correlation function $R_{hh}(\Delta t, \tau)$.

The Fourier transform of the channel autocorrelation function with respect to Δt is called the *scattering function* and under the WSSUS assumption is given by,

$$P(\nu, \tau) = \int_{-\infty}^{\infty} R_{hh}(\Delta t, \tau) \mathrm{e}^{-j2\pi f \Delta t} d\Delta t. \tag{2.7}$$

The scattering function gives the average power distribution of a channel in the delay, τ, and the Doppler frequency, ν domains. Two important parameters that can be extracted from the scattering function are the *power delay profile* and the *Doppler power spectrum*.

The power delay profile shows the received signal power intensity as a function of propagation delay, i.e.,

$$P_\tau(\tau) = \int_{-\infty}^{\infty} P(\nu, \tau) d\nu. \tag{2.8}$$

To measure the severity of the multipath channel, the *delay spread*, $\hat{\tau}_s$, is defined as the root-mean-square (RMS) widths of the power delay profile [16]. Alternatively, in the frequency domain the *coherence bandwidth* is defined as a statistical measure that indicates the range of frequency over which the channel can be considered frequency-flat and it is expressed as the inverse of the delay spread,

$$B_c = \frac{1}{\hat{\tau}_s}. \tag{2.9}$$

The Doppler power spectrum is a power spectral density that characterizes the distribution of the received signal power as a function of the Doppler frequency, i.e.,

$$P_\nu(\nu) = \int_{-\infty}^{\infty} P(\nu, \tau) d\tau. \tag{2.10}$$

In many practical conditions, the channel is non-stationary and/or correlated. But, due to slow variation of the channel in absence of relative speed between the transmitter and receiver which is created by motor force, it can be assumed that the channel behaves as a WSSUS channel for a restricted time interval and frequency band [9]. Under this assumption, the UWA channel can be fully described by Equation (2.1), (2.2), (2.6), (2.8), and (2.10). After modeling the time-variation due to random motion of the deployment statistically, the relative motion due to motor force can be added on top of the random time-variation.

Because the focus of this thesis is on developing a method to compensate for the of time-variability effect of a channel, the next section will explore and analyze this phenomenon.

2.3 Time Variability

Under the WSSUS assumption, channel modeling can be done in two steps. First, calculating the time-varying delay using ray theory for a given geometry and time-varying distance. This is accomplished by modeling the undersea environment as a semi-rectangular waveguide bounded by surface and bottom (or walls in the river environment). Second, calculating the time-varying path amplitudes using a given Doppler spectrum. These time-varying parameters will be described in Section 2.3.1 and Section 2.3.2, respectively.

2.3.1 Time-varying Delay

Time-varying delay generally happens due to relative motion between the transmitter and receiver. The relative motion is usually caused by transmitter/receiver random displacement which happens due to waves and currents, or motor force of the underwater vehicles which creates a certain relative velocity.

Random displacement usually makes small frequency shifts in the received signal spectrum. The value of these random frequency shifts are described by the Doppler spectrum.

The motion of the transmitter and receiver produced by motor force, i.e. deployment using two moving boats, creates a time-varying velocity that is superimposed on the effects of the channel. This adds another level of complexity to these systems as the received signal is now also dynamically time-scaled, an effect that is especially deleterious in wideband systems. Depending on the direction of this velocity, the *time-scaling* will be observed as received signal *dilation* or *compression* in the time-domain. In the frequency domain, the compression/dilation is observed as frequency dependent frequency shifts.

The time-varying path delay, $\tau_p(t)$, is directly related to the distance which the pth eigenray travels, $r_p(t)$, and can be obtained by dividing this distance by the speed of propagation, c_w. Specifically

$$\tau_p(t) = \frac{r_p(t)}{c_w}. \tag{2.11}$$

The time-varying distance between the transmitter and receiver with respect to the horizon can be obtained for a given relative speed, $v(t)$, and initial distance, d_0, using the kinematic laws and it is

$$d(t) = \int_0^t v(t)dt + d_0. \tag{2.12}$$

To simplify the modeling, first the random motions are neglected. The relative velocity, created by motor force will then be

$$\vec{v}(t) = \vec{v}_{tx}(t) - \vec{v}_{rx}(t), \tag{2.13}$$

where $\vec{v}_{tx}$ and $\vec{v}_{rx}$ indicate the transmitter and receiver vectorial velocity, respectively. This scenario is shown in Figure 2.1.

Then, the time-varying distance that each eigenray travels from the transmitter to the receiver, $r_p(t)$, can be calculated from the method of images using the time-varying distance with respect to the horizon and other geometrical parameters in a two dimensional plane [10].

Figure 2.2 shows some possible path arrivals. In a two dimensional plane, the geometrical parameters that are considered to calculate the distance of the eigenrays are: the total depth $H(t)$, the depth of receiver $h_{rx}(t)$, the depth of transmitter $h_{tx}(t)$, and the total number of upward and downward bounces n [10]. Note that the depth can vary with time and distance, due to surface waves and rough bottom conditions. The

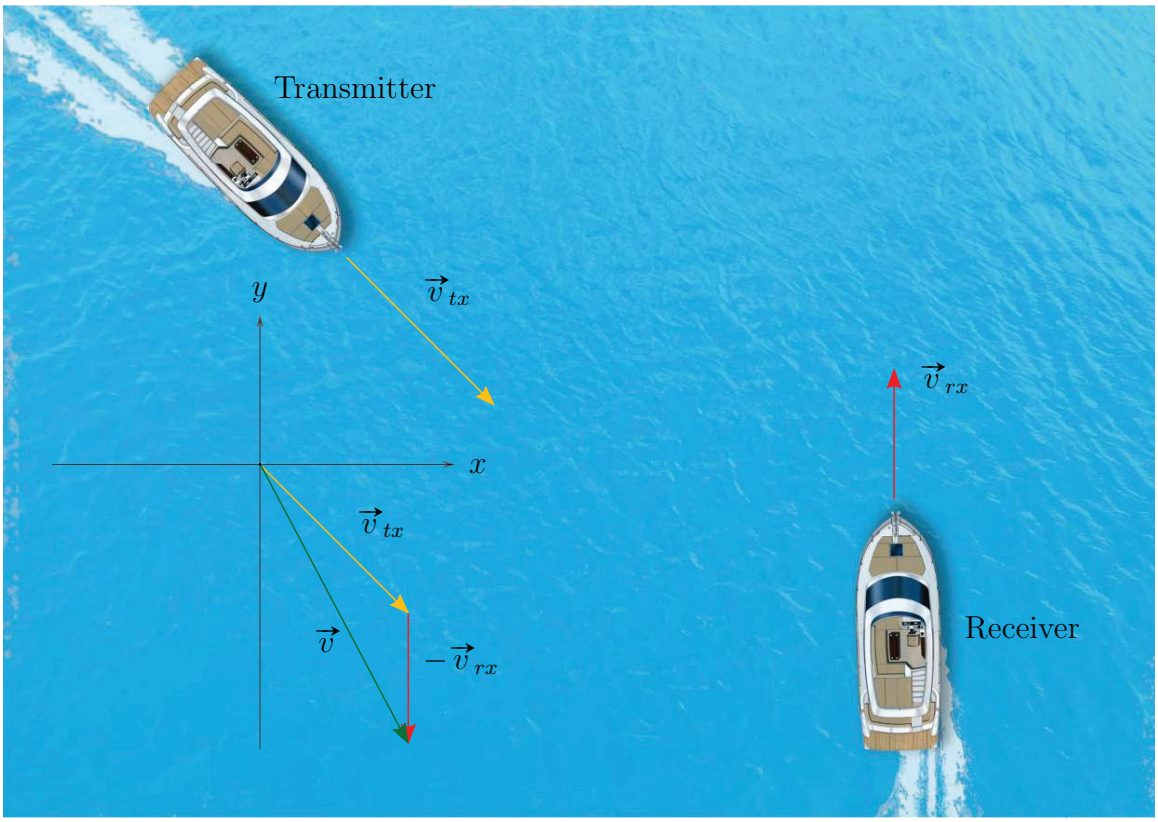

Figure 2.1: A vector demonstration of the relative velocity calculation in two dimensions.

distances are calculated form the following equations,

$$r_{\text{los}}(t) = \frac{d(t)}{\sqrt{d^2(t) - |h_{tx}(t) - h_{rx}(t)|^2}}, \tag{2.14}$$

$$r_n^u(t) = \frac{d(t)}{\sqrt{d^2(t) - \left|(n-\frac{1}{2})H(t) + h_{tx}(t) + (-1)^n\left(\frac{H(t)}{2} - h_{rx}(t)\right)\right|^2}}, \tag{2.15}$$

$$r_n^d(t) = \frac{d(t)}{\sqrt{d^2(t) - \left|(n+\frac{1}{2})H(t) - h_{tx}(t) + (-1)^{n+1}\left(\frac{H(t)}{2} - h_{rx}(t)\right)\right|^2}}, \tag{2.16}$$

where r_{los}, r_n^u, and r_n^d show the ranges of the line of sight, nth upward eigenray, and nth downward eigenray, respectively. Some of the other eigenrays that may be observed in real environments are refracted rays (in deep water) and rays from wall reflections. Because of the focus of this work on shallow water environment and to simplify the model, the refracted rays are neglected.

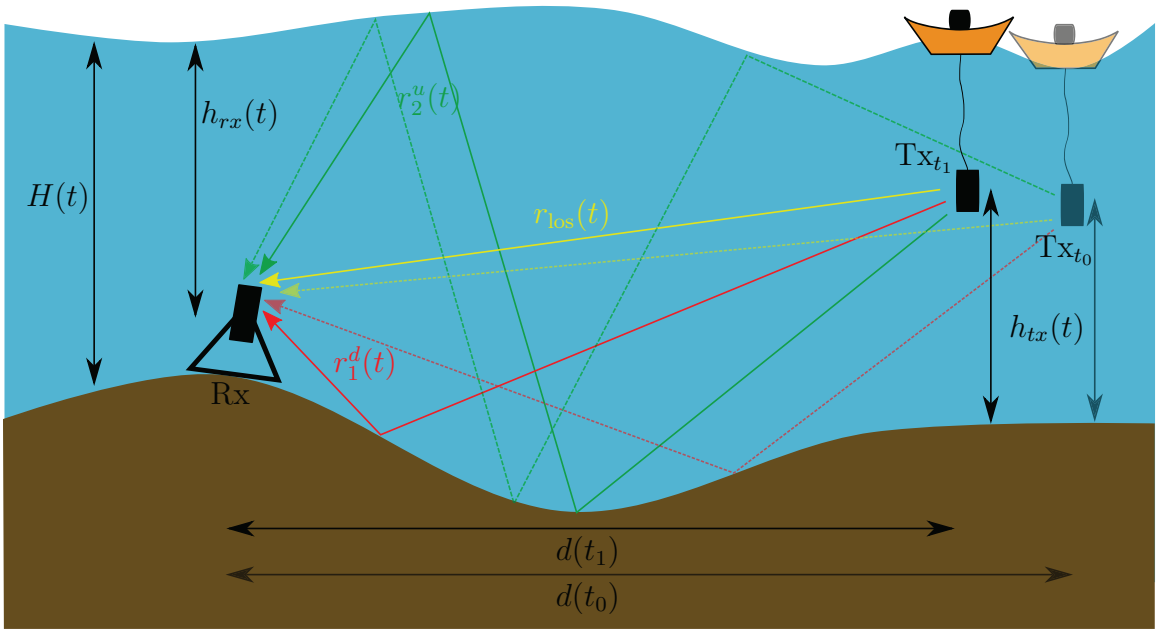

Figure 2.2: Underwater sound propagation in a two dimensional space.

According to [17], the angle of arrival of each eigenray is obtained using the following equation,

$$\phi_p(t) = \cos^{-1}(\frac{d(t)}{r_p(t)}). \tag{2.17}$$

As an example, a specific mobile deployment scenario is analyzed here. Assume that the relative velocity between the transmitter and receiver with respect to the horizon is constant in time, v. Also, it is assumed that the amplitude, h_p, and angle of arrival, ϕ_p, of each eigenpath remains constant. Then, the horizontal distance is,

$$d(t) = vt + d_0. \tag{2.18}$$

So, the time-varying delay of the pth path is expressed as,

$$\tau_p(t) = \frac{r_p(t)}{c_w} = \frac{1}{\cos(\phi_p)}\left(\frac{d_0}{c_w} + \frac{v}{c_w}t\right) = \tau_{0,p} - (1 - \alpha_p(t))t, \tag{2.19}$$

where $\tau_{0,p}$ is the initial delay of the pth path and α_p is the time-scaling factor which describes the rate of the received signal compression or dilation and it is,

$$\alpha_p = (1 + \frac{v_p}{c_w}), \tag{2.20}$$

where $v_p = \frac{v}{\cos(\phi_p)}$. When $v_p > 0$ and $\alpha_p > 0$, the path length is decreasing which causes compression in the time domain. Similarly, the signal would be dilated in time domain when $v_p < 0$ and $\alpha_p < 1$.

The time-varying channel impulse response, Equation (2.1), is then re-written as

$$h(t,\tau) = \sum_p h_p(t)\delta\left(\tau - \tau_{0,p} + (1-\alpha_p)t\right). \tag{2.21}$$

The channel frequency response at time instant t, is obtained by taking the Fourier transform of Equation (2.21) with respect to τ,

$$H(t,f) = \sum_p h_p \mathrm{e}^{-j2\pi f\tau_{0,p}} \mathrm{e}^{j2\pi\frac{v_p}{c_w}ft}, \tag{2.22}$$

where the first exponential term $\mathrm{e}^{-j2\pi f\tau_{0,p}}$ indicates that there is a frequency dependent phase shift of $2\pi\tau_{0,p}$ and the second term $\mathrm{e}^{j2\pi\frac{v_p}{c_w}ft}$ shows a frequency dependent frequency shift of $\frac{v_p}{c_w}f$ on the pth path due to the relative speed v_p.

A general narrowband assumption that is often made is that, for a given bandwidth, B, and carrier frequency, f_c, when the fractional bandwidth is much less than 1, $\frac{B}{f_c} << 1$, then $f \approx f_c$. This means that the Doppler effect can be modelled as a constant frequency shift, $\frac{v_p}{c_w}f_c$, for all frequencies [18].

In practical underwater communication systems the attenuation due to chemicals energy absorption, increases with frequency, so to realize a link with a range above a few kilometers, the carrier frequency should be low, below 200kHz [12]. Therefore to maintain a reasonable communication bandwidth, it can not be assumed that $\frac{B}{f_c} << 1$. Therefore the narrowband assumption does not hold. In addition, because of the low speed of sound underwater ($c_w \approx 1500\frac{\mathrm{m}}{\mathrm{s}}$) in comparison with RF wave propagation in the air (with speed of light $c_l \approx 300,000,000\frac{\mathrm{m}}{\mathrm{s}}$) any relative velocity will be substantial compared to c_w and makes a considerable scaling factor which can not be modeled with a constant frequency shift.

Note that, the approach which was used in this example, can be also used in analyzing the Doppler effect on the emitted signal in any mobile scenario.

2.3.2 Time-varying Path Gain

In underwater acoustic channels, each eigenray arrives with a different amplitude. This gain is time-varying, since the phenomena which cause path amplitude variation are the transmission loss and the superposition of the micropaths around each eigenpath. In this section, first the different types of transmission losses and their dependency in time are described. Then, the effect of amplitude fading is defined and analyzed.

2.3.2.1 Review of Transmission Loss

Spreading Loss: Refering to the physics of acoustic waves, the area of the wavefront gets larger while propagating underwater, but the total energy remains the same as it spreads out of the source. This means that the energy per unit length of the wave must get smaller. This reduction in the power density is called spreading loss. Two classes of spreading are defined: *spherical spreading* and *cylindrical spreading*. Spherical spreading is defined for sound propagation in deep water, where it is assumed that the source is located in a homogeneous, unbounded medium [14]. In this case the wave propagates from a small source uniformly in all directions, and the power is distributed over the surface of a sphere surrounding the source. When the medium is bounded from top and bottom, like in shallow water, the spreading is no longer spherical because the wave will hit the sea boundaries. In this case the spreading loss can be approximated by assuming that the power is distributed uniformly over the surface of a cylinder with a radius equal to the range and a height equal to the depth of the sea [14]. To model the spreading loss accurately, a piecewise function is used where spherical spreading is assumed when the transmission range r, is less than half of the depth of the water H, and cylindrical spreading is assumed when r is greater than H [19], i.e.,

$$\mathrm{TL}_{\mathrm{spreading}} = \begin{cases} 20\log r, & \text{if } r < H, \\ 20\log H + 10\log\left(r - H\right), & \text{if } r > H. \end{cases} \tag{2.23}$$

Reflection Loss: According to [20], when there is a reflection at a rough surface (bottom or wall), a part of the incident wave energy is scattered in directions out of the vertical plane of the multipath arrivals. This results in a loss of acoustic energy. This phenomenon is called reflection loss and it depends on physical parameters such as the roughness of the surface/bottom, water density, water pressure, and speed of wind at the surface. It also can be frequency dependent [20]. In this work, to simplify the calculations, constant reflection losses are assumed for the sea surface, Γ_s, sea bottom, Γ_b, and walls Γ_w. With this assumption, the overall reflection loss will only depend on the number of surface, bottom, or wall bounces. For example, the reflection loss of a path arrival with n_b bottom reflections, n_s surface reflection, and n_w reflections from the walls is calculated in linear scale as,

$$\mathrm{TL}_{\mathrm{reflection}} = (\Gamma_s)^{n_s}(\Gamma_b)^{n_b}(\Gamma_w)^{n_w}. \tag{2.24}$$

Absorption Loss: As an acoustic wave travels underwater, it gets absorbed by the molecules within the medium. Usually, the absorbed energy is converted to heat. In other words, the molecules steal some of the acoustic energy from the wave to overcome the viscosity of the medium through which the wave is propagating. In addition to the absorption due to viscosity, some of the chemicals that make the ocean salty also absorb sound and convert it to heat. In summary, the absorption decreases the power of the wave and causes transmission loss. The strength of this loss depends on the transmitted signal frequency. Depending on a certain set of physical parameters such as salinity, pressure and temperature, and the type of the chemicals in the medium, the absorption loss can be different. According to [14], by ignoring the pressure and temperature dependence, the frequency dependent attenuation due to viscosity can be approximated as,

$$\alpha_{\mathrm{a}}(f) \approx \frac{0.1f^2}{1+f^2} + \frac{40f^2}{4100+f^2} + 2.75\times 10^{-4} f^2 + 0.003, \tag{2.25}$$

where α_{a} is the attenuation parameter in $\frac{\mathrm{dB}}{\mathrm{km}}$ and f is the signal frequency in kHz. The absorption loss in the range of r, is calculated in linear scale as,

$$\mathrm{TL}_{\mathrm{absorption}}(f) = 10^{\alpha_a(f)\frac{r}{20}}. \tag{2.26}$$

This equation shows how the absorption loss increases by increasing the range and frequency. As the loss increases the power of the received signal decreases, so in the software model, the absorption loss is implemented by a lowpass filter using the following transfer function,

$$\mathrm{H}_{\mathrm{absorption}}(f) = (\mathrm{TL}_{\mathrm{absorption}}(f))^{-\frac{r}{2}} . \tag{2.27}$$

To apply the absorption loss in the channel simulator, the received eigenpaths pass through the absorption loss filter. An example of the this transfer function is shown in Figure 2.3.

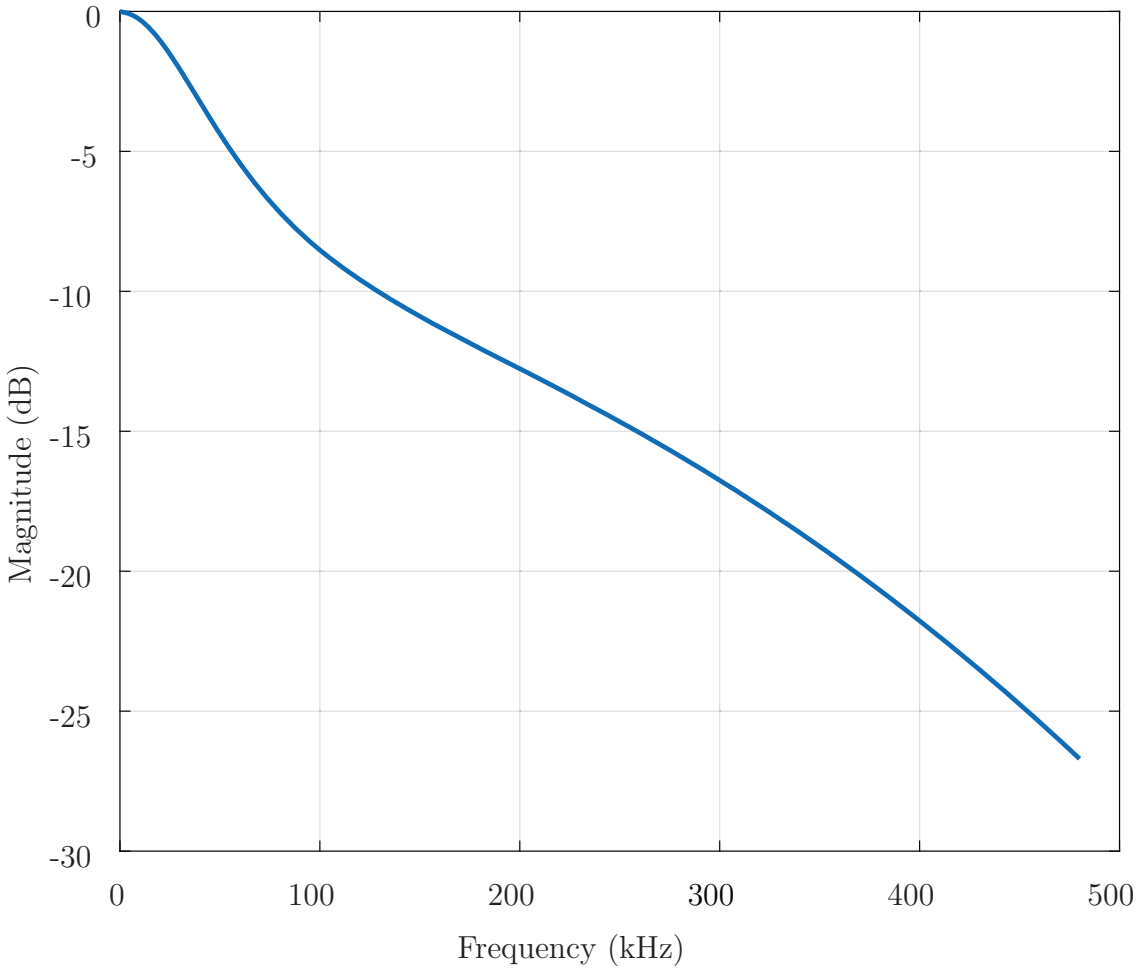

Figure 2.3: The transfer function of the absorption loss filter in the range of $r = 1$km.

To summarize, the transmission loss of each path can vary with different parameters such as distance, frequency, type of chemicals and number of reflections. Among

the aforementioned parameters, the distance is the one which is related to time directly. Therefore, the transmission loss can change with time (distance) when distance changes considerably.

2.3.2.2 Fading in the Time-domain

Fading is the random variation of the path amplitude with respect to time. Fading often is caused by the superposition of multiple copies of the transmitted signal within an eigenpath. As mentioned in Section 2.1 the superposition of the micropath with different Doppler shifts creates amplitude variations. By considering uncorrelated paths, a time-varying path amplitude can be generated as an independent Gaussian random process [9]. To simulate a fading amplitude, a white Gaussian process is generated and passed through the Doppler filter. The transfer function of the Doppler filter is extracted from the measured power Doppler spectrum. The fading amplitude is multiplied by the constant amplitude value which is obtained after the transmission loss calculation.

2.4 Software Channel Implementation

Because of the high variability of the UWA channel, the design of a model which fits into a big variety of undersea geometries, is challenging. In order to test wideband underwater communication systems, the effect of the channel needs to be accurately modeled in software as sea trials are often expensive and deployments can be complicated. Recently, there has been a growing effort to develop a computationally efficient channel model which considers both physical and statistical characteristics.

In this thesis a computationally efficient tool is utilized to develop a geometry based stochastic model by considering the time-varying relative velocity between the transmitter and receiver. Similar to the approach that was used in Section 2.3, the channel implementation is divided to the implementation of the path delay and path amplitude.

2.4.1 Implementation of the Path Delay

As described in Section 2.3.1, the delay of the eigenpath can be calculated from the geometrical parameters. The main challenge in this approach is the time-variance of the delay. This time-varying delay can be modeled with a time-varying time-scaling factor. In software models, the time-scaling is usually implemented by a *resampling* operation. Resampling is equivalent to changing the sampling frequency. Assume a signal $x(t)$ is sampled by a sampling frequency of F_s. If $x(t)$ is scaled by a constant factor, α, then the new sampling frequency is

$$F_{s,new} = \frac{1}{\alpha} F_s. \tag{2.28}$$

The time-scaling of a signal can be implemented by sampling the signal at $F_{s,new}$ and then running the resampled signal at the original sampling rate. For example, when time-scaling factor is bigger than 1, the new sampling frequency will be smaller than the original sampling frequency. If the transmitted signal be resampled with the new sampling frequency and then be recorded at the receiver side with the original sampling frequency, the received signal is observed as a dilated version of the transmitted signal.

As an alternative method, the time-scaling factor can be approximated by a rational number, M/N. Then resampling can be implemented by up-sampling (interpolating) by the rate of M and then down-sampling (decimating) the up-sampled signal by the rate of N. When the time-scaling factor is close to 1, M and N will be big numbers and the resampling process will be computationally expensive, which makes it inappropriate in hardware implementation when the memory is limited.

The *Time-Varying Fractional Delay Line* (TVFDL) is introduced as the third alternative method for resampling [1]. In this method the time-scaling is implemented by sampling the original signal with a time-varying delay. Using this approach, once the time-varying delay was calculated using Equation (2.11), it can be implemented using a dynamic resampling process. This process accounts for the delay using an interpolation filter that is fractionally spaced and resampling is realized by varying the position of the fractional delay with time. The desired delay for a certain eigenpath is converted to a delay in samples with both an integer and fractional part. The

integer part indicates what delays in the delay line need to be used to produce the value for that delay at a time instance, t, while the fractional part is used to calculate the proper weight for each sample. The position of this delay can then be varied at each new time instant in order to implement the desired time-varying resampling.

To describe TVFDL mathematically, assume $x(\alpha t)$ is a continuous-time time-scaled signal originally and $x_s(\alpha n T_s)$ is its sampled representation with a sampling period of T_s. Then, $x(\alpha t)$ can be expressed as

$$x(\alpha t) = x_s(\alpha n T_s) = x_s((1-(1-\alpha))nT_s) = x_s(nT_s - (1-\alpha)nT_s) \tag{2.29}$$

where n is a positive integer between 0 and $N_{max} - 1$. The original signal window size is N_{max}. So, the time-scaled signal can be written as

$$x(\alpha t) = x_s(nT_s - \tau[n]), \tag{2.30}$$

where

$$\tau[n] = (1-\alpha)nT_s. \tag{2.31}$$

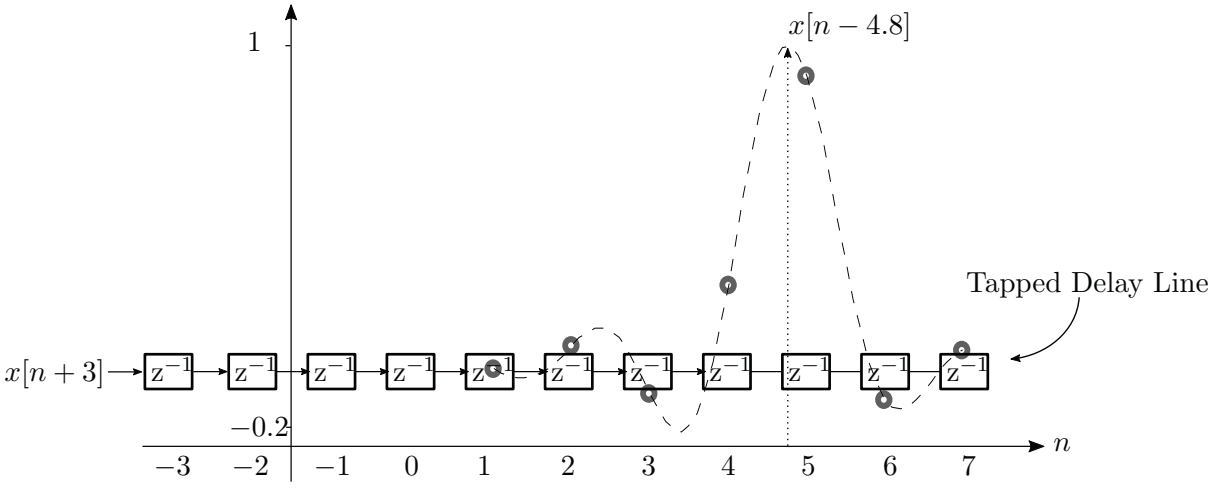

Figure 2.4: Example of the output for the fractional delay for a single instant in time. The dashed line indicates the continuous sinc interpolation filter and the grey circles indicate the discrete, sampled points of the function. (from [1])

The interpolation filter can be implemented by a tapped delay line, and if multiple fractional delays are required the same tapped delay line can be used. A sinc filter

can be used as interpolation filter. So the time delayed signal becomes

$$x_s(nT_s - \tau) = x_s[n - \tau_s] = \sum_{m=-\infty}^{\infty} \text{sinc}[m - \tau_s]x[n - m], \tag{2.32}$$

where τ_s is the normalized delay with respect to the sampling period, T_s. In fact Equation 2.32 shows that using this approach the resampling process is equivalent to convolution of the transmitted signal and the TVFDL which is implemented by a sinc filter. The normalized delay can be broken to the integer part, D_{τ_s}, and the fractional part, d_{τ_s},

$$\tau_s = \frac{\tau}{T_s} = D_{\tau_s} + d_{\tau_s}. \tag{2.33}$$

An example of this process is shown in Figure 2.4. In this example a sinc function with a length equal to 7 was chosen. The integer and fractional part of the delay are $D_{\tau_s} = 4$ and $d_{\tau_s} = 0.8$, and the sinc function samples from 1 to 7. The input signal, $x[n]$, has been previously delayed by 3 samples to maintain causality. This figure shows the output of fractional delay line in a single instant. The next instant is calculated by advancing the delay line by one.

Working with the fractional delay has two main benefits in channel implementation. First, any resampling rate can be implemented with low computational complexity since the time varying delay will simply be different for different resampling rates. Second, this model accounts for dynamically changing velocity between the receiver and transmitter, because it relies on the time-varying delay, $\tau_p(t)$, which can be simply calculated for any dynamic scenarios using the kinematic laws.

In order to verify the functionality of TVFDL, the resampling operation was applied to a reference waveform using the aforementioned resampling methods and the results are compared in Figure 2.5. In this simulation, the scaling factor $\alpha = 1.0167$ which is equivalent to a constant relative velocity of $v_c = +25\ \frac{\text{m}}{\text{s}}$ and compresses the received signal. As demonstrated in Figure 2.5, the TVFDL has a similar result to the other resampling methods.

In order to demonstrate the ability of TVFDL in implementing a wide variety of mobile deployment scenarios, a deterministic channel model with four eigenpaths was

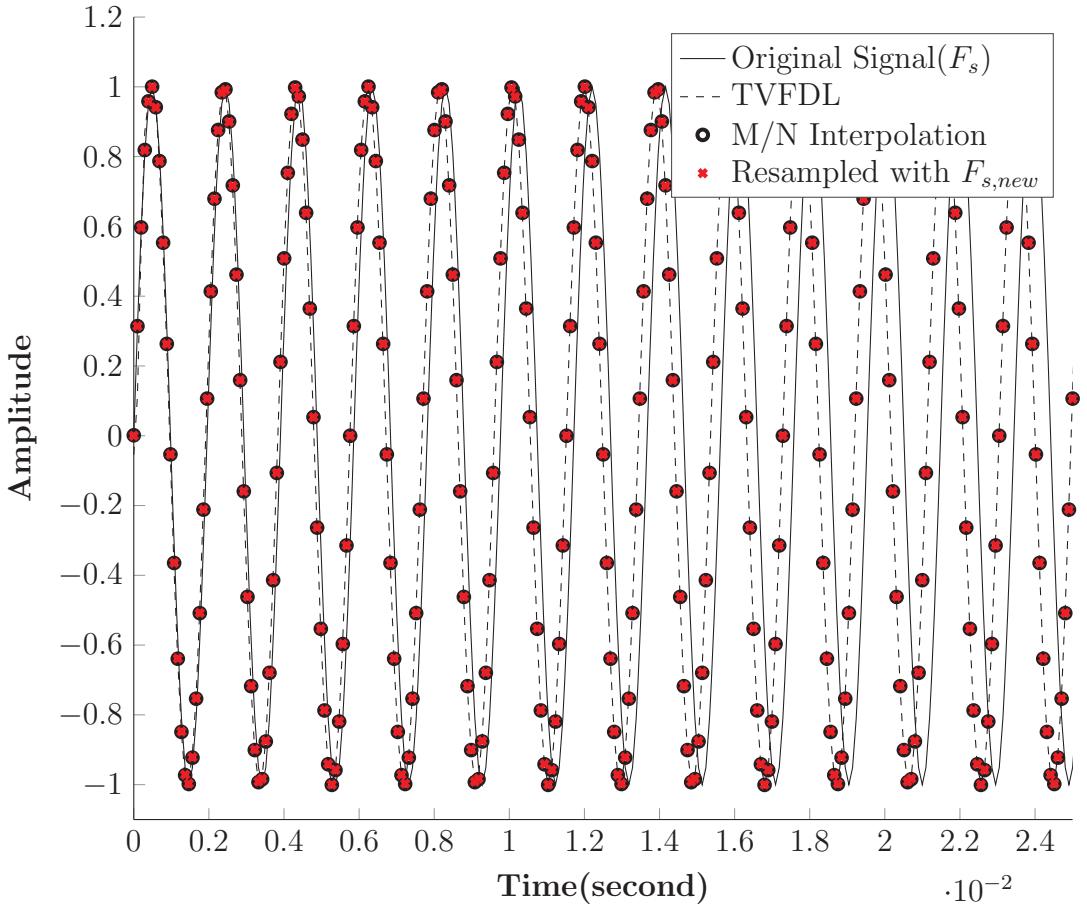

Figure 2.5: A comparison between different resampling methods that have been applied on a sine wave with sampling frequency $F_s = 10240\,\text{Hz}$ and carrier frequency $F_c = 512\,\text{Hz}$.

implemented as an example. In this simulation each eigenpath has a completely different time-varying delay function which listed below:

- The first path is time-invariant with the initial delay of $\tau_{0,1} = 25\,\text{ms}$.
- The second path models a scenario for which the relative velocity between the transmitter and receiver is $-2\frac{\text{m}}{\text{s}}$. In this simulation the time-scaling is constant, $\alpha = 0.9987$, and the initial delay is 31 ms.
- The third path shows a sinusoidal time-varying delay with a magnitude that is increasing linearly. This time-varying delay is described mathematically by

$$\tau_3(t) = \tau_{0,3} - c_l t \sin(2\pi f_l t), \tag{2.34}$$

where $c_l = 0.5$, $\tau_{0,3} = 78\,\text{ms}$ and $f_l = 7\,\text{Hz}$.

- The fourth path is a scenario where the underwater vehicles have a constant relative acceleration, $\bar{a}_l = 0.5\ \frac{\text{m}}{\text{s}^2}$, and an initial velocity of $v_{l,0} = 0.5\ \frac{\text{m}}{\text{s}}$. The initial delay is $\tau_{0,4} = 100\,\text{ms}$. In this case the distance equation of the path is

$$d_l(t) = d_{0,l} + v_{0,l}t + \frac{\bar{a}_l}{2}t^2, \tag{2.35}$$

where the $d_{0,l}$ is the initial path length. The time-varying delay then can be obtained as,

$$\tau_l(t) = \frac{d_{0,l}}{c_w} + \frac{v_{0,l}t}{c_w} + \frac{\bar{a}_l t^2}{2c_w} = \tau_{0,l} - (1 - \alpha_l(t))t \tag{2.36}$$

where

$$\tau_{0,l} = \frac{d_{0,l}}{c_w}, \tag{2.37}$$

and

$$\alpha_l(t) = 1 + \frac{1}{c_w}(v_{0,l} + \frac{\bar{a}_l}{2}t). \tag{2.38}$$

Note that the amplitude of these eigenpath is constant. To verify the functionality of this model, a channel sounder was simulated. The details of the channel sounder design can be found in Appendix A.

The channel impulse response is shown in a time-delay plot in Figure 2.6. Although, the examples demonstrate the capability of TVFDL in implementation of deterministic channel model in different highly dynamic deployments, the same tool can be utilized in stochastic models.

Referring to Section 2.3.1, in modeling the real world environment, the time-varying delays can be calculated from Equation (2.12), (2.14), (2.15), and (2.16). The channel model utilizes the TVFDL to implement these delays. The results of the channel simulation using this approach are shown in Section 2.4.3.

2.4.2 Implementation of the Path Gain

The approach that was explained in Section 2.3.2 is used to implement the path gain. In this model, for normalization purpose it is assumed that the input power of the

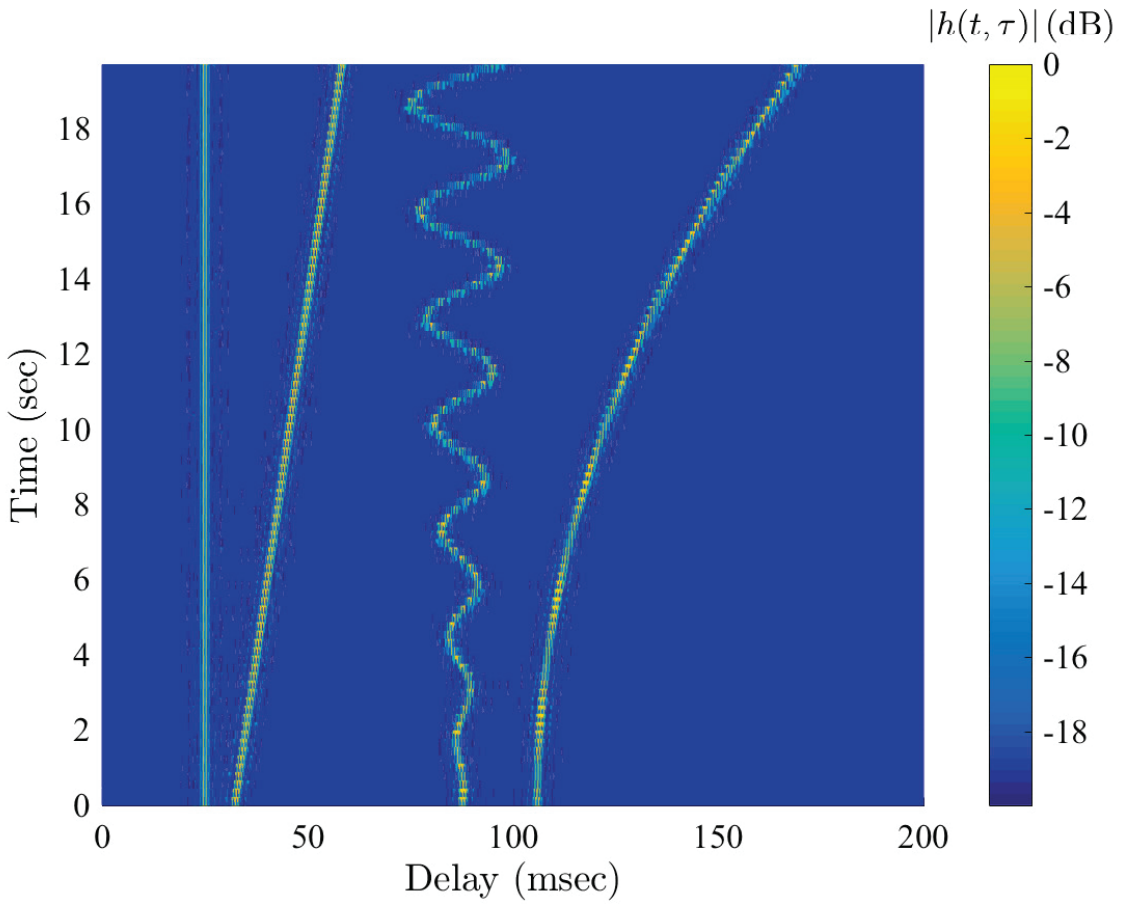

Figure 2.6: Examples of implementation of time-varying delay using TVFDL.

channel function is equal to 1Watt. After calculating the spreading and reflection loss using Equation (2.23) and Equation (2.23) respectively, the attenuated amplitude of the eigenpaths are calculated at each sample time. The implementation of the absorption loss is more complicated than the other kind of losses because it requires the implementation of multiple filters for different distances. To simplify the implementation of the absorption loss filter, it is only implemented for the maximum range of each path. It is due to slow variation of the absorption loss with respect to distance (and time). In this channel model, using the transfer function in Equation 2.27, the absorption loss filter is implemented by Kaiser window FIR filter design method, since it is an accurate model.

After applying the transmission losses on the multiple copies of the transmitted signal, the fading amplitudes should be generated using the approach which was described

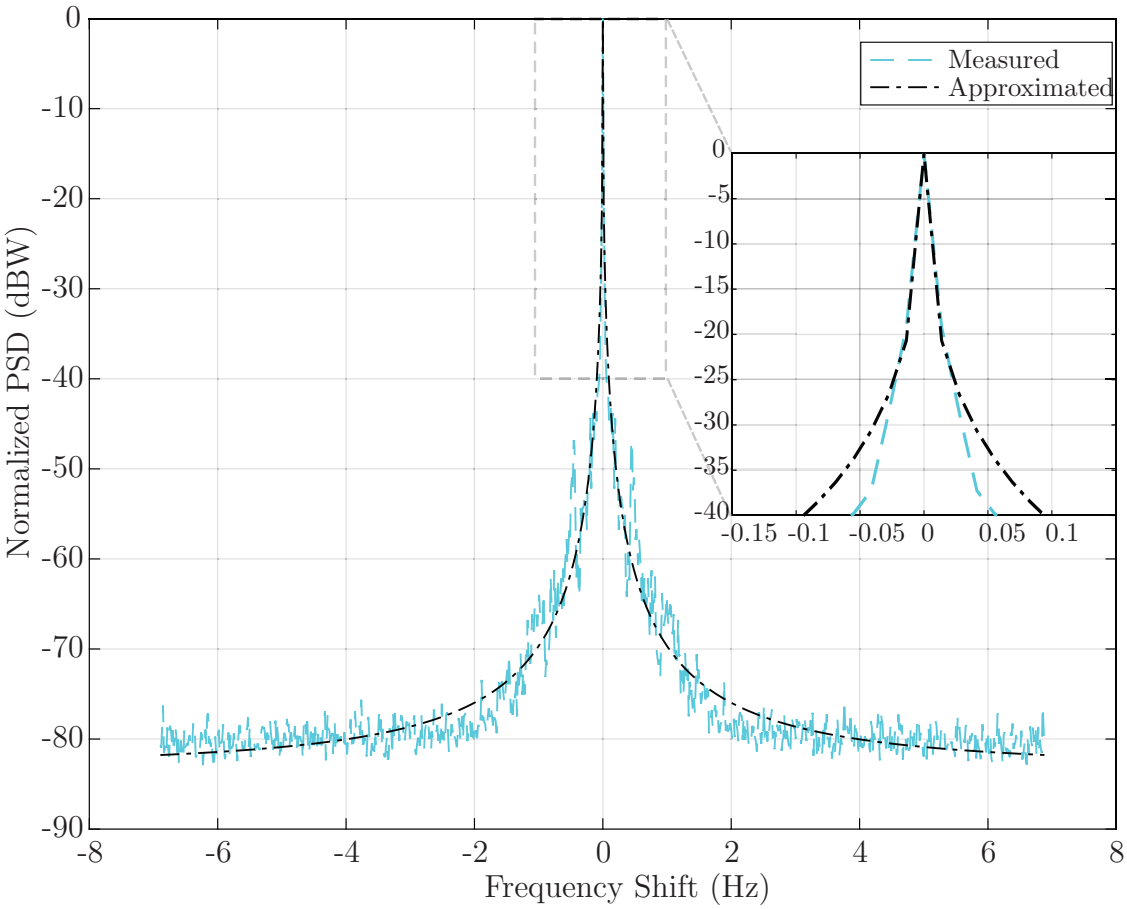

Figure 2.7: Example of Doppler power spectrum estimation. The estimated shape parameters are $c_1 = 0.2477$, $c_2 = 0.4326$, and the noise floor is $N_F = -83$ dB.

in Section 2.3.2. In this approach a white Gaussian noise sequence with power of 1 Watt is generated for each eigenpath. These noises pass through the Doppler filter and then are multiplied with attenuated amplitudes of the respective eigenpaths. In an accurate model, the Doppler filters have to be different for each eigenpath because each eigenpath has a different Doppler spectrum. However, the results of the channel measurements in different locations, show that the difference between the spectrum are not considerable for normalized power larger than -40 dB. Therefore, the average Doppler spectrum (Equation (2.10)) of the measured channels is calculated and utilized in this model.

In UWA channels, the measured Doppler spectrum usually has an exponential-like shape with a high degree of fluctuation (See Figure 2.7) on magnitude. The implementation of the Doppler spectrum as an FIR filter with these fluctuation needs a

huge number of taps. To simplify the design of the Doppler filter, instead of implementing the measured power Doppler spectrum an accurate approximation of it will be implemented. According to [21], results of channel sounding in different locations and different time periods show that the Doppler spectrum can be well described by an exponential function as,

$$\tilde{P}_\nu(\nu) \approx A\mathrm{e}^{(\frac{\nu}{c_1})^{c_2}} + N_F, \tag{2.39}$$

where A is a scaling factor, N_F is the noise floor and, c_1 and c_2 are the shape parameters of the exponential Doppler spectrum. The shape parameters are estimated with curve fitting methods. The transfer function of the Doppler filter is extracted from the approximation of the Doppler spectrum as,

$$H_{Doppler}(f) = \sqrt{\tilde{P}_\nu(f)}, \tag{2.40}$$

where f is the frequency parameter. In most of the practical scenarios the bandwidth of the Doppler filter is less than 10Hz, while the sampling frequency is in the order of a few hundred kilo Hertz. This makes the Doppler filter very narrowband. This narrowband filter is implemented with a multistage multirate approach [22].

Figure 2.7 shows the Doppler spectrum of a measured channel and its approximation. The detailed results of the measurements are discussed and the measured channel impulse response will be shown in the Section 2.4.3.

2.4.3 Channel Simulation Results

To validate the channel model against the real environment conditions, channel sounding was performed in shallow water environment in Shad Bay, Nova Scotia. The data was recorded at ultrasonic frequencies. All the parameters of the simulated channel (See Table 2.1) in this section are representative of the geometrical conditions in which the transmitter and receiver were deployed. In addition, the measured channel impulse responses were used to extract the Doppler spectrum, in order to model the fading amplitude.

To separate the random time-variance of the channel from the time-variance due to relative speed which creates time-scaling, the received sounding packet should be

Sampling Frequency (F_s)	960 kHz
Carrier Frequency (f_c)	170 kHz
Total Depth (H)	28 m
Depth of transmitter (h_{tx})	26.5 m
Depth of receiver (h_{rx})	1 m
Initial distance (d_0)	43 m
Distance between the walls (d_w)	500 m
Distance from the reference wall to the transmitter (d_{wt})	200 m
Distance from the reference wall to receiver (d_{wt})	220 m
Initial velocity (v_0)	$-0.3\ \frac{\mathrm{m}}{\mathrm{s}}$
Average acceleration (a)	$-0.005\ \frac{\mathrm{m}}{\mathrm{s}^2}$
Surface reflection loss (Γ_s)	6 dB
Bottom reflection loss (Γ_b)	12 dB
Wall reflection loss (Γ_w)	12 dB
Noise floor of the Doppler spectra (N_F)	-83 dB
Shape factors of the Doppler spectra	$c_1 = 0.2477$, $c_2 = 0.4326$
Signal to noise ratio	9.5 dB

Table 2.1: Parameter of the channel simulation.

resampled. This resampling should be done before the calculation of the spreading function.

To verify that the time-varying model can accurately recreate the effects of an underwater deployment, the channel model presented in this chapter is compared to a measured time-varying channel. In this test the transmitter was anchored at the bottom of the sea and the receiver was 1 m under the surface attached to the boat, while the boat was drifting due to surface waves. A chirp signal with a bandwidth of 7 kHz and central frequency of 170 kHz was used as the channel sounder signature. The procedure of the channel sounder design is explained in Appendix A. Also, the procedure of the sea trial will be explained in detail in Section 5.4.1.

The same channel sounder was used in simulations. The input parameters to the channel simulator are the geometrical specifications of the deployment and parameters used to approximate the Doppler spectrum of the deployment.

Figure 2.8 shows a comparison between the simulated and measured channel. This figure shows a high degree of resemblance using the CIR measurements as well as the delay-Doppler spreading functions.

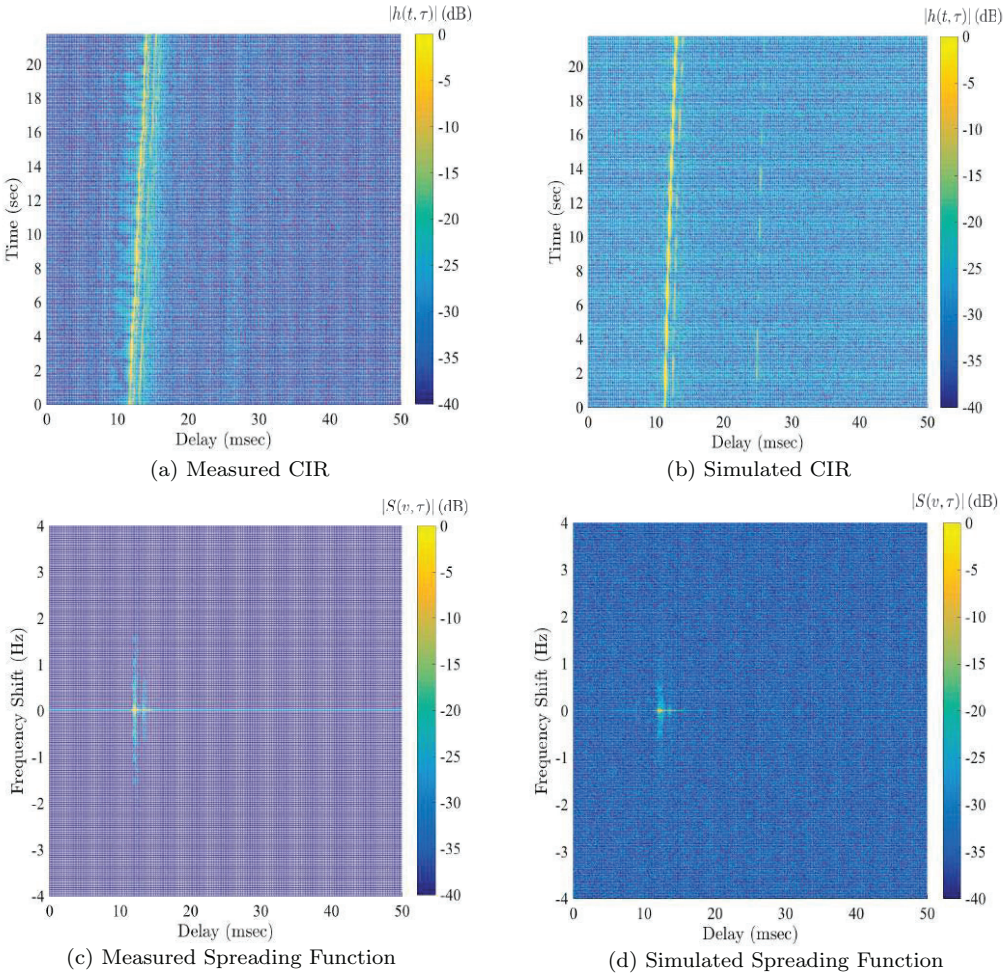

(a) Measured CIR

(b) Simulated CIR

(c) Measured Spreading Function

(d) Simulated Spreading Function

Figure 2.8: A comparison of the measured and simulated channels.

In the next Chapter the OFDM modulation scheme is introduced and the effect of the UWA channel on the OFDM signal is studied.

Chapter 3

The Effect of the UWA Channel on OFDM

Measurements show that the UWA channel is subject to multipath in which each path experiences a different time-scaling factor [23]. This phenomenon is called *multi-scale multipath* propagation [24]. In this chapter, the effect of multi-scale multipath on the communication performance is analyzed.

In the multipath scenario the received communication signal needs to be equalized to mitigate the effects of the channel. Assume a time-invariant multipath channel with an impulse response of

$$h(\tau) = \sum_{p=1}^{N_p} h_p \delta(\tau - \tau_p). \tag{3.1}$$

When the coherence bandwidth, B_c, of the channel is bigger than the bandwidth of the signal, B_{sys}, the frequency response of the channel is constant over the frequency band of the transmitted signal [25]. This channel usually is described as showing frequency-flat fading properties and of a single path arrival. The equalization of this channel can be done simply using complex multiplication between the estimated channel path and received signal.

When the data rate increases or the delay spread of the channel increases, the flat fading condition is not preserved and the channel must be treated as a channel with multiple path arrivals. In this case the received signal is represented as the delayed sum of multiple copies of the transmitted signal [25]. It means that a part or all of a given symbol will be spread into adjacent symbols, thereby distorting the received signal. This effect is called *inter-symbol interference (ISI)*. In addition, this effect causes a variation in the channel frequency response, which is called *frequency selectivity*. In a frequency selective channel the equalizer filter needs to have more taps in order to have an accurate estimate of the channel [26]. This can be quite computationally

expensive in a rich multipath environment with a large delay spread.

In Section 3.1 the OFDM modulation is introduced as a method which provides less complex channel equalization method in comparison to a single carrier modulation technique. Section 3.2 highlights the need to estimate the optimum time-scaling factor in the multi-scale multipath channel.

3.1 Orthogonal Frequency Division Multiplexing (OFDM)

One method that can be used to overcome the problem of equalization complexity is to divide the data stream into N different sub-streams and to send them over many different sub-channels. The data rate of each sub-stream is less than the total data rate, and corresponding sub-channel bandwidth, $B_N = B_{sys}/N$, is smaller than the system total bandwidth, B_{sys} [26]. Therefore, when the coherence bandwidth for the channel is larger than the system bandwidth, $B_c \geq B_{sys}$, N is set sufficiently large to obtain a sub-channel bandwidth which is much smaller than the coherence bandwidth, $B_N << B_{sys}$, to insure flat-fading on each sub-channel. Thus, each sub-channel can be equalized using a single complex multiplication. In this method, the nth sub-stream is linearly modulated (using BPSK or QPSK) with the sub-carrier frequency f_n and then transmitted in parallel with other sub-channels.

Orthogonal Frequency Multiplexing Division (OFDM) is a multi-carrier transmission scheme that has received increased interest for communications due to its low complexity channel estimation and equalization. The key feature that defines OFDM is that the sub-channels are separated by the minimum frequency separation while maintaining orthogonality. The orthogonality allows simultaneous transmissions on adjacent sub-channels to not interfere with each other.

According to [26], the discrete implementation of OFDM is called *discrete multitone modulation (DMT)*. The structure of a simple DMT system is shown in Figure 3.1. In this example, the bit stream is modulated using a BPSK modulator. Then, the digital symbol stream is converted to a parallel stream of symbols which are transmitted over each of the N orthogonal sub-carriers. The parallel BPSK symbols can

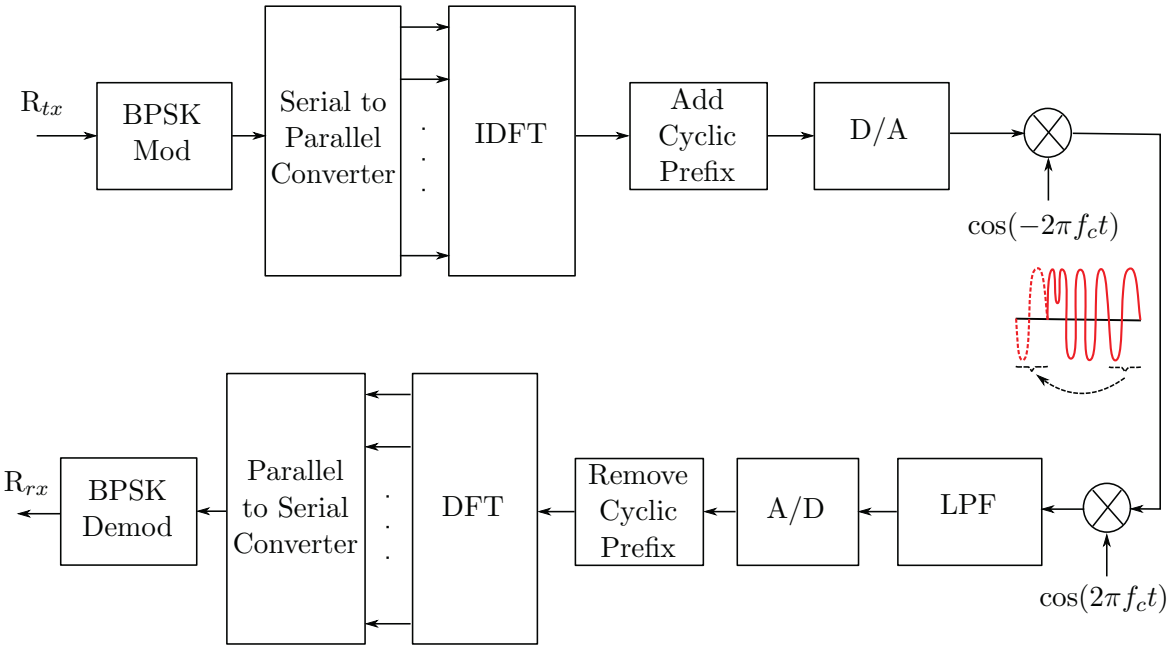

Figure 3.1: Discrete implementation of OFDM. The concept of cyclic prefixing is shown in red.

be considered as the discrete frequency components of the OFDM output signal [26]. At baseband, to convert these frequency components into the time-domain an inverse discrete Fourier transform (IDFT) is performed. Assuming N subcarriers, and defining the transmit information x_n at subcarrier n, the IDFT operation is defined as

$$X_k \overset{\text{def}}{=} \sum_{k=-\frac{N}{2}}^{\frac{N}{2}-1} x_n \cdot \mathrm{e}^{-j2\pi kn/N}, \quad k = 0, \cdots, N-1. \tag{3.2}$$

The subcarrier frequencies are given by $f_k = k/T$ where T is the duration of the OFDM symbol. It is possible to demonstrate orthogonality between subcarriers [26], i.e. $X_k \cdot X_j = 0$ for $k \neq j$. As such the transmitter can be implemented efficiently using the inverse fast Fourier transform (iFFT). Similarly, the receiver utilizes the discrete Fourier transform (DFT) to convert the received block from time domain to the frequency domain. The DFT block is implemented by a fast Fourier transform (FFT).

As described in [27], the time-varying channel with delay-spread causes two main problems for OFDM: inter-symbol interference (ISI) and inter-carrier interference (ICI). These phenomena are described in Section 3.1.1 and Section 3.1.2, respectively.

3.1.1 Analysis of ISI in OFDM System

Similar to single carrier modulations, when one symbol interferes with the adjacent symbols, ISI occurs. In the other words, ISI in OFDM causes the OFDM symbols, in time domain, to interfere with each other.

To avoid the ISI a guard interval is added between the OFDM symbols. The combination of an OFDM symbol and a guard interval is called an OFDM block. The most commonly used guard interval insertion method is the cyclic prefix (CP). In this method each OFDM symbol is pre-pended with a repetition of its tail (See Figure 3.1). This guard interval insertion approach has two purposes. First, it eliminates the ISI between the OFDM symbols. Second, it allows the linear convolution of the multipath channel to be modeled as a circular convolution. The benefit of working with circular convolution is described here.

The circular convolution of two finite-length sequences, $x_1[n]$ and $x_2[n]$ is described by

$$(x_{2_N} * x_1)[n] \stackrel{\text{def}}{=} \sum_{m=0}^{N-1} x_1[m]x_2[((n-m))_N], \quad 0 \leq n \leq N-1, \tag{3.3}$$

where $((.))_N$ defines a circular shift of N samples. According to [22], using linear convolution one sequence is multiplied by the time-reversed and linearly shifted version of the other sequence. In other words, to obtain the linear convolution of two sequences, they are successively shifted relative to each other along a linear axes. In comparison, in circular convolution the second sequence is circularly shifted with respect to the first.

It can be proven that similar to the continuous-time domain where the linear convolution is equivalent to multiplication in the frequency domain, multiplication in the DFT domain corresponds to circular convolution [22]. So, by choosing the length of the cyclic prefix, L_{cp}, greater than the expected channel length, the effect of the channel response on the OFDM block can be modeled mathematically using a circular convolution. Thus, after discarding the cyclic prefix at the receiver, the process of the convolution with the channel shows up as multiplication of the discrete Fourier domain sub-carriers and the signal can be simply equalized by a vector multiplication

in the discrete Fourier domain as

$$(x_N * h)[n] \xleftrightarrow{\mathcal{DFT}} H[k]X[k]. \tag{3.4}$$

One of the disadvantages of the cyclic prefix guard interval is that it requires sending more power per symbol. There is an alternative guard interval technique called zeros padding (ZP). Using zero-padding, in discrete-time domain, the OFDM symbol is padded with L_{zp} zeros. At the receiver the last L_{zp} samples are added to the first L_{zp} samples of the received OFDM symbol. This demodulation method is called *overlap and add (OLA)* which also converts the linear convolution of the OFDM block and the channel to a circular convolution and the equalization can be obtained by a simple multiplication in the DFT domain [22, 28].

The overlap and add operation is represented as,

$$y[n] = \begin{cases} y_{zp}[n] + y_{zp}[n + N + L_{zp}], & \text{if } 0 < n < L_{zp} - 1, \\ y_{zp}[n], & \text{if } L_{zp} < n < N + L_{zp} - 1. \end{cases} \tag{3.5}$$

where y_{zp} is the received zero-padded OFDM block. The purpose of zero-padding is to get the linear convolution to look like the circular convolution. It has been shown in [22] that, circular convolution is equivalent to linear convolution with time aliasing. Equation (3.5) can be expressed as a linear convolution which has been broken into two separate summations,

$$y[n] = \begin{cases} \sum_0^{L_h} h[m] \left(x_{zp}[n - m] + x_{zp}[n + N + L_{zp} - m] \right), & \text{if } 0 < n < L_{zp} - 1, \\ \sum_0^{L_h} h[m] x_{zp}[n - m], & \text{if } L_{zp} < n < N + L_{zp} - 1, \end{cases} \tag{3.6}$$

where x_{zp} is the transmitted OFDM block and L_h is the length of the channel. The first summation which shows the time aliasing can be viewed as the process of forming a circular convolution. Using this method, a full reception of the OFDM block plus the effect of the multipath channel has been observed and the equalization in the discrete Fourier domain can be done by a vector multiplication. The main disadvantage of the zero-padded OFDM is that because of integration of the received signal over a longer period than the OFDM symbol, the output of OLA operation will have a higher noise floor in comparison an OFDM system which utilizes cyclic prefix in the same setting. [28].

3.1.2 Analysis of ICI in OFDM System

One of the undesirable effects of the channel is time-variance, which can create a loss of orthogonality between the sub-carriers. This phenomenon usually happens due to frequency shift. In other words, the frequency of sub-carriers is shifted and the proportions between some of the sub-carrier frequencies are not integer numbers. In this case, the energy of a sub-carrier spills over to adjacent sub-carriers which is called *inter-carrier interference (ICI)*. Two main sources of the frequency offset are the relative motions between the transmitter and receiver, and the hardware timing impairments.

In the real world, the speed of the underwater vehicle will be time dependent. In other words, the speed is always changing with time with an acceleration rate which is time-variant as well. So, in most practical scenarios the average speed and acceleration is considered. Using these assumptions, the time-varying channel impulse response can be modeled by rewriting Equation (2.1) using Equation (2.38) as

$$h(t,\tau) = \sum_{l=0}^{P} h_p \delta\left(\tau - \tau_{p,0} + \frac{1}{c_w}\left(v_{p,0} + \frac{\hat{a}_p}{2}t\right)t\right) \tag{3.7}$$

where h_p, $\tau_{p,0}$, $v_{p,0}$ and $\hat{a}_p$ are the channel gain, the initial path delay, the initial velocity and the average acceleration of the pth path. The time-varying channel frequency response is obtained by taking the Fourier transform of Equation (3.7) with respect to τ as

$$H(t,f) = \sum_{l} h_l \mathrm{e}^{-j2\pi f \tau_{l,0}} \mathrm{e}^{j2\pi f(1-\alpha_l(t))t}. \tag{3.8}$$

where the $\alpha_l(t) = 1 - \frac{1}{c_w}\left(v_{l,0} + \frac{\hat{a}_l}{2}t\right)$, is the respective time-varying time-scaling factor.

The main purpose of this Section is to analyze the effect of the time-scaling on OFDM signals. For this purpose, it is assumed that the average acceleration rate is small enough, so the time-scaling factor approximately remains constant during one OFDM block. So, in order to estimate the time-varying time-scaling factor, it is assumed each OFDM block experiences a constant time-scaling factor ($\alpha_{b,l} = cte$), however this factor may change from one block to the other. This way an optimum time-scaling factor can be estimated for each OFDM block.

Thus, the time-varying channel frequency response in the time frame of the mth OFDM block is rewritten as

$$H_m(t,f) = \sum_{l=0}^{P} h_l \mathrm{e}^{-j2\pi f \tau_{l,0}} \mathrm{e}^{j2\pi f(1-\alpha_{l,m})t}, \quad t_m < t < t_m + T_b, \tag{3.9}$$

where t_m is the start of the mth OFDM block [24]. Also, in this mobile environment, the Mach factor, for path l, $\mu_{l,m}$, and discrete time index m, represents the equivalent constant speed, $v_{l,m}$, of each block divided by the velocity of sound underwater, c_w, and is equal to

$$\mu_{l,m} = \alpha_{l,m} - 1 = \frac{v_{l,m}}{c_w}. \tag{3.10}$$

To analyze the effect of a constant time-scaling on an OFDM symbol, the transmitted OFDM symbol is rewritten as a sum of a number of orthogonal complex sinusoidal functions as

$$s_m(t) = \sum_{k=0}^{N-1} s_k \mathrm{e}^{j2\pi f_k t} u(t) \tag{3.11}$$

where s_k is the kth data symbol and $u(t)$ is a rectangular pulse shaping function, expressed as

$$u(t) = \begin{cases} \sqrt{\frac{1}{T}}, & \text{if } t \in [0\, T] \\ 0, & \text{elsewhere.} \end{cases} \tag{3.12}$$

The kth sub-carrier frequency is $f_k = f_c + k\Delta f$, where Δf is the frequency separation between the sub-carriers and $k = -\frac{N}{2}, \cdots, \frac{N}{2} - 1$. The received symbol can be expressed as [24]

$$\begin{aligned} r_m(t) &= \sum_{l=0}^{P} h_l s((\mu_{l,m}+1)t - \tau_{l,0}) + n(t) \\ &= \sum_{l=0}^{P} h_l \sum_{k=0}^{N-1} s_k \mathrm{e}^{j2\pi f_k((\mu_{l,m}+1)t - \tau_{l,0})} u_l(t) + n(t) \\ &= \sum_{l=0}^{P} \sum_{k=0}^{N-1} h_l s_k \mathrm{e}^{j2\pi f_k t} \mathrm{e}^{-j2\pi f_k \tau_{l,0}} \mathrm{e}^{j2\pi(f_k \mu_{l,m})t} u_l(t) + n(t). \end{aligned} \tag{3.13}$$

As it was stated in Chapter 2, the kth sub-carrier of the mth OFDM symbol experiences a phase shift of $\mathrm{e}^{-j2\pi f_k \tau_{l,0}}$ and a frequency shift of $\mathrm{e}^{j2\pi(f_k \alpha_{l,m})t}$ at the lth path

arrival. At the receiver, the baseband signal is obtained by down-converting $r_m(t)$ and then sampling at T/N seconds [24], which is described by

$$\begin{aligned} \mathrm{r_m}[n] &= r_m(t)\mathrm{e}^{j2\pi f_c t}|_{t=nT/N} \\ &= \sum_{l=0}^{P}\sum_{k=0}^{N-1} h_l s_k \mathrm{e}^{-j2\pi f_k \tau_{l,0}} \mathrm{e}^{j2\pi k(1+\mu_{l,m})\frac{n}{N}} \mathrm{e}^{-j2\pi f_c \mu_{l,m} n \frac{T}{N}} + \mathrm{n}[n], \end{aligned} \tag{3.14}$$

where $n = 0, 1, \cdots, N-1$. The discrete-time received signal is then sampled at the data rate and represented in a vector form as [24],

$$\begin{aligned} \mathbf{r}_m &= [\mathbf{r}(0), \mathbf{r}(1), \cdots, \mathbf{r}(N-1)], \\ \mathbf{r}_m &= \sum_l h_l \mathbf{D}_l \mathbf{A}_l \mathbf{\Gamma} \mathbf{B}_l \mathbf{s} + \mathbf{n}, \end{aligned} \tag{3.15}$$

where, $\mathbf{D}_l$ and $\mathbf{B}_l$ are diagonal matrices which model frequency offset and phase shift in the lth path, respectively. A_l is a Vandermonde matrix that models frequency distortion due to time-scaling and $\mathbf{\Gamma}$ is a selection matrix which selects the active sub-carriers (N_a). These matrices are represented as,

$$\mathbf{D}_{l,m}[n] = \mathrm{e}^{-j2\pi f_c \mu_{l,m}(nT/N)}, \qquad n = 0, 1, \cdots, N-1, \tag{3.16}$$

$$\mathbf{B}_{l,m}[k] = \mathrm{e}^{-j2\pi f_k \tau_{l,0}}, \qquad m \in N_a, \tag{3.17}$$

$$[\mathbf{A}_{l,m}]_{nk} = \mathrm{e}^{j2\pi nk(1+\mu_{l,m})/N}, \qquad n, k = 0, 1, \cdots, N-1, \tag{3.18}$$

$$\Gamma_{n,k} = \begin{cases} 1, & \text{if } n = k \text{ and } k \in N_a, \\ 0, & \text{otherwise} \end{cases} \qquad n, k = 0, 1, \cdots, N-1. \tag{3.19}$$

As it was shown in Equation (3.9), each path has a different time-scaling factor. In the underwater acoustic receiver design, it is generally assumed that all paths have equal time-scaling factor, however, measurements show that in a real environment each path will experience a different time-scaling factor [23].

3.2 Optimal Time-Scaling Factor

In this Section, the necessity of estimating an optimal time-scaling factor in a multi-path environment is discussed. The methodology discussed in this work also accounts for the fact that the different path arrivals are subject to different time-scaling factors.

As described in Chapter 2, the acoustic propagation path delays can vary rapidly due to low speed of propagation of sound underwater. Some observations [23] show that, in an UWA channel, each path will arrive with a different velocity. Therefore, the velocity of each eigneray, v_p, at the receiver is observed as [29]

$$v_p = \overline{V}\cos(\theta_p) \tag{3.20}$$

where $\overline{V}$ is the average relative velocity between the transmitter and receiver tangential to the propagation vector and θ_p is the angle of the arrival of the pth path. Every change in the velocity of the received ray causes a change in the time-scaling factor. In [24], the authors studied the effect of resampling using a single time-scaling factor on the performance of the receiver in a multi-scale multipath channel. They showed that, when the spread of the time-scaling factor, called scaling spread, is large, resampling with respect to a single scaling factor can cause degradation of reliability, because of the residual Doppler shift after resampling. However, it was shown through measurements [23] that in most practical cases, the scaling spread is small and degradation of reliability after resampling can be neglected.

To design a receiver with an optimum single resampling factor, the channel statistics must be considered. Based on Equation 2.1, an approximation of the channel, $\hat{h}_k(t)$, on the kth subcarrier, with constant path amplitude, h_l, is defined by,

$$\hat{h}_k(t) = \sqrt{\frac{1}{T}} \sum_{l=0}^{L} h_l \mathrm{e}^{-j2\pi f_k \tau_l} \mathrm{e}^{j2\pi f_k bt} \tag{3.21}$$

where b is the resampling rate which is common for all paths [24]. The problem of finding the optimum resampling factor, b, is explained as the problem of minimizing the error of the channel approximation. In other words, the resampling factor, which minimizes the approximation error is the optimum time-scaling factor. The channel approximation is obtained from the received signal and its algorithm will be explained in Chapter 4. In order to extract the optimum scaling factor, the mean squared error (MSE) between the actual and the approximated channels on the kth sub-carrier, $\mathrm{MSE}_k(b)$, is defined as

$$\mathrm{MSE}_k(b) = \int_0^{t/(1+b)} \left| h_k(t) - \hat{h}_k(t) \right|^2 dt. \tag{3.22}$$

The integration interval, $[0, T/(1+b)]$, has been chosen as the scaled version of all the OFDM sub-carriers to complete an integer number of sub-carrier period in the interval [24]. Note that to explain the effect of resampling the received signal using optimum resampling factor, it is assumed that the channel parameters are known.

The aggregate mean squared error (AMSE) of the estimated sub-channels of an OFDM symbol represents the summation of the MSE over all discrete path arrivals and all sub-carriers. It is defined as $\text{AMSE}(b) = \sum_{l=0}^{L} \text{MSE}_m(b)$ [24] and is equal to

$$\text{AMSE}(b) = \sum_{k=0}^{N-1} \sum_{m,l}^{L} h_k h_l^* \mathrm{e}^{-j2\pi f_k(\tau_m - \tau_l)} \times \int_0^{T/(1+b)} \left(\mathrm{e}^{j2\pi f_k a_m t} - \mathrm{e}^{j2\pi f_k bt}\right) \times \left(\mathrm{e}^{j2\pi f_k a_l t} - \mathrm{e}^{j2\pi f_k bt}\right) dt \quad (3.23)$$

The optimum time-scaling factor then minimizes the AMSE between the actual and the approximated channels, and is expressed as

$$b_{opt} = \arg\min_b \text{AMSE}(b). \quad (3.24)$$

In [24], the authors considered two special cases for which they derived a statistical model to obtain the optimum time-scaling factor. The statistical examination, which obtains optimum time-scaling factor, is beyond the scope of this work. However, the results using the procedure are presented and, simulations are derived to confirm the results.

According to [24], the scaling spread of the channel, D_s, is defined as the maximum distance between the time-scaling factors of a multi-scale multipath channel,

$$D_s = \max_{i \neq j} |a_i - a_j| . \quad (3.25)$$

It can be shown that, when the time-scaling factors are too close to each other, i.e. when $D_s < 10^{-3}$, the optimum resampling factor is a weighted average of the time-scaling factors all paths [24]. Also, it can be proven that, the optimal time-scaling factor is equal to the time-scaling factor of the path which has the largest magnitude

when the scaling spread is large, $D_s > 10^{-3}$ [24]. This approximation works even under circumstances in which path amplitudes are only slightly different.

Simulations were conducted to confirm the results of the optimal time-scaling approximation. The channel model described by Equation (3.9) is used with three taps and different time-scaling factors which are constant in time. It is assumed the channel impulse response is known. Using this assumption, the MSE between the actual and the approximated channel is calculated as a function of the time-scaling factor for one sub-carrier, which is equivalent to a single tone. The optimal time-scaling factor must minimize this MSE. The AMSE of the OFDM symbol, which is a linear weighted average of the sub-channels will result in the same optimum time-scaling factor.

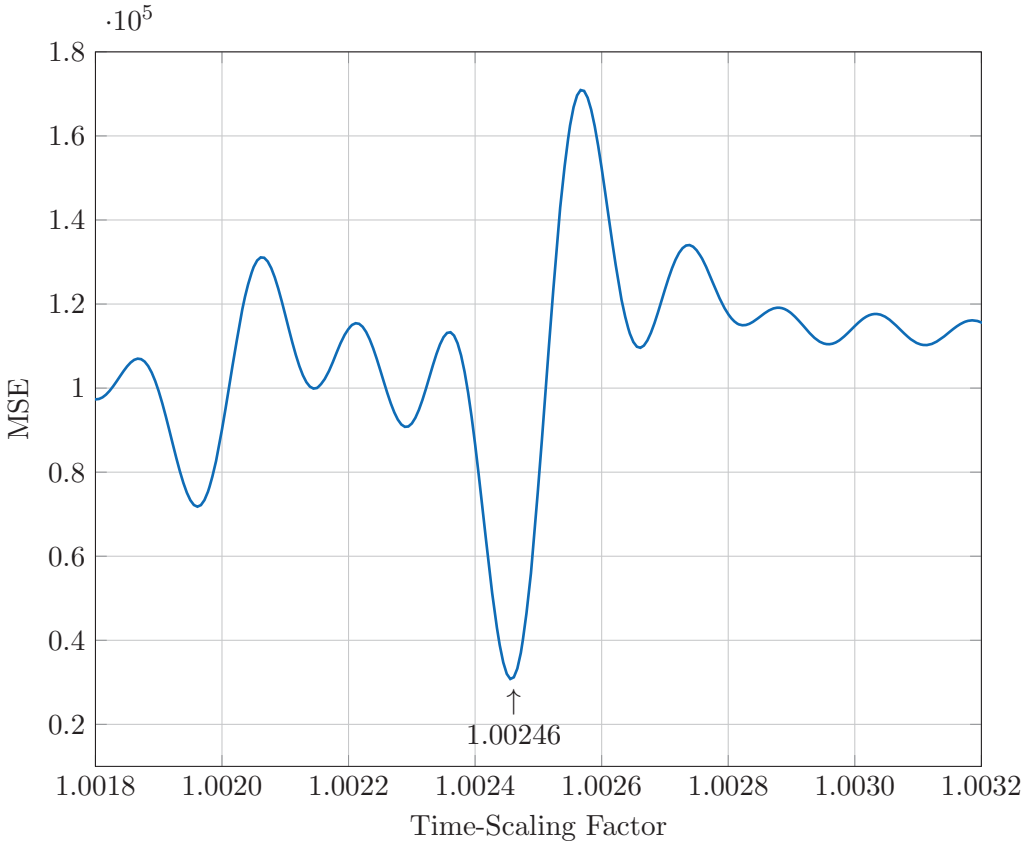

Figure 3.2: MSE of channel approximation as a function of the time-scaling factor for a single tone signal in a channel with small scaling spread.

Two different scenarios are defined. The channel parameters are chosen to show two specific scenarios and are not necessarily matched with the real world measurements.

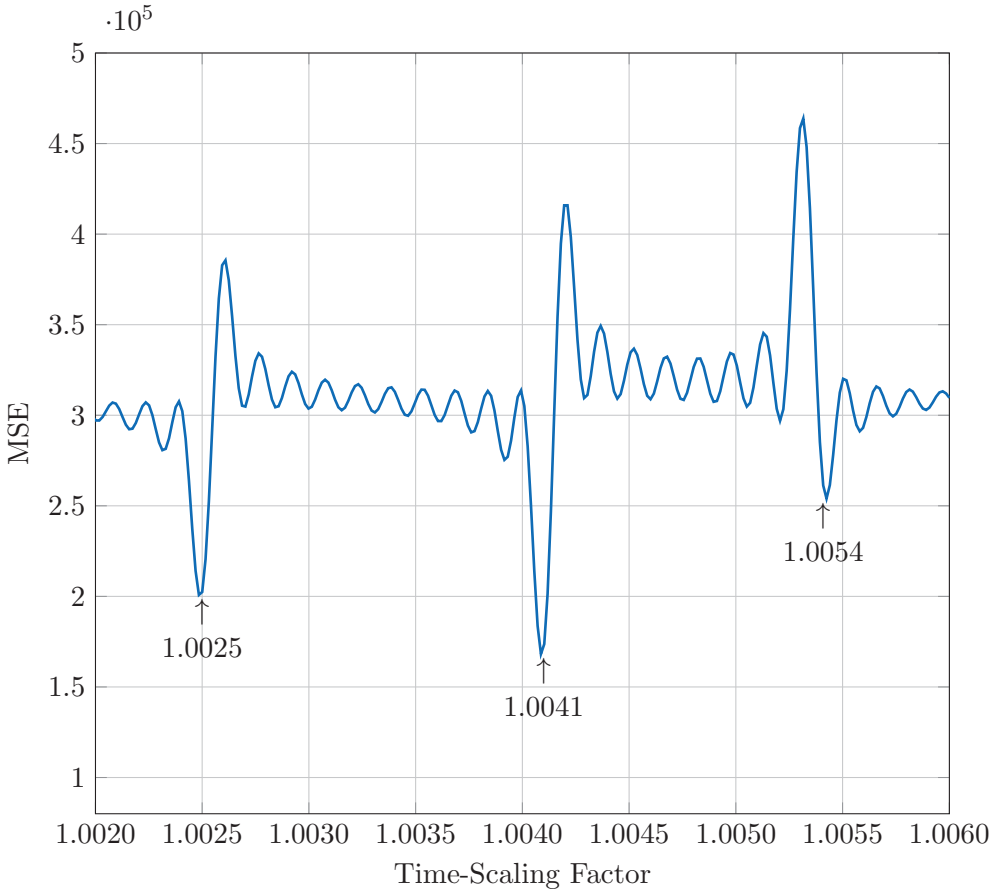

Figure 3.3: MSE of the channel approximation as a function of the time-scaling factor for a single tone signal in a channel with large scaling spread.

First, a channel with small scaling spread ($D_s = 8 \times 10^{-4}$) is tested. The path magnitudes, time-scaling factor, and central frequency of this channel are equal to $\mathbf{h} = [1, 0.4, 0.1]$, $\alpha = [1.0025, 1.0020, 1.0028]$, and $f_c = 2048$ Hz, respectively. The second channel has large scaling spread ($D_s = 2.8 \times 10^{-3}$). The path magnitudes, time-scaling factor, and central frequency of this channel are equal to $\mathbf{h} = [1, 0.75, 0.9]$, $\alpha = [1.0041, 1.0025, 1.0053]$, and $f_c = 2048$ Hz, respectively.

The results of the first test is shown in Figure 3.2. This figure shows that the optimal time-scaling factor, a_{opt}, is equal to the weighted average of time-scaling factors, which is equal to

$$a_{opt} = \frac{\sum_{l=0}^{L} h_l^2 a_l}{\sum_{l=0}^{L} h_l^2} = 1.00244. \tag{3.26}$$

Note that in this scenario, the optimal time-scaling factor is close to the scaling factor

of the first path, because the magnitude of this path dominates.

Figure 3.3 shows the MSE as a function of time-scaling for the second scenario. Three local minima are shown at the time-scaling factor of each path, however the global minimum is equal to the time-scaling factor of the strongest path.

Measurements reported in [23] show that in shallow water the multi-scale multipath effects can degrade the performance of the communication systems. In Moreover, in practical situations, the time-scaling factor changes with time. In this work, a method will be proposed to compensate for the optimum time-varying time-scaling. Specifically, in the next section a time-varying Doppler compensation method is developed.

Chapter 4

Doppler Compensation and Synchronization

Coherent single-carrier modulations are traditionally used for high data rate, bandwidth-efficient underwater communications. Some of these systems use adaptive joint phase synchronization and decision-feedback equalization [30]. Although single carrier communication systems perform successfully in a variety of underwater environments, they require careful tuning of the time-domain equalizer parameters [30]. These equalizers are usually very complex because they need too many taps in realization as a FIR filter. OFDM systems have been introduced as an alternative solution, because of their low complexity channel estimation and equalization. As mentioned in Section 3.1, while OFDM equalization in frequency domain reduces the complexity of the system, this signaling scheme is very sensitive to time-variant propagation, particularly when it creates frequency distortion. Essentially, any frequency offset in OFDM causes loss in sub-carriers' orthogonality and creates inter-carrier interference (ICI).

As far as the underwater acoustic OFDM (UWA-OFDM) transmission is concerned, researchers focus on different approaches for synchronization in the presence of time-variance. Earlier work on UWA-OFDM focused on designing an OFDM detector with low complexity synchronization method in a scenario that the transmitter and the receiver are deployed in shallow water [30]. In [30], the Doppler effect is modeled as a motion induced frequency offset which is common for all of the paths and is canceled in a block by block processing.

Also, a number of researchers studied the design of the OFDM system for high-rate communications when the transmitter and receiver are moving at a relative speed up to 5 $\frac{\mathrm{m}}{\mathrm{s}}$ [18, 23, 31]. Researchers in [18] used a two-step approach to mitigate the Doppler effect. The first step is the frequency dependent Doppler compensation via time-rescaling which is done by resampling with respect to an estimated time-scaling

factor. In [18] a constant time-scaling factor is estimated for all the OFDM blocks within a packet. After resampling, due to error in time-scaling factor estimation, a small frequency shift remains within each OFDM symbol. To remove the ICI completely in the second step, the residual frequency shift is estimated using a technique which utilizes null sub-carriers. Using this method the frequency shift which minimizes the energy in the null sub-carrier position is the optimum estimated residual frequency shift.

In [18], to estimate the time-scaling factor, the rate of change in the length of the transmitted packet is measured. For this purpose, two identical chirp sequences, are used as the preamble and the postamble at the leading edge and the final edge of the packet, respectively. A number of OFDM symbols are concatenated between the preamble and postamble. The distance between the two training sequences can be obtained by cross-correlating the whole packet with the reference chirp signal. The time-scaling factor over the packet can be estimated by comparing the length of the transmitted and received packets. Because this method requires buffering the whole packet, the researchers in [31] proposed a novel method for time-scaling estimation which avoids buffering the whole packet. Specifically, in [31] the Doppler scale estimation is obtained based on the correlation metrics from a bank of correlators, each matched with a different time-scaling factor.

In all the aforementioned papers, it was assumed that the time-scaling factor remains constant during the packet. However, as mentioned in Chapter 2 it is not a practical assumption in most practical cases.

To combat the problem of time-varying time-scaling during the period of a packet, Parrish *et al.* [32] proposed an algorithm which is able to estimate the carrier frequency offset (CFO) of each OFDM block within a packet. In [32], it is assumed that the statistics of the channel is known and the elements of channel impulse response are independent Rayleigh fading arrivals. However, this system shows promising results in simulations, there is no guaranty that it can work properly in the UWA channel, since this channel usually can not be described by Rayleigh fading arrivals. Also, Abdelkareem *et al.* [33] proposed a novel method for underwater OFDM transmission in a scenario of vehicle acceleration and sudden changes in direction. In this algorithm,

the time-offset estimator utilizes the cross-correlation of the cyclic prefix and its replica at the end of OFDM symbol [33].

The drawback which is common in all the works which have been discussed above, is that the time-scaling factor is assumed to be common to all paths. The authors in [24], proposed an algorithm which minimizes the MSE between the reference and received pilots' block to estimate the optimal time-scaling factor in a multi-scale multipath environment. However it was assumed that the time-scaling factor remains constant during the packet.

The algorithm which is proposed in this thesis, estimates the optimal time-scaling factor of each OFDM block by utilizing the pilot tones and a linear approximation. This algorithm uses the same mathematical bases as the technique which was described in [24], with three major differences. First, in this thesis the time-scaling factor is assumed to be changing from one OFDM block to the next. Second, instead of using a block of pilots at the start of each packet, the comb-type pilot insertion is used and the time-scaling factor is estimated for each OFDM block. Third, the time-varying time-scaling factor across the packet is approximated and to compensate for Doppler effect, instead of resampling with respect to a constant time-scaling factor, the TVFDL is utilized to implement a time-varying Doppler compensation.

In this Chapter, first the the coarse packet synchronization and channel estimation method is described in Section 4.1. Then, the proposed Doppler compensation method is described in detail in Section 4.2.

4.1 Packet Synchronization and Coarse Channel Estimation

In the receiver design, it is essential to find the point where the packet starts. As such, the packet synchronization is a basic requirement of any receiver. Data aided synchronization using preambles is a traditional method to deal with this problem. For this purpose, a known training sequence is inserted at the start of the packet as a preamble. At the receiver, the location of the peak of the cross-correlation between the received signal and the known preamble gives a coarse estimate of the start of the

packet.

A training sequence, often used in underwater telemetry, is the chirp signal. The chirp signal is chosen becuase it has a desirable ambiguity function in both time and frequency, which makes it tolerant to frequency shifts [31]. Also, the chirp signal has good autocorrelation characteristics [34]. More information on the characteristics of this signature and its ambiguity function can be found in Appendix A.

In system architecture of this thesis, a chirp is placed at the leading edge of the packet. The length of each chirp signal is equal to the length of an OFDM symbol (N). This length is chosen in such a way that it covers the whole period of the multipath channel. A guard of zeros with length of cyclic prefix L_{cp} is added after the preamble and before the OFDM blocks. The structure of the transmitted packet is depicted in Figure 4.1.

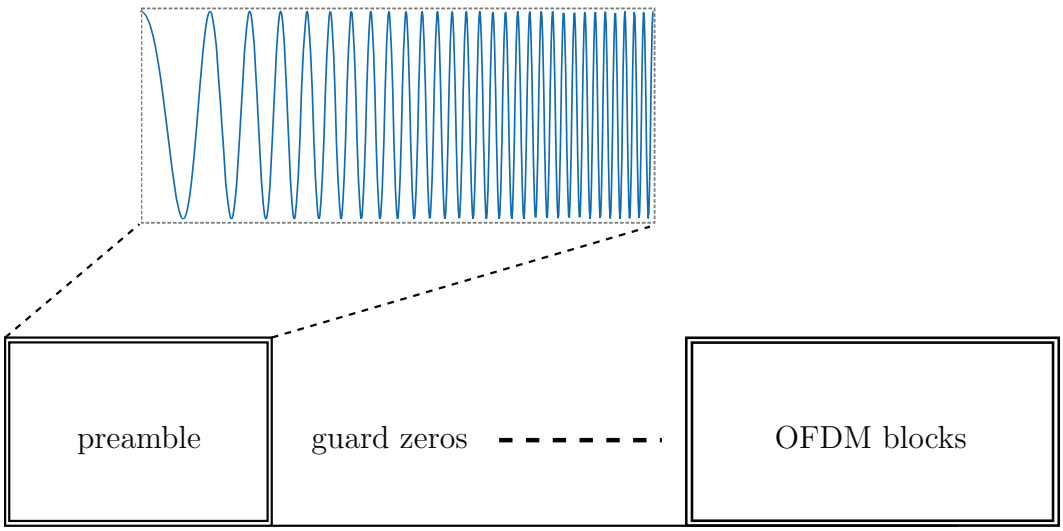

Figure 4.1: Packet structure

At the receiver, first the leading edge of the packet including the preamble is buffered. The cross-correlation between the known training sequence and the buffered signal is obtained. The results of cross-correlation are used for two purposes, packet detection and coarse channel estimation. The packet detection is obtained by finding the

location of the cross-correlation peak.

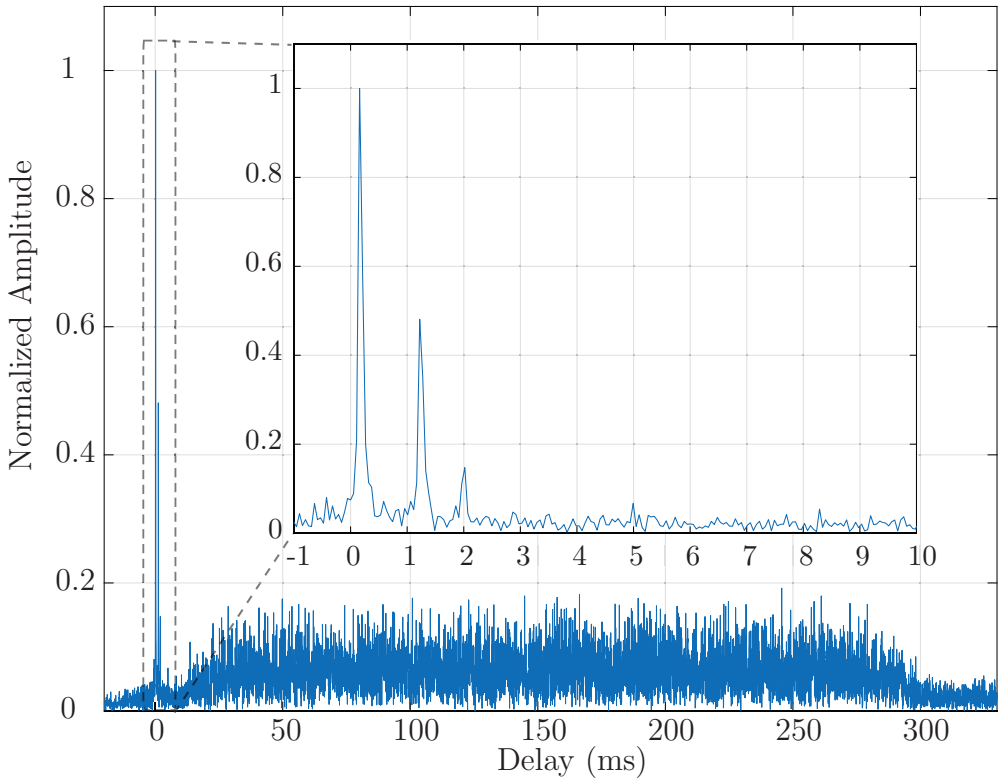

Figure 4.2: An example of initial estimate of the channel impulse response.

An initial estimate of the path delays and amplitudes can be also obtained from the result of the cross-correlation. The cross-correlation is performed at the baseband and using the symbol rate.

Figure 4.2 shows an example of the coarse channel estimation and frame synchronization. In this test the channel parameters are the same as described in Table 2.1 and the normalized delays of the three strongest eigenpaths were equal to $\tau = [0, 1.0632, 1.8174]$ ms. The estimated path delays, with respect to the delay of the first path are $\hat{\tau} = [0, 1.0625, 1.8594]$ ms which are very close to the actual delays, τ.

After finding the start of the packet, it should be partitioned for Doppler estimation purposes. The partitioning in baseband requires accurate estimation of the starting

point of each OFDM block. In this receiver design, the OFDM block synchronization has been integrated with the time-scaling estimation unit, which is discussed in, the next section.

4.2 Time-Scaling Estimation and Compensation

Pilot tones or pilot carriers are traditionally used for synchronization and channel estimation purposes. In OFDM systems, pilot tones are the symbols which are inserted between the data sub-carriers and they are known at the receiver side. These sub-carriers are usually used for channel estimation in the frequency domain which is described in Chapter 5.

There are two basic methods for pilot arrangements in OFDM sub-carrier allocations: block-type and comb-type. In the block-type pilot arrangement, the pilot tones are inserted into all sub-carriers of OFDM symbols within a specific period [35]. In the comb-type pilot arrangement, the pilots are inserted in some certain sub-carriers of each OFDM symbol [35]. These two basic pilot arrangement methods are shown in Figure 4.3.

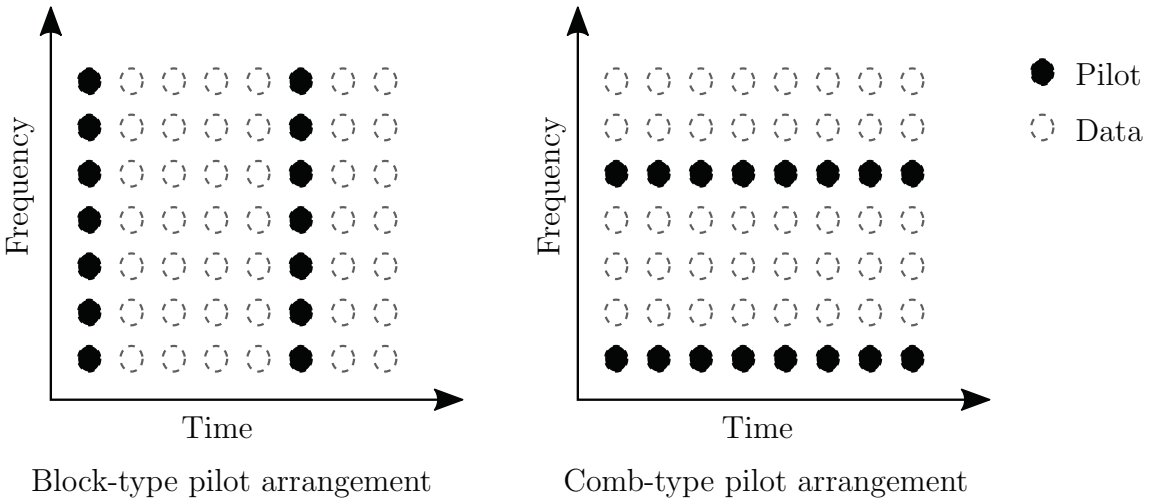

Figure 4.3: Basic pilot arrangements for OFDM systems

Pilot sub-carriers can be also utilized to estimate the Doppler frequency offset and time-scaling factor. Some earlier research on channel parameters estimation, including

Doppler effect, utilize pilot sub-carriers to compensate for Doppler effect [24, 30, 32]. In most of these works the Doppler shift was assumed, to be constant during the packet and the estimation was performed using a block-type pilot arrangement. One of the disadvantages of the block-type based channel estimation methods is that they are unable to track a fast time-varying channel.

In this work, a comb-type pilot aided time-scaling estimation is developed. This method is a modification of the block-type pilot estimator that was described in [24]. One of the basic assumptions in this estimator design is that the time-scaling factor remains constant during one OFDM block. Under this assumption a single optimum resampling factor is estimated for each OFDM block. For this purpose the receiver needs to find an accurate estimation of the start point of each OFDM block. The method which is proposed in this work, integrates the time-scaling estimation and OFDM block synchronization components at the receiver.

4.2.1 Time-scaling Estimation

In this work, it is assumed that the relative velocity is changing slowly with time, so the time-scaling factor can be assumed constant during the length of an OFDM block. By this assumption, the optimum time-scaling factor can be estimated block by block, by minimizing the error between the received baseband symbols and the approximated symbols. The time-varying time-scaling factor then can be estimated by using an interpolation between the estimated time-scaling factors of the multiple OFDM blocks.

To describe the estimation method, the received mth OFDM symbol can be expressed from Equation (3.14) using a single optimum resampling factor, b. This approximated received symbol can be written as

$$r_m[n] = \sum_{l=0}^{P} h_l \mathrm{e}^{-j2\pi f_k \tau_{l,0}} \sum_{k=0}^{N-1} s_k \mathrm{e}^{j2\pi k(1+b)\frac{n}{N}} \mathrm{e}^{j2\pi f_c bn\frac{T}{N}} + \mathbf{n}[n]. \tag{4.1}$$

By separating the effect of multipath and Doppler, and by neglecting the effect of the

noise, the approximated received vector is expressed as,

$$\hat{\mathbf{r}} = \mathbf{D}_b \tilde{\mathbf{A}}_b \mathbf{x}, \tag{4.2}$$

where $\hat{\mathbf{r}}$ is an $N \times 1$ vector which shows the samples of the received OFDM symbol and $\mathbf{x} = \mathbf{Hs}$ demonstrates the effect of multipath on the transmitted symbol, where $\mathbf{H}$ and $\mathbf{s}$ are the multipath channel matrix and transmitted signal vector, respectively. $\mathbf{D}_b$ was described by Equation (3.16) and it models the frequency offset. Also, as explained by Equation (3.18), $\tilde{\mathbf{A}}_b$, which is equal to $\tilde{\mathbf{A}} \times \mathbf{\Gamma}$, models the frequency distortion due to time scaling and $\mathbf{\Gamma}$ is a selection matrix which selects the symbols in pilot sub-carriers.

By using the Equation (4.2), the mean squared error between the actual and the approximated received vector is defined as a cost function which is the following L_2 norm,

$$\varepsilon(\mathbf{x}, b) = \|\mathbf{r} - \hat{\mathbf{r}}\|^2 = \left\|\mathbf{r} - \mathbf{D}_b \tilde{\mathbf{A}}_b \mathbf{x}\right\|^2. \tag{4.3}$$

Equation (4.3) is a function of the resampling factor, b, and the multipath channel parameters, shown in $\mathbf{x}$. When the channel parameters are known, the distorted reference signal in multipath, $\mathbf{x}$, and in the absence of Doppler is

$$\mathbf{x} = \mathbf{SFh}, \tag{4.4}$$

where $\mathbf{S}$ is the diagonal $P \times P$ matrix of the pilot vector $\mathbf{s}$, and P is the length of the reference pilot vector. The matrix of $\mathbf{F}$ (with size $P \times L$) provides a relationship between the phase shift of each sub-carrier to the channel gain of each path and is given as

$$\mathbf{F} = \begin{bmatrix} \mathrm{e}^{-j2\pi f_{p_1}\tau_1} & \mathrm{e}^{-j2\pi f_{p_1}\tau_2} & \cdots & \mathrm{e}^{-j2\pi f_{p_1}\tau_L} \\ \mathrm{e}^{-j2\pi f_{p_2}\tau_1} & \mathrm{e}^{-j2\pi f_{p_2}\tau_2} & \cdots & \mathrm{e}^{-j2\pi f_{p_2}\tau_L} \\ \vdots & \ddots & \vdots & \\ \mathrm{e}^{-j2\pi f_{p_P}\tau_1} & \mathrm{e}^{-j2\pi f_{p_P}\tau_2} & \cdots & \mathrm{e}^{-j2\pi f_{p_P}\tau_L} \end{bmatrix}, \tag{4.5}$$

and $\mathbf{h} = [h_1, h_2, \cdots, h_L]^T$ is the $L \times 1$ vector of the channel gain on each path. An initial estimate of the channel impulse response, $\hat{\mathbf{h}}$, can be extracted from the preamble, so the cost function in Equation (4.3) is changed to

$$\varepsilon(\hat{\mathbf{h}}, b) = \|\mathbf{r} - \hat{\mathbf{r}}\|^2 = \left\|\mathbf{r} - \mathbf{D}_b \tilde{\mathbf{A}}_b \mathbf{SF}\hat{\mathbf{h}}\right\|^2. \tag{4.6}$$

In multipath fading scenarios the path amplitudes change from one block to the next. Thus, the coarse channel gain estimation from preamble can not be used for all the OFDM symbols.

Since the statistical characteristics of the channel are unknown, the path amplitudes can be considered as unknown deterministic parameters [36]. To eliminate the nuisance parameter, $\mathbf{h}$, the deterministic maximum-likelihood (DML) method, described in [36] is utilized. The ML estimate of $\mathbf{x}$ and b is a choice of these parameters, which locally minimizes the L_2 norm of Equation (4.3). The DML estimate of $\mathbf{x}$, corresponding to a candidate b, is [36]

$$\hat{\mathbf{x}} = \tilde{\mathbf{A}}_b^{\dagger}\mathbf{D}_b^H\mathbf{r}. \tag{4.7}$$

By replacing $\hat{\mathbf{x}}$ in Equation (4.7) with $\mathbf{x}$ in Equation (4.4), the approximation of distorted received signal, $\hat{\mathbf{x}}$ can be expressed as

$$\hat{\mathbf{x}} = \tilde{\mathbf{A}}_b^{\dagger}\mathbf{D}_b^H\mathbf{r} = \mathbf{SF}\hat{\mathbf{h}}. \tag{4.8}$$

Then an estimation of the path amplitude, $\hat{\mathbf{h}}$ can be obtained by applying some matrix inversion and multiplication on Equation (4.8) and it is

$$\hat{\mathbf{h}} = \mathbf{F}^{\dagger}\mathbf{S}^H(\tilde{\mathbf{A}}_b)^{\dagger}\mathbf{D}_b^H\mathbf{r}. \tag{4.9}$$

The cost function then can be reduced to a one dimensional function of the optimum resampling factor, b, by replacing Equation (4.9) in Equation (4.6) which is

$$\varepsilon(b) = \left|\mathbf{r} - \mathbf{D}_b\tilde{\mathbf{A}}_b\mathbf{SFF}^{\dagger}\mathbf{S}^H(\tilde{\mathbf{A}}_b)^{\dagger}\mathbf{D}_b^H\mathbf{r}\right|^2. \tag{4.10}$$

To summarize, the optimum time-scaling factor is estimated by minimizing the new cost function as,

$$b^* = \arg\min_b \varepsilon. \tag{4.11}$$

It can be proved that the minimization problem is equivalent to maximizing the projection of the received signal onto the approximated received signal defined as [24]

$$b^* = \arg\max_b \mathbf{r}^H\mathbf{D}_b\tilde{\mathbf{A}}_b\mathbf{SFF}^{\dagger}\mathbf{S}^H(\tilde{\mathbf{A}}_b)^{\dagger}\mathbf{D}_b^H\mathbf{r}. \tag{4.12}$$

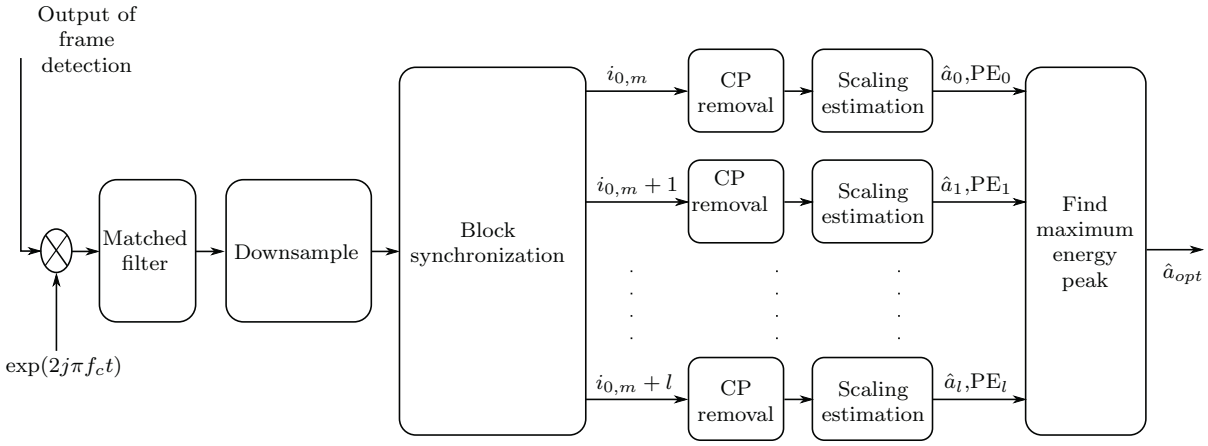

Figure 4.4: The time-scaling factor estimation block diagram

4.2.2 OFDM Block Synchronization and Simulation Results

As explained in Chapter 2, the Doppler effect can create dilation/compression in the packet, which causes a loss of block synchronization. Block synchronization is the process of finding the starting point of each OFDM block before partitioning at the receiver. It can be shown that when block synchronization is prefect the projected energy of the OFDM block has the highest peak. So by considering this fact, fine block synchronization can be performed in three steps:

1. Find a coarse estimate of the starting point of the mth OFDM block, $i_{0,m}$, by counting $m \times (N + L_{cp})$ samples after the preamble in the baseband.
2. Shift the starting point of the mth block around $i_{0,m}$ by an integer number of samples, l. Then, calculate for each delay the projected energy from the $(i_{0,m} + l)$th point. The range of l depends on the intensity of Doppler and number of OFDM samples in discrete time-domain.
3. Choose the point which gives the maximum peak between the energy functions as the optimum start point of the mth OFDM block.

The block diagram of the time-scaling estimator is shown in Figure 4.4. The range of l depends on the rate of dilation/compression.

A simulation was carried out for a packet of five OFDM symbols which were concatenated one after the other. The packet passes through a deterministic multi-scale

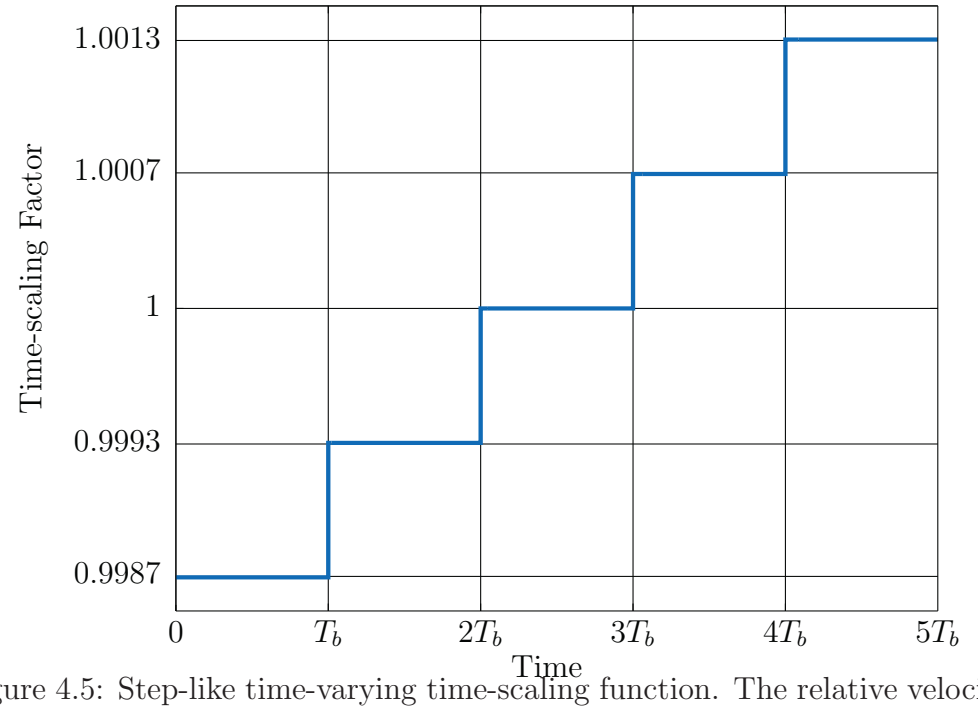

Figure 4.5: Step-like time-varying time-scaling function. The relative velocity during each OFDM block remains constant and it is changing from one block to the next. The vector of the relative velocity is $\mathbf{v_r} = [-2, -1, 0, 1, 2]\ \frac{\text{m}}{\text{s}}$. The OFDM block duration is $T_b = 1.9$ s

multipath channel with delay spread of $\overline{\tau} = 59.3$ ms and a maximum scaling spread of $D_s = 2.2 \times 10^{-4}$. The signal to noise ratio is 10 dB. The time-scaling factor is constant during each OFDM symbol, but is changing from one block to the next (see Figure 4.5).

The maximum of the cost function for each OFDM symbol is obtained by a linear search on b. The result of the linear search is shown in Figure 4.6 where the estimation algorithm is able to track the time-scaling factors created by a relative speed up to $2.5\frac{\text{m}}{\text{s}}$. Although this example demonstrates a constant speed for each block, it will be shown through simulations that the estimation algorithm works in a continuously time-varying speed condition if the rate of acceleration remains small.

When the time-scaling factor changes continuously in time, the received packet needs to be compensated with a time-varying resampling process. The time-varying time-scaling factor of the packet can be approximated with an interpolation between the estimated optimum time-scaling factors. Depending on the accuracy and hardware limitations, different kinds of interpolation methods can be used. Linear interpolation

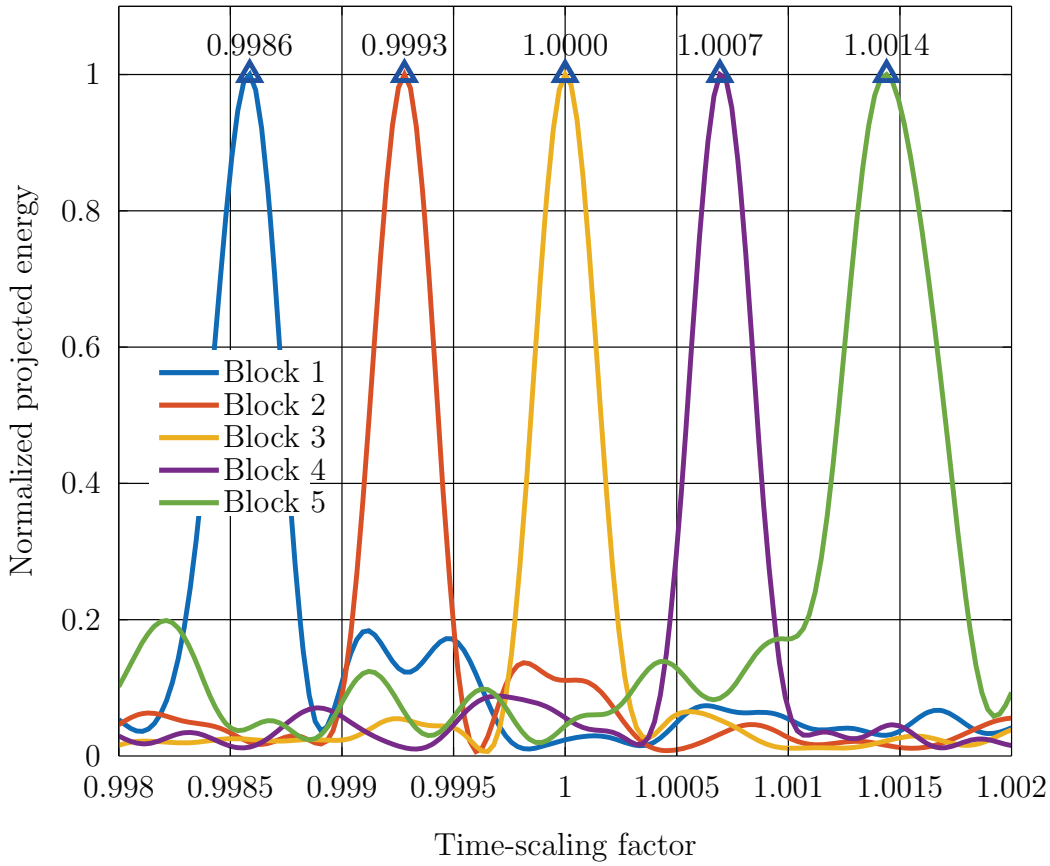

Figure 4.6: An example of linear search for time-scaling factor estimation in a packet of five OFDM block. Different colors show different OFDM blocks. The points that the energies are maximized, show the optimum time-scaling factors. In this example each OFDM symbol has 512 sub-carriers that 128 nulls and 128 pilots have been inserted in between them. The length of cyclic prefix is 100 samples in discrete-time domain. The transmitted bandwidth is 320 Hz. The range of integer search for the block synchronization is $l = [-4, 4]$.

is one of the simplest methods that can approximate the time-scaling factor between two successive OFDM symbols as,

$$\hat{a}_i(t) = \frac{\hat{a}_i - \hat{a}_{i-1}}{T} t + \hat{a}_{i-1}, \tag{4.13}$$

where a_i and a_{i-1} are the estimated scaling factors of the ith and the $(i-1)$th OFDM block, respectively. The initial estimate of the time-scaling factor over the preamble can be used in the approximation of the time-varying time-scaling factor over the first OFDM block.

Once the time-varying time-scaling factor over the packet was approximated by interpolation, the passband received signal can be ressampled in a time-varying manner using TVFDL. An example of the approximation of the time-varying delay is shown in Figure 4.7. In this channel simulation, the relative velocity between the receiver and transmitter is increasing continuously from -1 $\frac{\text{m}}{\text{s}}$ up to 2.5 $\frac{\text{m}}{\text{s}}$. The negative speed shows a positive delay and the positive speed creates a negative delay. The delay is varying with time like a quadratic function because the acceleration rate remains constant during the packet. Equation (2.35) expresses this case mathematically.

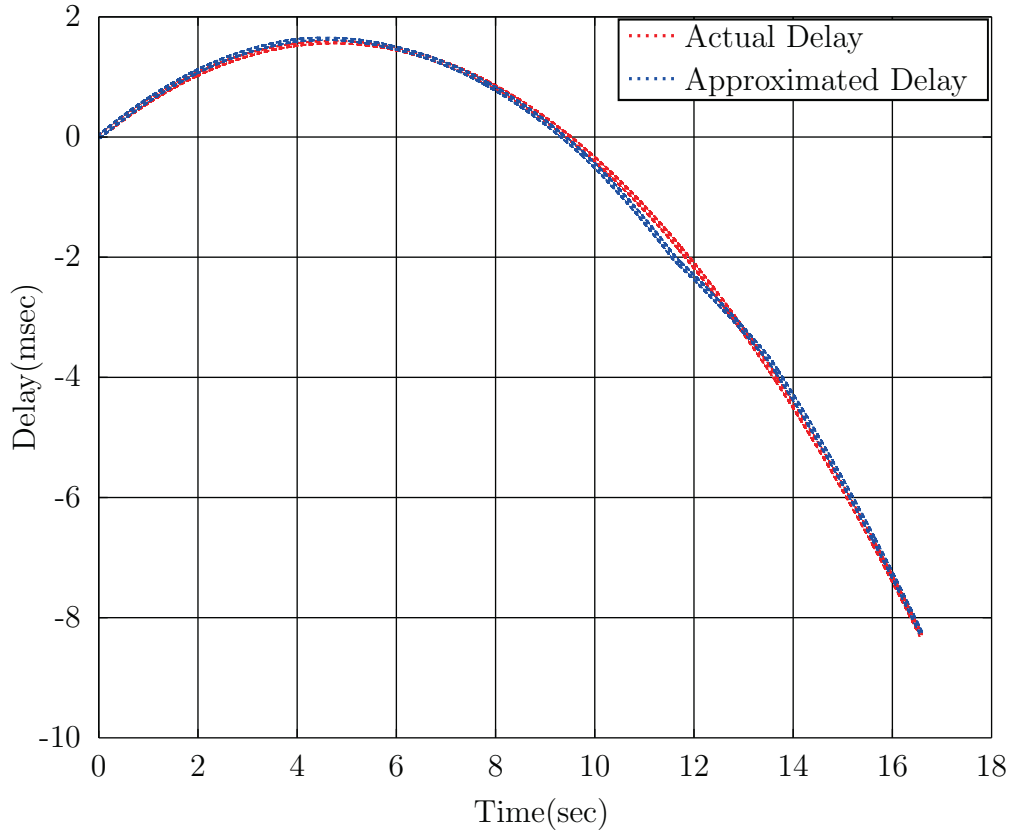

Figure 4.7: An example of time-varying delay estimation. The delay of the strongest path is changing with time like a quadratic function.

As shown in Figure 4.7, the linear interpolation can effectively approximate the time-varying time-scaling factor and consequently time-varying delay. But, this approximation has an error which sometimes can create considerable frequency dependent frequency shifts after resampling. These residual frequency shifts can be modeled as a

common frequency shift for the all sub-carriers, if they are smaller than the frequency separation between the sub-carriers, Δf. This means that, it can be canceled out by an opposite frequency shift. By this assumption the maximum tolerable error in the time-scaling factor approximation, Δa_{max}, can be defined as

$$\Delta a_{max} \times f_{k_{\max}} < \Delta f, \tag{4.14}$$

where $f_{k_{max}} = f_c + (\frac{N}{2} - 1)\Delta f$ is the maximum frequency component of the OFDM signal in passband. Equation (4.14) can be re-written as,

$$\Delta a_{max} < \frac{\Delta f}{f_c + (\frac{N}{2} - 1)\Delta f}. \tag{4.15}$$

In other words, when the approximation error is less than Δa_{max}, the residual frequency shifts would be negligible. Therefore, in a mobile UWA communication system design, choosing the optimum frequency separation and central frequency should be considered carefully, as well as the optimum sub-carrier allocation.

In addition to Doppler compensation, the received symbols should be equalized before decoding, to combat the effect of frequency selectivity. This step will be explained in the next Chapter in combination with the receiver design approach.

Chapter 5

OFDM System Design

This chapter discusses a communication system architecture that uses the Doppler compensation method which was described in Chapter 4. The design parameters and the communication blocks will be explained in detail in Section 5.1. Then, a channel estimation method is proposed in Section 5.2. The necessity of using null sub-carriers between the pilot and data sub-carriers and their optimum placement is discussed in Section 5.3. The procedure of sea trial is described in Section 5.4.1. Finally, Section 5.4.2 will compare the bit error rate performance of the simulated and measured systems.

5.1 System Architecture

The block diagram of the proposed transmitter is shown in Figure 5.1. This block diagram shows how information bits are modulated and transmitted to passband. In this design the BPSK modulation scheme is used because of its simplicity. After serial to parallel conversion (S\P block in Figure 5.1), the nulls and the pilot tones are inserted into predefined sub-carrier locations. The symbols are converted to the time domain using inverse Fourier transform (IFFT). Then the cyclic prefix is added as a guard interval.

In order to limit the bandwidth of the transmitted pulse, it is passed through a band limited filter, which in this case is a pulse shaping filter. To realize the filtering easily and convert the signal to analog domain, the signal is upsampled. A raised cosine filter with a roll-off factor, $\beta = 0.5$, is used for pulse shaping. After pulse shaping, the signal is shifted to passband using a frequency mixer. The output of this module is a passband OFDM block which will be concatenated with the preamble and the other

OFDM blocks to create a packet. The packet structure was described in Section 4.1.

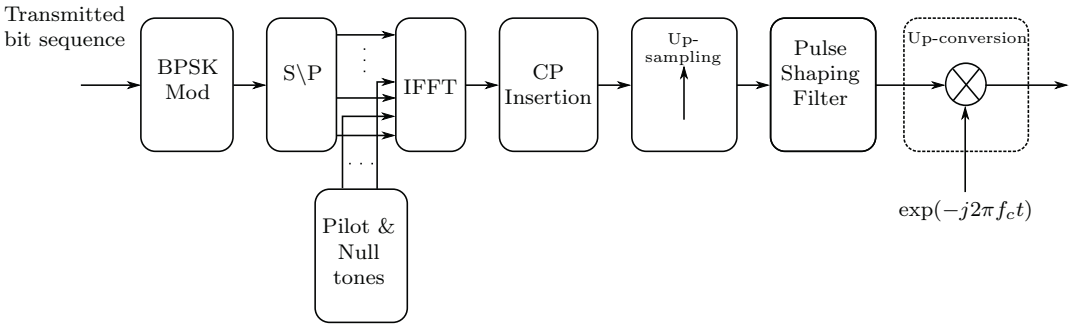

Figure 5.1: The block diagram of the transmitter.

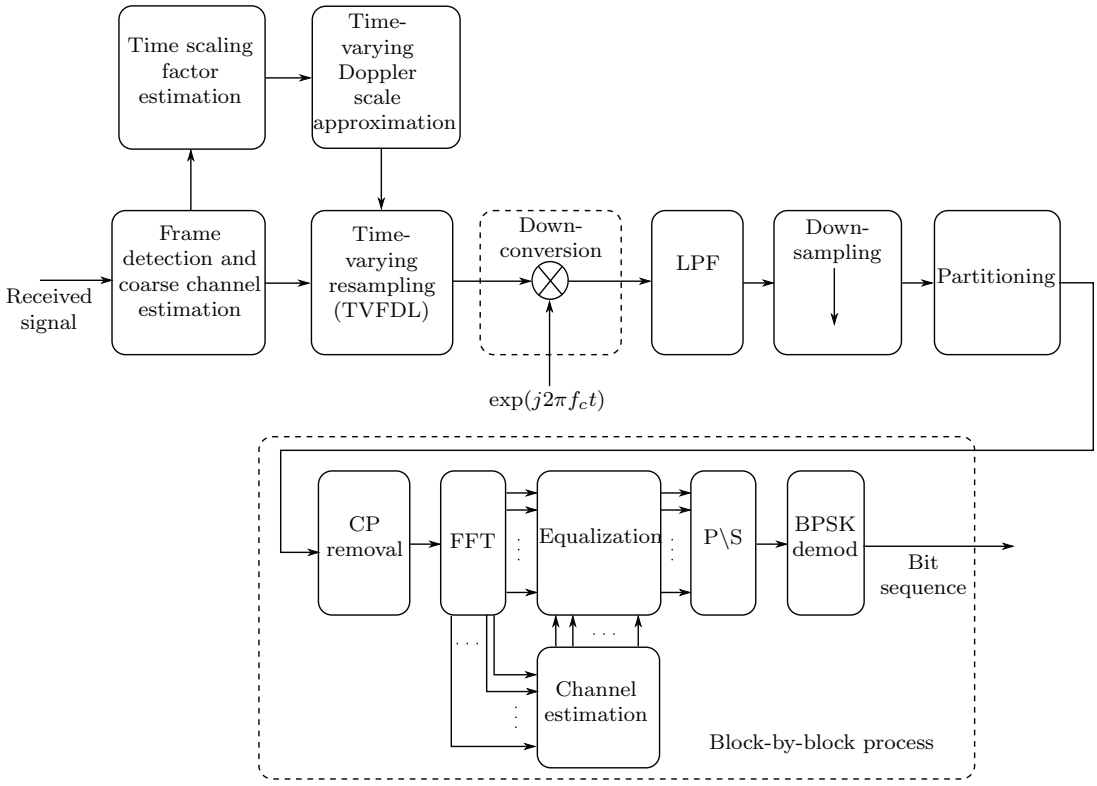

Figure 5.2: The block diagram of the receiver

At the receiver, the TVFDL block operates in passband. So, to utilize it for Doppler compensation the signal will be processed in two stages. As it is shown in Figure 5.2, after coarse channel estimation, the time-scaling factors of the OFDM blocks are estimated in baseband. Then, the time-varying time-scaling factor is approximated and the signal is resampled in passband using the TVFDL.

Every receiver needs a low-pass filter (LPF) after the mixer to extract the baseband signal and ignore the high frequency images. After partitioning and the guard interval removal (CP removal block in Figure 5.2), the signal is converted to the frequency domain, using the FFT block, to extract the channel information and demodulation. The channel information can be estimated using the pilot tones. One of the advantages of OFDM systems is that the signal can be equalized easily in the frequency domain by a vector multiplication. Some of the channel estimation techniques are reviewed in the next Section.

5.2 Channel Estimation

As described in Chapter 2, in underwater communications the signal is transmitted through a multi-scale multipath channel. In order to achieve a reliable coherent decoding, the effect of the multipath channel has to be compensated after resampling. In other words, an equalizer should be designed to compensate for the frequency selectivity of the channel.

The channel estimators can be categorized into blind and non-blind estimation methods [37]. The blind estimation utilizes the statistical behaviour of the received signal and it requires a large amount of data [38]. The most popular non-blind OFDM channel estimation method is pilot based channel estimation. In this method the pilot tones are inserted in between the sub-carriers in the frequency domain. As explained in Section 4.2 the pilot tones can be inserted using block-type or comb-type arrangement. While in OFDM systems the pilots are usually inserted in the frequency domain, the authors in [39] presented a channel estimation method which utilizes the pilot tones in both time and frequency domains. In this system which is called *Known Symbol Padding OFDM (KSP-OFDM)*, instead of using cyclic prefix, a known symbol, like a modulated PN sequence, is padded at the end of each OFDM symbol as a guard interval. This known symbol then is utilized as a time-domain pilot for the channel estimation purposes [39].

In the design of the data aided channel estimator, two aspects should be considered, as explained in [35]. First, the best pilot arrangement in the sub-carrier allocation

should be examined. Then, a statistically optimum estimator with low complexity and good channel tracking ability which uses the pilots to estimate the channel, should be designed.

In a time-varying environment in which the channel characteristics are changing from one OFDM block to the next, a comb-type pilot estimation is the best solution. This method requires interpolation to estimate the channel conditions on the other sub-carriers' locations. In addition, a combination of the block-type and comb-type arrangement, like KSP-OFDM system, can sometimes be beneficial, because it can track the channels characteristics in both time and frequency domains. But, this approach is more computationally expensive and has less bandwidth efficiency in comparison with comb-type pilot arrangement.

According to [37], "One of the objectives of the receiver design is to minimize the detection error". So, the equalizer should be designed in a way to minimize the symbol/bit detection error. In [37], the channel estimator was designed based on maximizing the likelihood function which is equivalent to the joint probability of the received sequence conditioned on the information sequence. In [40], two conventional channel estimation methods were compared: *Least Square* (LS) and *Minimum Mean-Square Error* (MMSE). When the number of pilot subcarriers is bigger than the length of the discrete channel path arrivals, the LS estimator can be used [35, 40]. Although the LS estimators are calculated with very low complexity, their performance is degraded dramatically as the signal to noise ratio (SNR) decreases.

In low SNR scenarios the MMSE estimator would be a better alternative, because it uses a coarse estimate of SNR to make the estimation less sensitive to the noise. To design a MMSE estimator, a *priori* knowledge of the channel autocorrelation should be also available [35, 40]. Since the channel statistics are usually unknown, the authors in [41] have studied the mismatch of the estimator to channel statistics and proposed a channel estimation method which is insensitive to the channel statistics.

Also, a novel method has been suggested in [42], which uses the LS estimated channel impulse response to extract the autocorrelation matrix and the noise variance for the MMSE estimation. This method considers the fact that the energy of the channel is

concentrated in a short time period in comparison to the period of guard intervals between OFDM symbols. But, this assumption is not reasonable in shallow water communications, because the channel usually has a large delay spread (in order of 100 ms). In this case, a guard interval much longer than the length of the channel must be chosen, which may increase the latency of the system. The other disadvantage of this MMSE estimator is its high complexity in comparison with the LS estimator. More examples of application of the conventional channel estimators in underwater acoustic systems can be found in [18, 33, 43].

Besides the conventional methods which were introduced, the *sparse channel estimation* algorithms have recently attracted a lot of interest. These estimation techniques have been developed based on compressed sensing theory, which presents a method of problem solving which in, the number of measurements are less than the number of the unknown parameters. In this technique it is known that the solution is sparse in some domain. According to [44], the common assumption is that a sparse multipath channel leads to a baseband channel model where most of the paths amplitudes are negligible.

The sparse channel estimation methods can perform well in some high data rate communication links, for instance in deep underwater communications where the channel shows sparsity [45]. But, measurement shows that assumption of the sparse channel does not necessarily hold in shallow water communication, like in a shallow river where there are too many reflection from the rough bottoms and walls [46].

In this work, to avoid added receiver complexity, a pilot aided LS estimator is used. The estimation algorithm is described in the next section.

5.2.1 Least Square (LS) Estimator

The problem of LS estimation is defined as minimizing the squared error of the received signal vector in the frequency domain, $\mathbf{z}$, and its estimation, $\hat{\mathbf{z}}$. So, the LS estimate of the channel frequency response, $\hat{\mathbf{H}}_{\mathbf{LS}}$, is

$$\hat{\mathbf{H}}_{\mathbf{LS}} = \arg\min_{\mathrm{H}} \left\{ (\mathbf{z} - \tilde{\mathbf{z}}) (\mathbf{z} - \tilde{\mathbf{z}})^H \right\}. \tag{5.1}$$

The estimation of the received signal in frequency domain is expressed as

$$\hat{\mathbf{z}} = \hat{\mathbf{H}}\mathbf{y} + \mathbf{n} \tag{5.2}$$

where $\mathbf{y}$, $\hat{\mathbf{H}}$ and $\mathbf{n}$ are the transmitted signal vector, estimation of the channel frequency response matrix and the noise vector, respectively. Thus, the $\hat{\mathbf{H}}$ should be chosen to minimize the squared error of the received signal and its estimation. Therefore, the LS estimate of the channel frequency response can be obtained by replacing Equation (5.1) into Equation (5.2) as

$$\hat{\mathbf{H}}_{\mathbf{LS}} = \arg\min_{\mathbf{H}} \left\{ (\mathbf{z} - \mathbf{H}\mathbf{y} - \mathbf{n}) (\mathbf{z} - \mathbf{H}\mathbf{y} - \mathbf{n})^H \right\}. \tag{5.3}$$

It can be proven that, by ignoring the effect of the noise, the $\hat{\mathbf{H}}$ which minimizes the square error of Equation (5.3) is equal to the vector multiplication between $\mathbf{z}$ and $\mathbf{y}^*$. Consequently,

$$\hat{\mathbf{H}}_{\mathbf{LS}} = \mathbf{z}\mathbf{y}^*. \tag{5.4}$$

The channel frequency response can be found in the pilot positions as,

$$\hat{H}_{LS_p} = z_p y_p^* \tag{5.5}$$

where $p \in S_P$, shows the index of the pilot tones.

To estimate the channel at the data sub-carriers a linear interpolation is used. The channel impulse response can be obtained by the discrete Fourier transform (DFT) of $\hat{\mathbf{H}}_{\mathbf{LS}}$.

5.3 Sub-carrier Allocation

As described in Section 4.2 and Section 5.2, the Doppler compensation and channel estimation blocks utilize a comb-type pilot arrangement to estimate the desired parameters. In the presence of ICI, the problem that occurs is that the unknown data sub-carriers interfere with the pilot sub-carriers. This phenomenon may reduce the estimation accuracy. Therefore, the sub-carrier allocation method must handle the Doppler effect with pilot sub-carriers.

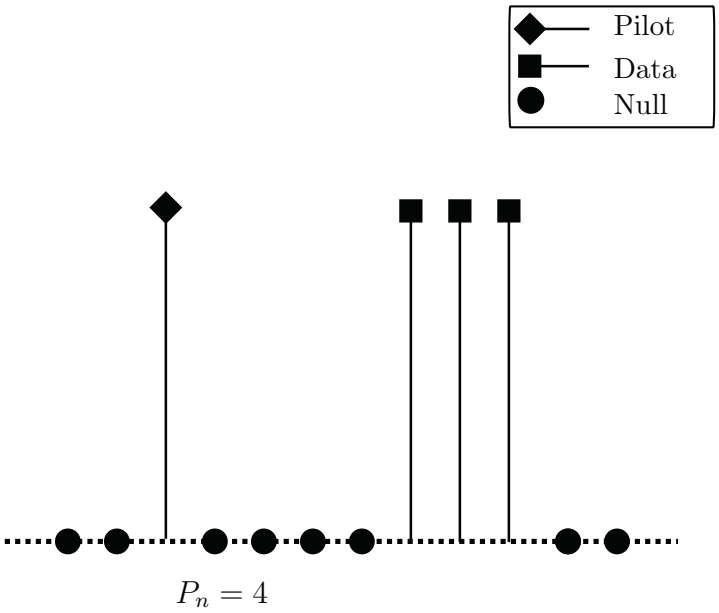

Figure 5.3: An example of OFDM sub-frame. One pilot tone and three data sub-carrier are inserted and the pilots are protected with four null sub-carriers.

To mitigate the effect of ICI on pilot tones in this system, some guard intervals consisting of zeros (nulls) are inserted on either side of pilot sub-carriers [47]. Figure 5.3 shows an example of a sub-frame of OFDM sub-carriers. The number of nulls is related to the value of the maximum Doppler shift. If it is assumed that the Doppler shift only occurs because of the relative velocity between the transmitter and receiver, then the maximum frequency shift, $f_{d_{\max}}$, is related to the maximum velocity, $v_{\max}$, and the maximum sub-carrier frequency. The maximum sub-carrier frequency, $f_{\max}$, of an OFDM system in passband is calculated as,

$$f_{\max} = f_c + \frac{B}{2}. \tag{5.6}$$

The maximum Doppler shift, $f_{d_{\max}}$, due to maximum velocity then is calculated as,

$$f_{d_{\max}} = \frac{v_{\max}}{c_w} f_{\max}. \tag{5.7}$$

The guard interval between the pilots and data sub-carriers should mitigate the interference between a shifted pilot and a shifted data symbol. Therefore, the number of nulls at each side of pilots, P_n, should be chosen in such a way that, it creates a frequency separation bigger than the maximum frequency shift, and is expressed as

$$P_n > \frac{f_{d_{\max}}}{\Delta f}, \tag{5.8}$$

where Δf is the frequency separation between two sub-carriers.

After designing the sub-frame, the final OFDM frame is created by concatenating multiple sub-frames. In the next section, the sub-frame design for two OFDM systems will be analyzed and the performance of the proposed system will be evaluated using MATLAB simulations and measurements.

5.4 System Evaluation

5.4.1 System Deployment Procedure

In Fall 2016, a sea trial was run in Shad Bay, Nova Scotia, to characterize the undersea channel conditions and to evaluate the performance of the communication link. The physical and geometrical parameters of the channel are summarized in Table 5.1. Note that one of the main applications of the proposed communications system is in underwater mobile networks for aquaculture industry. The Shad Bay geometry is a good representative of aquaculture sites, so it is chosen for the measurements.

In this test, the core of the transmitter (receiver) consists of a digital signal processing core which can transmit and record the acoustic wave using a custom front-end designed at Amirix Systems Inc.

During the deployment, the transmitter is equipped with a wideband projector that is approximately 26.5 meters deep and is driven by a power amplifier. The power amplifiers' output power is controlled to maintain a reasonable signal-to-noise ratio at the receiver without saturating the electronics. Pre-recorded sound files are sent using a 16-bit data acquisition card. The sample rate of the data converter is 960 kHz. In this work, a channel sounder and two OFDM communication systems, with different specifications, are tested. The pre-recorded sound file, which is uploaded into the DSP memory, consists of a chirp sequence for channel sounding purpose, a packet of system #1 and a packet of system #2. These files are concatenated sequentially with a short guard interval of zeros between them. The number of continuously transmitted chirp sequences, the packets of system #1 and the packets of system #2 are 300, 12 and

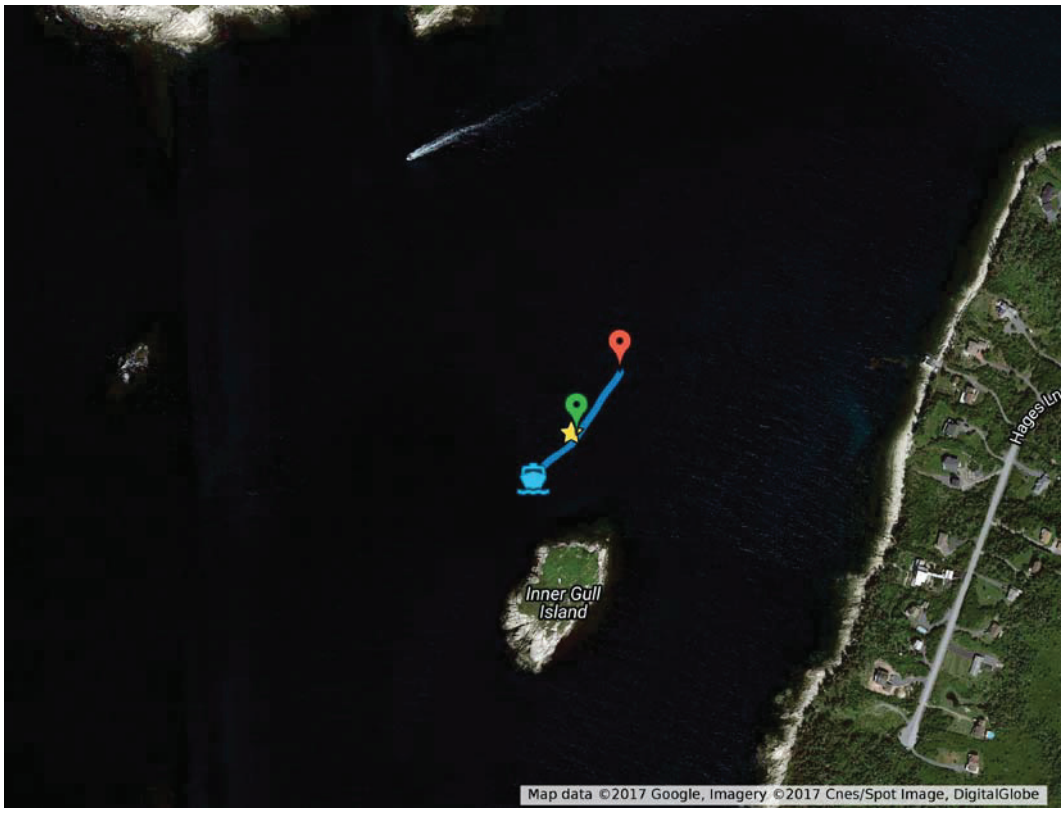

Figure 5.4: Demonstration of the location of the sea trial on the map. The total traveled distance is 161m. The maximum measured speed is $0.9\frac{\mathrm{m}}{\mathrm{s}}$. The boat icon shows the point that the boat started drifting. The star shows the location of the transmitter. The green icon represents the point where the receiver started recording and the red icon shows the point where the receiver stopped recording.

12, respectively.

At the receiver, the hydrophone projector is lowered to approximately 1.5 meters from the sea surface. The receiver is attached to a boat which is drifting at the surface with an average speed of 0.3 $\frac{\mathrm{m}}{\mathrm{s}}$, which is simply calculated using the information in Table 5.1. The speed of the wind is approximately 1 $\frac{\mathrm{m}}{\mathrm{s}}$ and the dark brown color of water shows a high level of turbidity. The turbidity results in a low signal to noise power ratio at the receiver side in short range. The traveled path between the transmitter and receiver is shown on the map in Figure 5.4. The digital acquisition card samples the received signal at 480 kHz and saves the digital information to a sound file for post-processing. The channel sounding algorithm is explained in Appendix A. Figure 5.5a shows the channel impulse response of the measured channel.

Parameter	**Value**
Total depth (H)	28 m
Depth of the transmitter (h_{tx})	26.5 m
Depth of the receiver (h_{rx})	1.5 m
Initial distance (d_0)	68 m
Distance between the walls (d_w)	400 m
Distance from the reference wall to the transmitter (d_{wt})	200 m
Distance from the reference wall to the receiver (d_{wt})	200 m
Initial velocity (v_0)	$-0.29\ \frac{\text{m}}{\text{s}}$
Maximum velocity ($v_{\max}$)	$-0.9\ \frac{\text{m}}{\text{s}}$
Average acceleration (a)	$-0.001\ \frac{\text{m}}{\text{s}^2}$
Surface reflection loss (Γ_s)	10 dB
Bottom reflection loss (Γ_b)	14 dB
Wall reflection loss (Γ_w)	14 dB
Noise floor of the Doppler spectra (N_F)	-71.5 dB
Shape factors of the Doppler spectra	$c_1 = 0.0049$, $c_2 = 0.2271$
Signal to noise ratio	5.5 dB

Table 5.1: Geometrical parameters of sea trial and input parameters of the channel simulator.

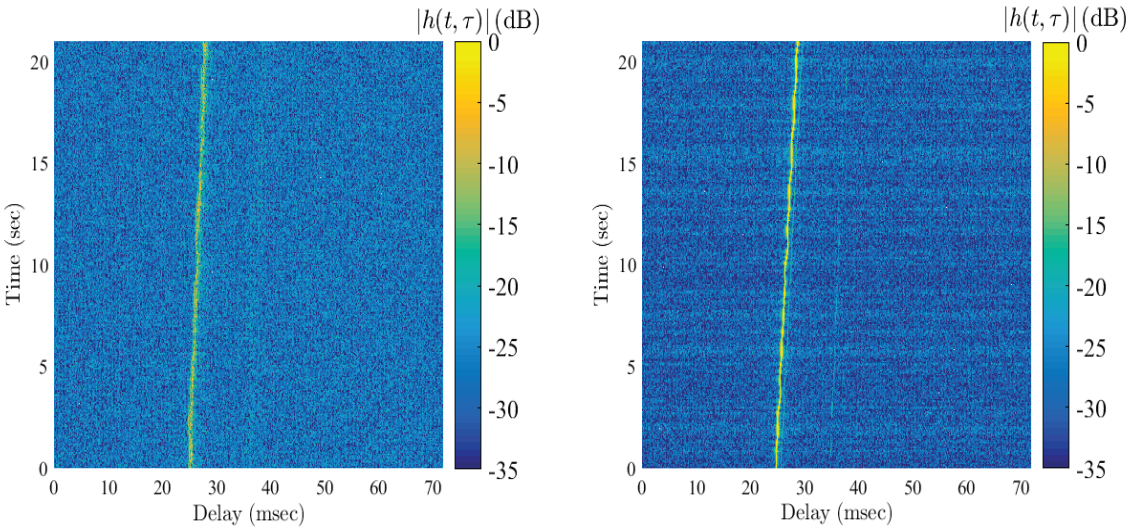

(a) Measured CIR

(b) Simulated CIR

Figure 5.5: Measured and simulated channel impulse responses.

The Doppler power spectrum of this channel and its approximation are demonstrated in Figure 5.6.

In this system design, the packet structure, which was explained in Section 4.1 is

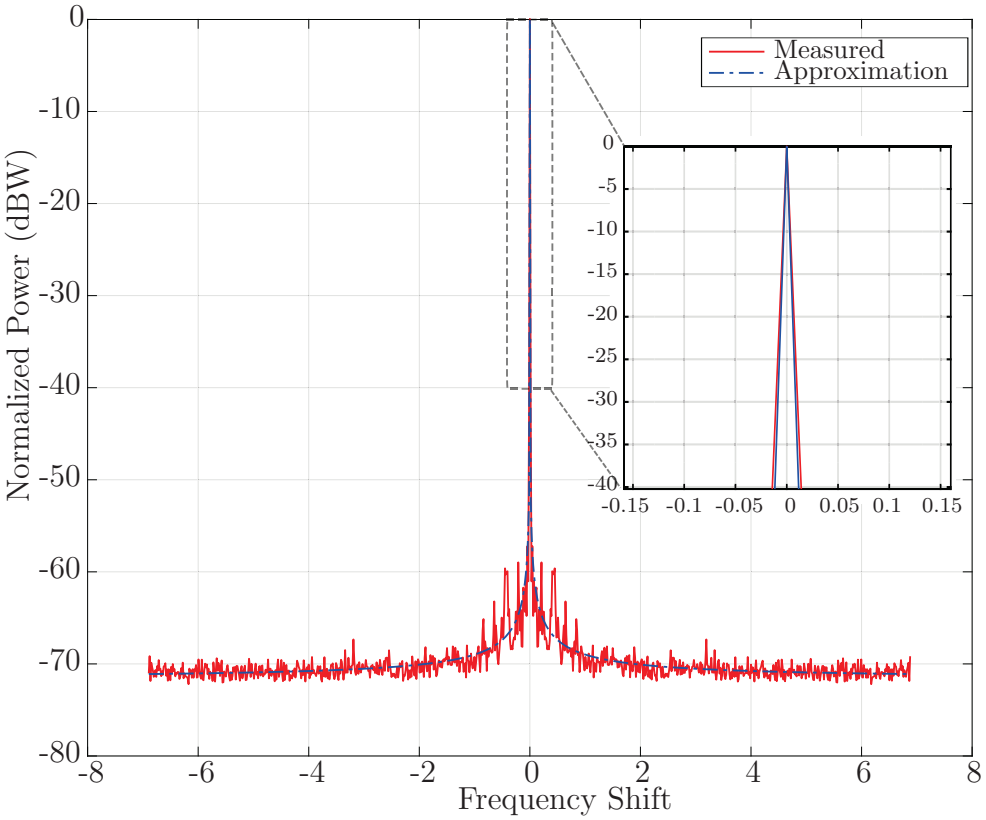

Figure 5.6: Measured Doppler power spectrum and its approximation.

utilized. Each OFDM packet contains a chirp sequence as a preamble, 6 OFDM blocks and a guard of zeros between the preamble and the OFDM blocks. The parameters of the two communication systems are summarized in Table 5.2. Note that system parameters are chosen based on the hardware limitations and they are adjusted to be used in underwater sensors, produced by Amirix System Inc.

Different sets of parameters such as, total number of sub-carriers, total number of pilot sub-carriers, bandwidth, central frequency, maximum tolerable frequency shift, and etc. are chosen for the system #1 and system #2, to compare the performance of the Doppler compensation and equalization components, using different settings.

The packet synchronization approach which was explained in Section 4.1, is used here to find the start of each packet. Figure 5.7 shows the results of the cross-correlation of the reference preambles and the received packets of system #1 and system #2.

Parameter	**System #1**	**System #2**
Total Number of sub-carriers (N)	512	1024
Total Number of data sub-carriers (K_d)	64	160
Total Number of pilot sub-carriers (K_p)	64	96
Total Number of null sub-carriers (K_n)	384	768
Number of data sub-carriers in a sub-frame (P_d)	2	4
Number of pilot sub-carriers in a sub-frame (P_p)	2	3
Number of null sub-carriers in a sub-frame (P_n)	6	12
Modulation	BPSK	BPSK
Sampling frequency (f_s)	960 kHz	960 kHz
Bandwidth (B)	19 kHz	20 kHz
Carrier frequency (f_c)	121 kHz	130 kHz
Fractional bandwidth $\left(\frac{B}{f_c}\right)$	15.7%	15.4%
Frequency separation (Δf)	37.1 Hz	19.5 Hz
Maximum tolerable frequency shift ($P_n \times \Delta f$)	222.6 Hz	234.4 Hz
Block duration (T_b)	33.6 ms	60.2 ms
Cyclic prefix duration (T_{cp})	6.4 ms	9 ms
Number of blocks in each packet (M)	6	6
Length of preambles	27.2 ms	51.2 ms

Table 5.2: Parameters of communication systems

The average signal to noise ratio during this test was 5.5 dB which was measured by averaging the power of noise within the guard zeros. However, as it is observed in Figure 5.7, the average power of noise is higher for some packets because of the presence of a bursty noise, i.e. packets number 7 and 8 in system #1. The bursty noise which can occur because of the biological sounds, degrades the performance of the system, effectively. The correlation peak to noise floor ratio is higher in system #2 because, the length of the reference preamble is longer in this system (See Table 5.2).

After frame synchronization, the received packets are down-converted and decimated to the symbol rate. Then, the time-varying time-scaling factor estimation method is applied on each packet. The constant estimated time-scaling factor of each OFDM block is directly related to the relative velocity between the transmitter and receiver that is observed on that block. Some examples of estimated relative velocities are shown in Figure 5.8. As can be seen from the Figure 5.8, the relative speed is changing from one OFDM block to the next with a random pattern. This observation proves the

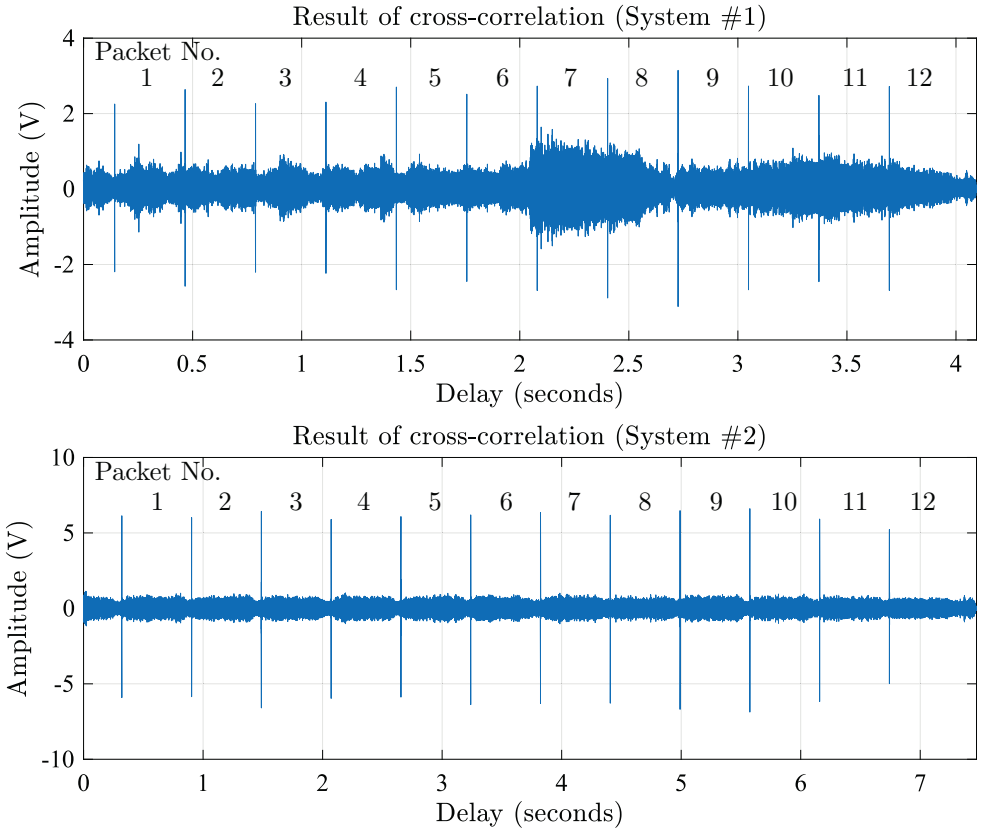

Figure 5.7: The result of the cross-correlation between the received packets and reference preambles. The length of reference preamble in the system #1 and system #2 are 27.2 ms and 51.2 ms, respectively.

necessity for using a time-varying Doppler compensation method, as the innovative method that is proposed in this thesis.

After Doppler compensation and block synchronization, the channel impulse response on each OFDM block is estimated using the LS method and the received block is equalized. Finally, the equalized signal is fed into the demodulation and decoding blocks. The decoded bits are compared to the transmitted bits to calculate the detection error. This procedure is called bit error rate (BER) analysis.

In this work the OFDM systems are evaluated in MATLAB simulations, as well. The channel simulator, which was developed in Chapter 2, is used for the simulation. The geometrical parameters of the channel are the same as sea trial. The results of the BER analysis of the measured and simulated systems are presented and compared in

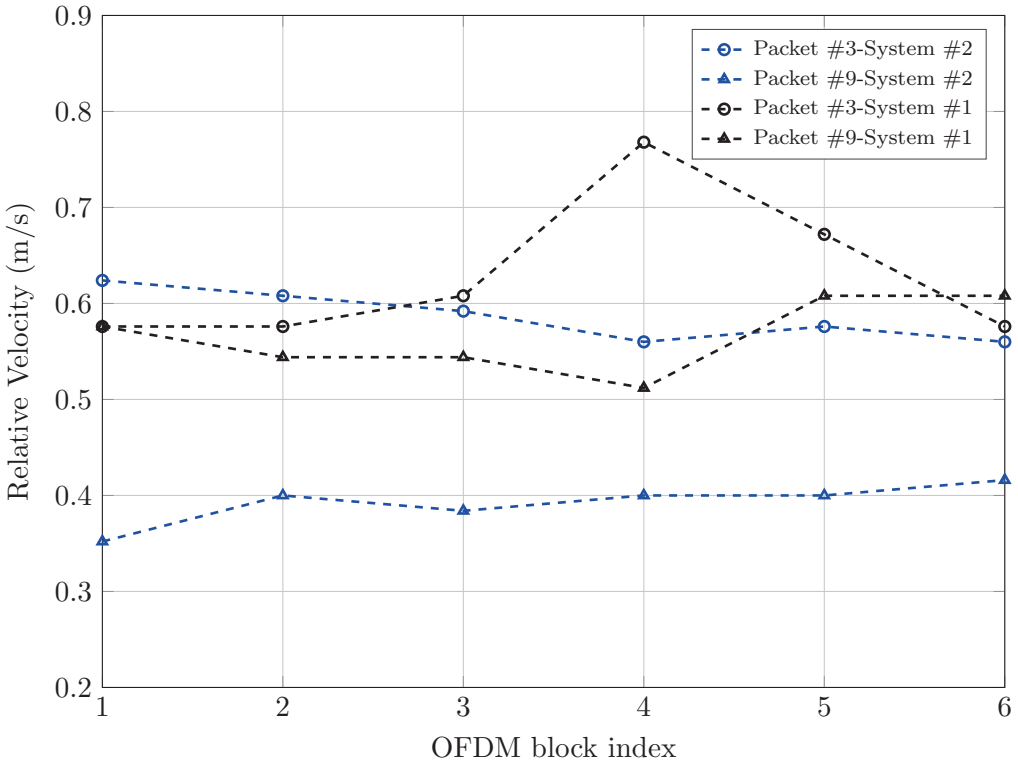

Figure 5.8: Examples of the estimation of the relative speed.

the next section.

5.4.2 Bit Error Rate Analysis

BER analysis is a testing method for digital communication systems in which the performance of the system is evaluated by sending a long sequence of symbols through the channel and calculating the detection errors at the receiver.

As mentioned in Table 5.1, the maximum velocity is equal to $v_{\max} = 0.9\frac{\mathrm{m}}{\mathrm{s}}$. By considering Equation (5.6), the maximum frequency components of the system #1 and system #2 are 130.5 kHz and 150 kHz, respectively. The respective maximum Doppler shifts are calculated using Equation (5.7), and they are equal to 78.3 Hz and 90 Hz. These frequency shifts are smaller than the maximum tolerable Doppler shift of either of the proposed systems (See Table 5.2). Therefore, the pilot placement should work efficiently in this scenario.

Because of the necessity of using an error-correction code in improving the performance of an OFDM communication link subject to frequency selectivity, a simple 1/3 repetition code is applied to these systems. This means that for this coding scheme, each OFDM block is retransmitted three times in the time-domain [48]. At the receiver side, the repetition decoding is done using majority logic detection. In this method, to determine the value of a particular bit, the received copies of the bit in the stream are verified and the value that occurs more frequently is chosen. Although this technique is suboptimal in contrast for example to using convolutional codes, the purpose of applying redundancy here is to demonstrate the reliability of the Doppler compensation method.

To examine the reliability of the proposed Doppler compensation method, another set of simulations is conducted in two scenarios. In the first scenario it is assumed that the time-varying delay of the strongest path is known and it is used for the Doppler compensation. The time-scaling spread is small in the simulated channel, therefore referring to Section 3.2 the time-scaling factor of the strongest path is equal to the optimum resampling factor. Also, in this scenario it is assumed that the multipath delay and amplitudes are known and the channel equalization is optimum. Thus, the first scenario is called the optimum channel equalization. Moreover, in the second scenario, the proposed Doppler compensation method, pilot aided (PA) compensation, is tested.

The physical and geometrical parameters of the channel which were described in Table 5.1 are used in these simulations. The simulated BER curves of the system #1 and system #2 are shown in Figure 5.9a and Figure 5.10a, respectively.

As observed, the proposed system (PA) shows a reliable BER performance in high SNRs (higher than 15 dB). However, the optimum equalization generally has a much better BER performance than the pilot aided compensation scenario. In addition a comparison between the BER curves of system #1 with 64 pilot sub-carriers and system #2 with 96 pilot sub-carriers shows that the Doppler and channel estimation is improved by increasing the number of pilot sub-carriers.

The UWA channel model simulates a multi-scale multipath scenario in which each

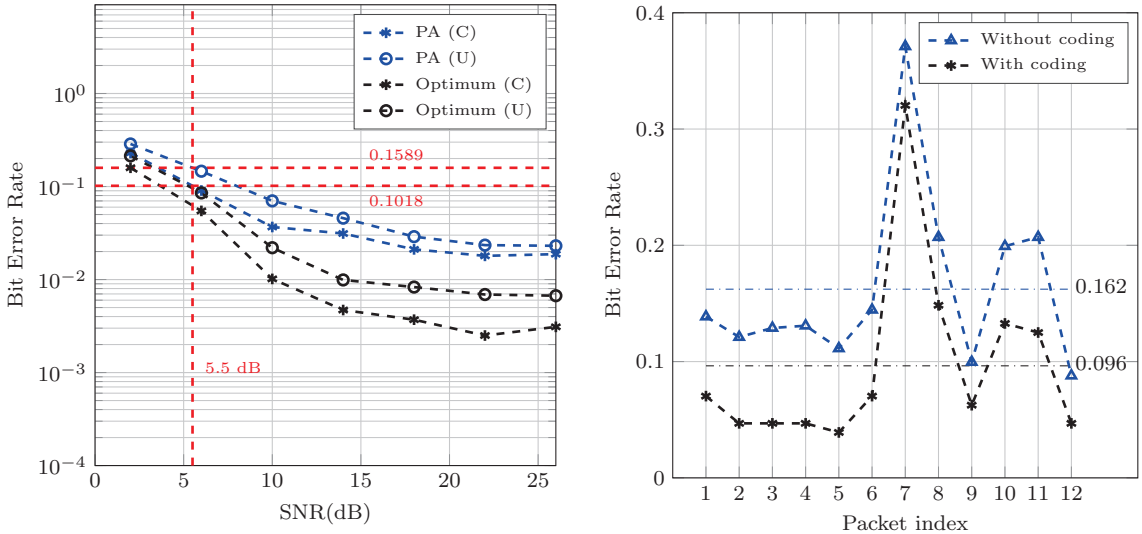

(a) Simulated BER

(b) Measured BER

Figure 5.9: BER analysis of system #1. The red lines in (a) show the value of BER in 5.5 dB for system with PA compensation (with and without coding).

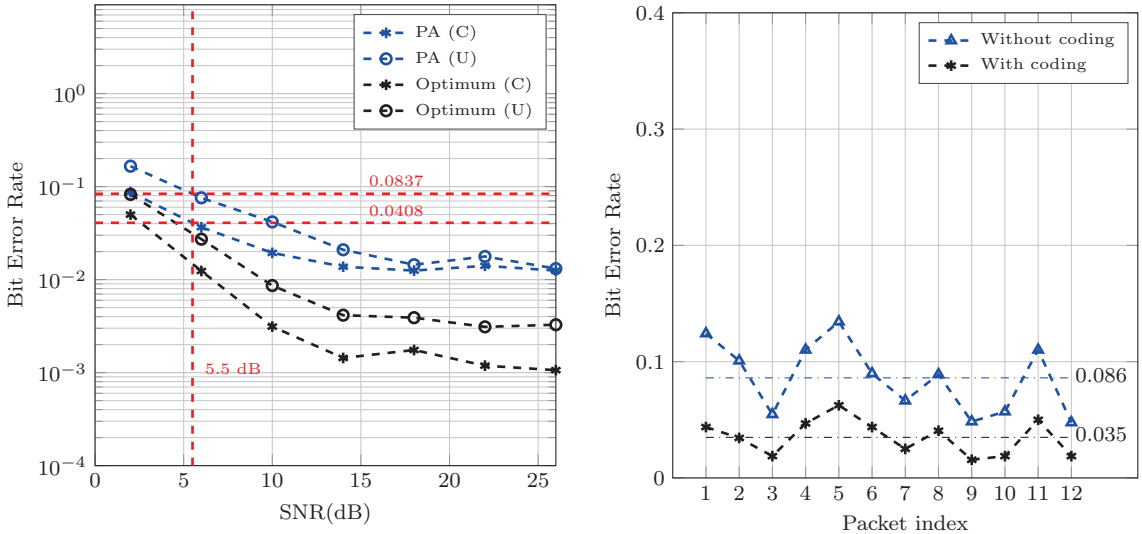

(a) Simulated BER

(b) Measured BER

Figure 5.10: BER analysis of system #2. The red lines in (a) show the value of BER in 5.5 dB for system with PA compensation (with and without coding).

path arrival has a different time-scaling factor. Therefore, the Doppler compensation with respect to the time-varying delay of the strongest path (optimum scenario) is not perfect in either of these systems. As a result, the BER curves converge to zero BER slowly and they may reach to an error floor.

The other channel effect which deteriorate the performance of the systems is fading amplitude. An interesting observation is that applying the repetition codes can improve the performance deterioration that happens due to fading.

One way that the total BER performance of the system can be improved, is by increasing the number of hydrophones at the receiver and applying diversity techniques such as Maximum Ratio Combining (MRC) [18]. Also, an alternative approach to enhance the BER performance of the system effectively is to use an efficient error correcting coding technique in the sub-carriers (frequency) domain, such as linear block codes or convolutional codes [18]. Some of the techniques that can lead to a better system performance are discussed in Section 6.2.

In addition to simulations, the BER of both systems is evaluated in measurements and the results are presented in Figure 5.9b and Figure 5.10b. Although the SNR does not remain constant during the measurement, the average measured SNR in both cases is 5.5 dB.

System #1 with and without repetition coding has a bit rate of 560 bits/s and 1680 bits/s, respectively. According to Figure 5.9a the respective BERs of the system #1 using PA compensation at SNR = 5.5 dB, are 0.102 and 0.159. These BERs are very close to the average measured BERs which are 0.096 and 0.162, respectively for system with and without repetition coding (See Figure 5.9b). More accurately, with 95 % confidence, the measured BERs of the coded and uncoded system are in the ranges of $(0.153, 0.172)$ and $(0.082, 0.112)$, respectively.

Also, system #2 with and without repetition coding has a bit rate of 776 bits/s and 2328 bits/s, respectively. As shown in Figure 5.10a the BERs of system #2 with and without coding and by using PA compensation at a SNR = 5.5 dB, are 0.041 and 0.084, respectively. According to Figure 5.10b, the measured respective BERs are, 0.035 and 0.086 which are very close to simulated values. The respective measured BER intervals of the coded and uncoded system with 95 % confidence are $(0.029, 0.041)$ and $(0.082, 0.091)$, respectively.

The results of measurement and simulation of system #2 are even closer in comparison to system #1, because no bursty noise occurs during the measurement of system #2.

Therefore, by comparing the results of the bit error rate analysis of simulated and measured systems, it is concluded that the proposed channel simulator presents a software tool for testing communication systems which simulates a condition that is very similar to the real world condition.

Chapter 6

Conclusion

In this thesis a time-varying Doppler compensation method for a coherent communication system relying on OFDM receiver was proposed to create a reliable communication link in the underwater environment with time-varying relative speed between the receiver and transmitter. In this chapter a summary of the results is presented in Section 6.1. Section 6.2 discusses some particular techniques to help the improvement of capabilities of the proposed system in the future.

6.1 Summary of Contributions and Results

This thesis had two main contributions. The first contribution was covered in Chapter 2, and it is the development of a realistic stochastic UWA channel model based on the geometry of specific deployments. First, the physical effects of the UWA channel were analyzed in detail. Then, based on the WSSUS assumption for shallow underwater environments, the mathematical model of the time-varying multipath channel is presented by dividing the time-variability effect of the channel into two parameters: time-varying delay and time-varying amplitude.

The time-varying delay is calculated for a given geometry using the physics of wave propagation in a bounded environment like the ocean. This time-varying delay then is implemented in the software channel simulator using a creative resampling method which is called TVFDL. Later in Section 2.4.1 it was shown, through simulations, that the TVFDL is able to realize any kind of high order time-variation of the channels.

The effect of time-varying amplitude of the received paths is related to two parameters, time-varying transmission loss and time fading. The time-varying transmission

loss is calculated using the time-varying distance between the transmitter and receiver. On the other hand, the fading amplitude is generated based on the Doppler spectrum of the measured channels. The procedure of fading amplitude generation was described in Section 2.4.2. Using this method the Doppler spectrum of a set of measured channels can be completely recreated.

The channel sounder, which was used in the sea trial, was run through the channel simulator using the same geometrical and statistical parameters to obtain a fair comparison between the measured and simulated channels. The results that were presented in Section 2.4.3 show a high degree of similarity between the measured and simulated channels.

In Chapter 3, the OFDM system was introduced as a reliable technique for frequency selective channels. The multi-scale multipath channel was defined as a time-varying multipath channel with different time-scaling factors on each path which is a scenario that is usually observed in UWA channel. Then, the effect of the multi-scale multipath channel on the OFDM system is analyzed and the necessity of estimation of an optimum time-scaling factor for Doppler compensation was discussed.

The second contribution of this thesis was developed in Chapter 4. First a traditional packet synchronization and coarse channel estimation technique using training sequences was discussed. Then, in Section 4.2, an innovative time-varying time-scaling compensation technique was developed. The time-scaling factor of each OFDM block is estimated by adjusting a conventional method which utilizes the pilot sub-carriers for this purpose. In this adjustment the block-type pilot arrangement of the conventional method is changed with an optimum comb-type pilot arrangement and the packet by packet Doppler compensation is changed to block (OFDM block) by block process. Then, the time-varying time-scaling factor is approximated over the whole OFDM packet using an interpolation method. Finally, the packet is resampled in a time-varying manner using the estimated time-varying time-scaling factor by utilizing the TVFDL. In this case, again TVFDL is utilized for resampling because of its flexibility and simplicity in dynamic resampling.

To assess the functionality of the proposed Doppler compensation method, it was

integrated into a full OFDM receiver in Chapter 5. To simplify the system design, the least square estimator was chosen for channel estimation purpose. The importance of developing an optimum sub-carrier allocation method to handle the Doppler estimation using pilot sub-carriers was stated. This was followed by the procedure of a reliable sub-carrier allocation technique.

The proposed OFDM system was tested using MATLAB simulations with the developed channel simulator. The results of BER rate analysis show how the Doppler compensation method can effectively improve the reliability of the system in mobile communication scenarios. The simulations show that the BER performance of the system which uses the proposed Doppler compensation method reaches to the BER performance of the system which uses the optimum Doppler compensation.

Finally in Section 5.4, the performance of the system was tested in a sea trial. The procedure of the sea trial was explained and the BER rate of multiple OFDM frames was measured for the proposed system with two different adjustments. The purpose of testing the system with different parameters, such as different bandwidths, carrier frequencies, numbers of sub-carriers and sub-carrier allocations, was to show the impact of optimum pilot design in increasing the performance of the OFDM system. In the particular case of this measurement, the system with a higher number of pilots and better pilot protection showed a better performance than the other system.

The most important assertion of this measurement was the high degree of resemblance between the measured and simulated BER. The absolute error between the measured and simulated BER of the system #1 and system #2 in an SNR=5.5 dB is 6×10^{-3} for both systems which is relatively small. This shows the ability of the channel simulator to model the real world conditions.

6.2 Future Works

There are certain signal processing and digital communication techniques that can improve the viability of the proposed channel model and communications system. They are summarized below.

In Chapter 2 it is assumed that the time-varying delay is a result of the relative motion of the transmitter and receiver due to motor force and/or drifting of the underwater vehicle. In fact, the random motion of scatterers, such as random waves, was not considered in the delay variance. These effects can be added to the channel model by analyzing each source of random time-variation separately and adding more physical parameters such as the speed of the wind at the surface, the temperature and the pressure at various depths. However, considering these parameters requires some accurate stochastic analysis and it can make the channel implementation of the channel significantly complicated.

In Chapters 4 and 5 developing a more efficient sub-carrier allocation can improve the accuracy and feasibility of the Doppler and channel estimation in specific conditions. Therefore, as future research, exploring the effect of placing the pilots and nulls in different fashions and with different densities can be valuable.

In addition, in the proposed communications system, replacing the LS channel estimation technique with a more accurate channel estimation methods such as the MMSE can improve the performance of the system considerably. Also, as shown in [18], utilizing an array of hydrophones at the receive side and applying different diversity techniques, such as Maximum Ratio Combining can be advantageous in improving the BER performance.

Finally, the repetition coding technique, which was used in this thesis is very simple but it is not bandwidth efficient. The other area that could improve the performance of the communications is applying more efficient coding techniques across the sub-carriers, such as cyclic error correcting codes.

Bibliography

[1] G. McIntyre, "Sparse directional estimation of the time-varying underwater acoustic channel," master's thesis, Dalhousie University, Halifax, NS, Canada, September 2015.

[2] "Discovery of sound in the sea." `http://www.dosits.org/people/history`. Accessed: 2017-02-14.

[3] L. Lanbo, Z. Shengli, and C. Jun-Hong, "Prospects and problems of wireless communication for underwater sensor networks," *Wireless Communications and Mobile Computing*, vol. 8, no. 8, pp. 977–994, 2008.

[4] "BLUECOMM underwater optical communication." `https://www.sonardyne.com/product/bluecomm-underwater-optical-communication-system/`. Accessed: 2017-02-14.

[5] P. Qarabaqi and M. Stojanovic, "Statistical characterization and computationally efficient modeling of a class of underwater acoustic communication channels," *IEEE Journal of Oceanic Engineering*, vol. 38, pp. 701–717, Oct 2013.

[6] M. B. Porter, "Bellhop code." `http://oalib.hlsresearch.com/Rays/index.html`.

[7] J. C. Peterson and M. B. Porter, "Ray/Beam tracing for modeling the effects of ocean and platform dynamics," *IEEE Journal of Oceanic Engineering*, vol. 38, pp. 655–665, Oct 2013.

[8] S. M. Kay and S. B. Doyle, "Rapid estimation of the range-Doppler scattering function," in *OCEANS, 2001. MTS/IEEE Conference and Exhibition*, vol. 1, pp. 34–39 vol.1, 2001.

[9] P. A. van Walree, T. Jenserud, and M. Smedsrud, "A discrete-time channel simulator driven by measured scattering functions," *IEEE Journal on Selected Areas in Communications*, vol. 26, pp. 1628–1637, December 2008.

[10] E. Baktash, M. J. Dehghani, M. R. F. Nasab, and M. Karimi, "Shallow water acoustic channel modeling based on analytical second order statistics for moving transmitter/receiver," *IEEE Transactions on Signal Processing*, vol. 63, pp. 2533–2545, May 2015.

[11] C. Liu, Y. V. Zakharov, and T. Chen, "Doubly selective underwater acoustic channel model for a moving transmitter/receiver," *IEEE Transactions on Vehicular Technology*, vol. 61, pp. 938–950, March 2012.

[12] M. Stojanovic and J. Preisig, "Underwater acoustic communication channels: Propagation models and statistical characterization," *IEEE Communications Magazine*, vol. 47, pp. 84–89, January 2009.

[13] F. X. Socheleau, C. Laot, and J. M. Passerieux, "Stochastic replay of Non-WSSUS underwater acoustic communication channels recorded at sea," *IEEE Transactions on Signal Processing*, vol. 59, pp. 4838–4849, Oct 2011.

[14] R. J. Urick, *Principle Of Underwater Sound*. McGraw-Hill, 2nd ed., 1983.

[15] S. M. Flatte, "Wave propagation through random media: Contributions from ocean acoustics," *Proceedings of the IEEE*, vol. 71, pp. 1267–1294, Nov 1983.

[16] F. Hlawatsch and G. Matz, *Wireless Communications Over Rapidly Time-Varying Channels*. Academic Press, 1st ed., 2011.

[17] M. A. Chitre, "A high-frequency warm shallow water acoustic communications channel model and measurements," *The Journal Of The Acoustical Society Of America*, vol. 122, pp. 2580–2586, Nov 2007.

[18] B. Li, S. Zhou, M. Stojanovic, L. Freitag, and P. Willett, "Multicarrier communication over underwater acoustic channels with nonuniform Doppler shifts," *IEEE Journal of Oceanic Engineering*, vol. 33, pp. 198–209, April 2008.

[19] X. Lurton, *An Introduction to Underwater Acoustics (2Nd Ed.)*. UK: Springer Praxis Books, 2010.

[20] A. D. Jones, A. J. Duncan, A. Maggi, J. Sendt, and P. A. Clarke, "Modelling acoustic reflection loss at the ocean surface for small angles of incidence," in *OCEANS 2010 IEEE - Sydney*, pp. 1–10, May 2010.

[21] P. A. van Walree, "Propagation and scattering effects in underwater acoustic communication channels," *IEEE Journal of Oceanic Engineering*, vol. 38, pp. 614–631, Oct 2013.

[22] A. V. Oppenheim, R. W. Schafer, and J. R. Buck, *Discrete-time Signal Processing (2Nd Ed.)*. Upper Saddle River, NJ, USA: Prentice-Hall, Inc., 1999.

[23] C. Liu, Y. V. Zakharov, and T. Chen, "Doubly selective underwater acoustic channel model for a moving transmitter/receiver," *IEEE Transactions on Vehicular Technology*, vol. 61, pp. 938–950, March 2012.

[24] S. Yerramalli and U. Mitra, "Optimal resampling of OFDM signals for multiscale-multilag underwater acoustic channels," *IEEE Journal of Oceanic Engineering*, vol. 36, pp. 126–138, Jan 2011.

[25] T. Rappaport, *Wireless Communications: Principles and Practice*. Upper Saddle River, NJ, USA: Prentice Hall PTR, 2nd ed., 2001.

[26] A. Goldsmith, *Wireless Communications*. New York, NY, USA: Cambridge University Press, 2005.

[27] Z. Wang, S. Zhou, J. Catipovic, and J. Huang, "Factor-graph-based joint IBI/ICI mitigation for OFDM in underwater acoustic multipath channels with long-separated clusters," *IEEE Journal of Oceanic Engineering*, vol. 37, pp. 680–694, Oct 2012.

[28] S. Plass, A. Dammann, S. Kaiser, and K. Fazel, eds., *Multi-carrier spread spectrum 2007*. Springer, 2007.

[29] I. R. Capoglu, Y. Li, and A. Swami, "Effect of doppler spread in OFDM-based UWB systems," *IEEE Transactions on Wireless Communications*, vol. 4, pp. 2559–2567, Sept 2005.

[30] M. Stojanovic, "Low complexity OFDM detector for underwater acoustic channels," in *OCEANS 2006*, pp. 1–6, Sept 2006.

[31] S. F. Mason, C. R. Berger, S. Zhou, and P. Willett, "Detection, synchronization, and Doppler scale estimation with multicarrier waveforms in underwater acoustic communication," *IEEE Journal on Selected Areas in Communications*, vol. 26, pp. 1638–1649, December 2008.

[32] N. Parrish, S. Roy, and P. Arabshahi, "Symbol by symbol doppler rate estimation for highly mobile underwater OFDM," in *Proceedings of the Fourth ACM International Workshop on UnderWater Networks*, WUWNet '09, (New York, NY, USA), pp. 1:1–1:8, ACM, 2009.

[33] A. Abdelkareem, B. Sharif, and C. Tsimenidis, "Adaptive time varying Doppler shift compensation algorithm for OFDM-based underwater acoustic communication systems," *Ad Hoc Netw.*, vol. 45, pp. 104–119, July 2016.

[34] S. Boumard and A. Mammela, "Robust and accurate frequency and timing synchronization using chirp signals," *IEEE Transactions on Broadcasting*, vol. 55, pp. 115–123, March 2009.

[35] Yushi Shen and Ed Martinez, NXP Semiconductor, "Channel Estimation in OFDM Systems, Application Note." `http://www.nxp.com/files/dsp/doc/app_note/AN3059.pdf`, 2006.

[36] A. B. Salberg and A. Swami, "Doppler and frequency-offset synchronization in wideband OFDM," *IEEE Transactions on Wireless Communications*, vol. 4, pp. 2870–2881, Nov 2005.

[37] J. K. Tugnait, L. Tong, and Z. ding, "Single-user channel estimation and equalization," *IEEE Signal Processing Magazine*, vol. 17, pp. 16–28, May 2000.

[38] M. K. Ozdemir and H. Arslan, "Channel estimation for wireless OFDM systems," *IEEE Communications Surveys Tutorials*, vol. 9, pp. 18–48, Second 2007.

[39] D. V. Welden and H. Steendam, "Near optimal iterative channel estimation for KSP-OFDM," *IEEE Transactions on Signal Processing*, vol. 58, pp. 4948–4954, Sept 2010.

[40] J. J. van de Beek, O. Edfors, M. Sandell, S. K. Wilson, and P. O. Borjesson, "On channel estimation in OFDM systems," in *Vehicular Technology Conference, 1995 IEEE 45th*, vol. 2, pp. 815–819 vol.2, Jul 1995.

[41] Y. Li, L. J. Cimini, and N. R. Sollenberger, "Robust channel estimation for OFDM systems with rapid dispersive fading channels," *IEEE Transactions on Communications*, vol. 46, pp. 902–915, Jul 1998.

[42] J. Ma, H. Yu, and S. Liu, "The MMSE Channel Estimation Based on DFT for OFDM System," in *5th Intl. Conf. Wireless Commun. Netw. Mob. Comput.*, pp. 1–4, Sept 2009.

[43] M. Stojanovic, "MIMO OFDM over underwater acoustic channels," in *2009 Conference Record of the Forty-Third Asilomar Conference on Signals, Systems and Computers*, pp. 605–609, Nov 2009.

[44] C. R. Berger, Z. Wang, J. Huang, and S. Zhou, "Application of compressive sensing to sparse channel estimation," *IEEE Communications Magazine*, vol. 48, pp. 164–174, November 2010.

[45] C. R. Berger, S. Zhou, J. C. Preisig, and P. Willett, "Sparse channel estimation for multicarrier underwater acoustic communication: From subspace methods to compressed sensing," *IEEE Transactions on Signal Processing*, vol. 58, pp. 1708–1721, March 2010.

[46] P. van Walree, "Channel sounding for acoustic communications: techniques and shallow-water examples." `http://rapporter.ffi.no/rapporter/2011/00007.pdf`.

[47] S. Mason, C. Berger, S. Zhou, K. Ball, L. Freitag, and P. Willett, "An OFDM design for underwater acoustic channels with Doppler spread," in *2009 IEEE 13th Digital Signal Processing Workshop and 5th IEEE Signal Processing Education Workshop*, pp. 138–143, Jan 2009.

[48] J. Proakis and M. Salehi, *Digital Communications (5th Ed.)*. New York, NY, USA: McGraw-Hill, 2008.

Appendix A

Channel Sounder Design

Channel sounding consists of sending a known signature through the channel and then processing the received signal to effectively obtain the channel information. Different types of channel sounders can be designed based on the type of signature signal and the procedure for signal processing. The selection of the signature signal depends on the channel characteristics. According to [46] a correlative channel sounder is suitable for UWA channels. In this type of channel sounder, the reference signature is continuously concatenated and repeated, without guard intervals, to create the sounding packet. Then, this packet is converted to passband and applied to a UWA channel.

At the receiver side, the received packet is down-converted and stored in memory for further offline processing to extract the channel impulse response.

The mathematics of the channel sounding procedure in the continuous time domain are summarized here. Applying a transmit sequence, $x_{\text{ref}}(t)$ to a time-invariant multipath channel with impulse response of $h(\tau)$ produces an output which is described as,

$$y(t) = \int_{-\infty}^{\infty} x_{\text{ref}}(t-\tau)h(\tau)d\tau. \tag{A.1}$$

The auto-correlation of the reference signature is,

$$R_{xx}(t) = \int_{-\infty}^{\infty} x^*_{\text{ref}}(t)x(t+\nu)d\nu. \tag{A.2}$$

Also, the cross-correlation between the received signature, $y(t)$ and reference signature is,

$$R_{xy}(t) = \int_{-\infty}^{\infty} x^*_{\text{ref}}(t)y(t+\nu)d\nu. \tag{A.3}$$

By replacing Equation A.1 in Equation A.3, it is changed to,

$$R_{xy}(t) = \hat{h}(\tau) = \int_{-\infty}^{\infty} R_{xx}(t-\tau)h(\tau)d\tau. \tag{A.4}$$

where $\hat{h}(\tau)$ is the estimation of the time-invariant multipath channel. According to Equation A.4, if the reference signature is chosen in such a way that the auto-correlation has a shape like a Delta function, $\delta(t)$, the estimation of the channel impulse response is equal to the cross-correlation between the reference signature and the received signal. Therefore, the auto-correlation properties play an essential role in the design of the reference signature.

In a time-varying channel, like UWA channel, the period of reference signature, T, must be at least as long as the channel delay spread, $\hat{\tau}_s$, in order to cover the entire impulse response in each slice of time. Also, the chip rate, T^{-1}, must be high enough to track the time variability. The other important parameter in channel sounder design is the central frequency, f_c. This parameter is important because it determines where the sounding is happening. In other words, by changing the central frequency, some of the characteristics of the channel, such as attenuation rate and Doppler shift, may change which can affect the channel impulse response.

After selecting the sounding signature, to extract a time-varying channel impulse response, a long packet of M passband reference signatures are concatenated after each other and sent through the channel. At the receiver side, first, the received packet is segmented into M parallel sequences in windows of equal duration to the reference. Then the cross-correlation between each partitioned sequence and the reference signature is calculated. The results of the cross-correlation are stacked on top of each other to make the channel impulse response in time-delay plot.

Two characteristics of the signature signal should be considered in the time-varying channel sounder design, the resolution of the auto-correlation in the delay domain and the sensitivity of the signature to Doppler effect. The second characteristic is observed as time-scaling or constant frequency shift.

The two main types of signature signals that are usually used in channel sounder design are the *Pseudorandom Noise (PN) sequence* and *Linear Frequency Modulated (LFM) sequence* (also known as *chirp*). These signals are usually used because of their appropriate auto-correlation properties.

In the digital world, the PN code is a sequence of zeros and ones which is generated

deterministically. This sequence has a spectrum similar to white noise. It means that, the PN code has a wide frequency flat spectrum. The PN codes can be modulated with one of the conventional digital modulation techniques such as BPSK or QAM, to form the sounding signature.

The LFM sequence is a signal in which the frequency is increasing (or decreasing) linearly with time. The spectrum of the LFM sequence has a rectangular pulse shape which is flat in a certain frequency range, which makes it suitable for wide-band channel sounding.

To compare the properties of the LFM and PN sequences, the ambiguity function of the signature is defined as a two-dimensional function of time delay and Doppler frequency shift, which shows the distortion of the signal due to Doppler shift. To simulate the ambiguity function of the LFM and PN sequences, each signature is shifted with a different constant frequency shift and then is cross-correlated with the reference sequence. The results of the cross-correlation are stacked on top of each other in delay-Doppler plane. The ambiguity functions of the PN and LFM sequences are shown in Figure A.1. The bandwidth, central frequency, number of chips and period of signals are $B = 7.083$kHz, $f_c = 170$kHz, $N = 512$, and $T = 72.53$ms respectively.

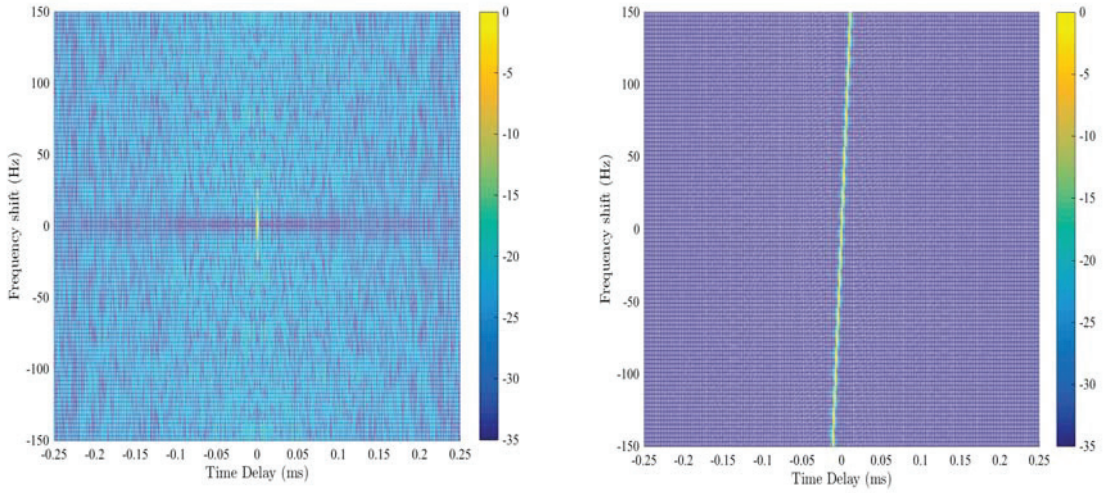

(a) PN sequence

(b) LFM sequence

Figure A.1: The ambiguity function of the LFM and PN sequence.

When the frequnecy is equal to 0Hz, the value of the ambiguity function is the same for both the PN and the LFM sequences. This means that both signatures have the same cross-correlation peak value when there is no Doppler shift. The PN sequence offers high resolution in detection of the energy of the channel in both delay and Doppler domain, but its correlation peak drops fast when the absolute value of the Doppler shift increases.

Referring to [46], the chirp signal has a higher correlation peak to noise floor ratio and it is more insensitive to Doppler shift than PN sequence. However, as the Doppler shift increases, the location of the peak of the LFM correlation is shifted in delay. According to [46], this delay shift is equal to $\Delta\tau = f_d \times T/B$, where f_d is the Doppler shift. This phenomenon makes the LFM signatures less accurate than PN sequences in delay domain.

The ambiguity function shows the sensitivity of the signatures to a constant frequency shift. However, in most practical cases the Doppler effect is observed as a dilation or compression of the received signal in the time domain which is called time-scaling. To explore the effect of time-scaling on LFM and PN signals another set of simulations was run. In this simulation the LFM and PN channel sounders are designed with equal communication parameters. The sounding signals pass through a deterministic channel with three paths where each path has a different time-scaling factor that is equivalent to different relative velocities between transmitter and receiver. In this channel, the delays are $\tau = [40, 60, 80, 100]$ ms and the respective path arrival velocities are $v = [0, 0.1, 0.3, 1]$ $\frac{\text{m}}{\text{s}}$. The amplitude of all paths is equal to 1. The communication parameters are the same as the previous simulation.

Figure A.2 shows the simulated power delay profiles of the channel, which are measured using the LFM and PN channel sounders. As it is shown the peak to noise floor ratio of the PN sounder decreases as the velocity (time-scaling factor) increases. This sensitivity to time-scaling can be reduced by re-sampling the received PN sequence before the channel sounding process. But, this procedure needs to obtain an estimate of the time-scaling factor which makes the implementation of the channel sounder more complicated.

Moreover, the LFM sequence is able to detect the paths with higher time-scaling factors, but it suffers from broadening in the delay domain, i.e. the third and forth path with $v = 0.3\ \frac{\text{m}}{\text{s}}$ and $v = 1\ \frac{\text{m}}{\text{s}}$, respectively.

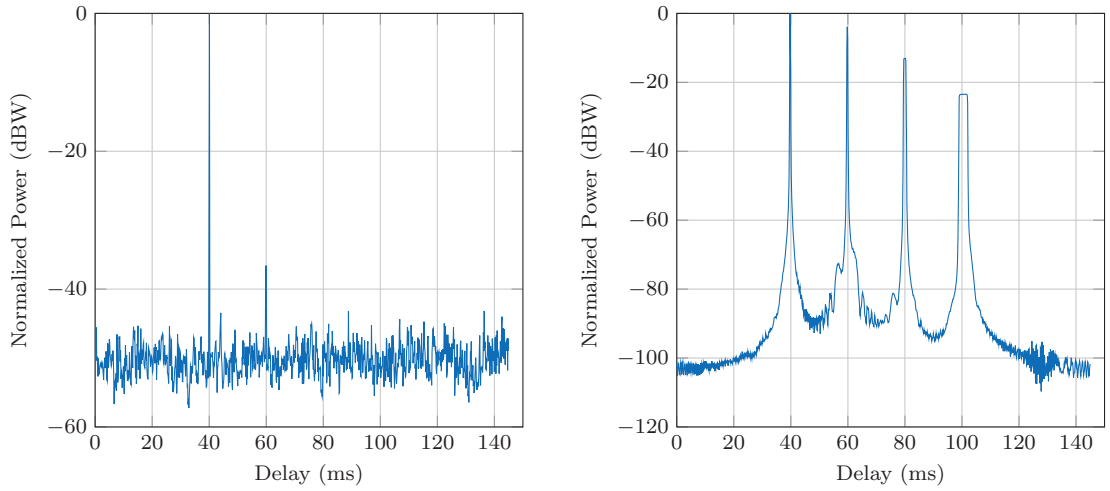

(a) Channel sounder with PN

(b) Channel sounder with Chirp

Figure A.2: Power delay profile measured by correlative channel sounder using LFM and PN sequences.

Therefore depending on the deployment of the channel sounder, both LFM and PN sequences can yield reliable results. Because the focus of this work was on characterization of the UWA channel in a fast time-varying scenario, the chirp signal was chosen due to its less sensitivity to Doppler effect. The results of channel sounding are shown in Chapter 2 and Chapter 5.